

Dissertation
submitted to the
Combined Faculty of Mathematics, Engineering and Natural Sciences
of Heidelberg University, Germany
for the degree of
Doctor of Natural Sciences

Put forward by
Javier Morán Fraile
born in: Valladolid, Spain
Oral examination: April 30th, 2024

Simulating the dynamical interaction of white dwarf stars in binaries

Referees:

Prof. Dr. Friedrich Röpke
Prof. Dr. Stefan Jordan

Zusammenfassung

Die Wechselwirkungen von Binärsternen, die auf dynamischen Zeitskalen stattfinden, gehören zu den anspruchsvollsten Prozessen, die in der Astronomie modelliert werden müssen. Sie werden am besten durch multidimensionale und multiphysikalische Simulationen beschrieben. Der Schwerpunkt dieser Arbeit liegt auf der numerischen Modellierung einiger der am wenigsten erforschten stellaren Wechselwirkungen, wobei ein besonderes Augenmerk auf solche mit weißen Zwergen gelegt wird. Diese Arbeit präsentiert drei verschiedene Studien unter Verwendung von dreidimensionalen hydrodynamischen Simulationen. An erster Stelle wird die Emission von Gravitationswellen während gemeinsamer Hüllenvorgänge untersucht, wobei die Chancen für ihre Entdeckung mit zukünftigen weltraumbasierten Detektoren abgeschätzt werden. Gegenstand der zweiten Studie ist die Gezeitenzerstörung eines weißen Zwergs durch einen Neutronenstern. Hier wird gezeigt, wie die genaue Modellierung dieser Ereignisse die Berücksichtigung einer Vielzahl von physikalischen Prozessen erfordert. Dabei wurden Magnetfelder, Kernreaktionen und Neutrinoemission in der Studie berücksichtigt. Zuletzt wird in einer dritten Studie aufgezeigt, wie Verschmelzungen zwischen niedrigmassigen weißen Zwergen (deren Gesamtmasse deutlich unter dem Chandrasekhar-Limit liegt) unter den richtigen Bedingungen zu thermonuklearen Explosionen führen können. Die Ergebnisse dieser Arbeit betonen, wie dynamische Wechselwirkungen zwischen Sternen eine Vielzahl von hellen Transienten hervorrufen können und wie der Einsatz fortschrittlicher multidimensionaler und multiphysikalischer Codes für ihre Modellierung dazu beitragen wird, unser Verständnis der Physik und der damit verbundenen Prozesse zu verbessern.

Abstract

Binary stellar interactions that take place on dynamical timescales are some of the most challenging processes to model in astronomy, and are best described by multidimensional, multi-physics simulations. The focus of this thesis is on the numerical modeling of some of the least explored stellar interactions, with a special emphasis on those involving white dwarfs. This work presents three different studies using three-dimensional hydrodynamic simulations. In the first place, the emission of gravitational waves during common-envelope events is studied, estimating the chances for their detection with future space-based detectors. Secondly, the tidal disruption of a white dwarf by a neutron star is studied, showing how the accurate modeling of these events requires the inclusion of a multitude of physical processes including magnetic fields, nuclear reactions and neutrino emission. Finally, through a third simulation, it is shown how mergers between low-mass white dwarfs, with total masses substantially below the Chandrasekhar limit, can lead to thermonuclear explosions under the right conditions. The results of this thesis stress how dynamical interactions between stars can produce a multitude of bright transients, and how the use of advanced multidimensional, multi-physics codes for their modeling will help improve our understanding of the physics and processes involved.

*In memory of
Anita and Luis*

Contents

List of abbreviations	1
List of physical constants	3
1. Context and theoretical background	5
1.1. White dwarfs	6
1.2. Binary stars	9
1.3. Stellar interactions	11
1.4. Numerical modeling in astrophysics	19
2. Results	23
2.1. Publication I: Gravitational wave emission from dynamical stellar interactions	25
2.2. Publication II: Self-consistent magnetohydrodynamic simulation of jet launching in a neutron star – white dwarf merger	39
2.3. Publication III: Faint calcium-rich transient from a double-detonation of a $0.6 M_{\odot}$ carbon-oxygen white dwarf star	53
3. Conclusions	63
3.1. Summary of the individual publications	63
3.2. Discussion and future work	68
3.3. Closing remarks	76
Acknowledgments	77
List of publications	79
Bibliography	81

List of abbreviations

GW	Gravitational waves
WD	White dwarf
HeWD	Helium white dwarf
COWD	Carbon-oxygen white dwarf
ONeWD	Oxygen-neon white dwarf
NS	Neutron star
BH	Black hole
CE	Common-envelope
EM	Electromagnetic
SN	Supernova
GR	General relativity
EoS	Equation of state
RLOF	Roche Lobe Overflow
LIGO	Laser Interferometer Gravitational-Wave Observatory
GRB	Gamma-ray burst
sGRB	Short gamma-ray burst
EM	Electromagnetic
BBH	Binary BH
BNS	Binary NS
LVK	LIGO-Virgo-KAGRA
IPTA	International Pulsar Timing Array
MHD	Magnetohydrodynamic
SNR	Signal to noise ratio
RG	Red giant
FBOT	Fast blue optical transient
SPH	Smoothed-particle hydrodynamics

List of physical constants

M_{\odot}	Solar mass
R_{\odot}	Solar mass
G	Gravitational constant
m_e	Electron mass
m_u	Atomic mass unit
c	Speed of light in a vacuum
h	Planck constant
pc	Parsec

1. Context and theoretical background

The fate of stars in binary systems is dictated by how they interact with each other. These interactions not only shape the evolution of the stars, but also give rise to some of the brightest events in the Universe. Modeling them involves accounting for a wide variety of physical processes such as fluid dynamics, nuclear reactions, magnetic fields, gravitational waves, neutrino emission, or radiative transfer, spanning an incredibly broad range of temporal scales. Interactions that take place on dynamical timescales are among the most challenging to model and are responsible for a multitude of different astronomical transients. The next generation of automated transient facilities and observatories is expected to be able to detect an unprecedented number of transients, and having accurate models will be crucial for their interpretation.

In this thesis, we make use of the advances in numerical techniques, especially the development of advanced, nearly Lagrangian, adaptive-mesh-refinement magnetohydrodynamic (MHD) codes, which coupled with the growing accessibility of computational resources, allow us to study, with an extraordinary level of detail, several types of astrophysical events not yet fully understood. In particular, we place special emphasis on events involving white dwarfs (WDs), as they are the most common type of stellar remnant, and they are known to originate some of the brightest events in the cosmos, such as Type Ia supernovae. Their interactions with other stars have the potential of resulting in highly energetic events, but the large parameter space, and the difficulties in the modeling of fast-evolving astrophysical interactions, mean that only a handful of possible events have been thoroughly studied.

This has been explored in three articles published in the peer-reviewed journal *Astronomy & Astrophysics*¹ and which constitute the results section of this thesis (Chapter 2). In Section 2.1 we studied the emission of gravitational waves (GW) during common-envelope events having WDs as the companion of the giant star, and analyzed their detectability by the next-generation GW detectors. Section 2.2 looks at one of the strongest regimes of interaction as we study the merger of a WD with a neutron star (NS), performing the first ever three-dimensional (3D) MHD simulation of such an event. In Sec. 2.3 an *intermediate* regime of interaction is studied as we look at the explosive outcome of the merger between a helium white dwarf (HeWD) and a low-mass carbon-oxygen white dwarf (COWD), combining 3D MHD simulations with radiative transfer to unveil a new type of thermonuclear transient.

¹<https://www.aanda.org/>

As each article shown in Chapter. 2 includes an introduction to the corresponding topic, the introduction of this thesis provides instead a general overview of several relevant aspects of astrophysics, and it is structured as follows: Section 1.1 introduces WDs, some of the physics relevant for their modeling, and transients that can be produced by these stars. Section 1.2 gives a brief overview of the importance of binary systems, how they may affect the evolution of the stars, and the difficulties in modeling them. The different types of interactions between the stars forming a binary are described in Sec. 1.3, including a brief introduction to the topic of GWs in Sec. 1.3.3 in order to highlight the important role that multi-messenger astronomy will play in the coming decades. Finally, Sec. 1.4 discusses the relevance of numerical modeling in modern astrophysics, what the current challenges are, and how they were addressed in our simulations.

1.1. White dwarfs

White dwarfs are the most common type of stellar remnant, and are generally understood as the end product of the evolution of stars born with masses below $\sim 11 M_{\odot}$ (Siess, 2007). These stars have been extensively researched, and a complete review of the topic is out of the scope of this thesis. Here, we will only give a brief overview of some of the basic properties of WDs and the physical principles governing them. A much more comprehensive description of WDs and the evolutionary phases that stars go through until reaching this stage can be found in reviews such as Koester and Chanmugam (1990) or Althaus et al. (2010). At this final stage of the star’s life, nuclear burning has stopped, and the stellar material, composed of a fully degenerate plasma, is supported by electron degeneracy pressure. This makes WDs a peculiar type of stellar object. With sizes on the order of a couple of thousand kilometers (Shipman and L., 1979; Carvalho et al., 2016), they are much more compact than stars undergoing nuclear reactions. But they are still considerably larger than NSs and stellar-mass black holes (BHs), the other two types of stellar remnants that have their origin in more massive stars.

The nuclear composition of this degenerate plasma varies depending on the initial mass of the progenitor of the WD. For those stars that are not massive enough to begin burning helium in their core (initial masses below $\sim 2.3 M_{\odot}$ according to Kippenhahn et al., 2012), what remains at the end of their evolution is the bare helium core after the outer layers of the star are shed, forming a so-called HeWD. According to standard stellar evolution, and excluding binary interactions, HeWDs can only reach masses up to $\sim 0.48 M_{\odot}$ (Kippenhahn et al., 2012), since stars with cores more massive than this will eventually reach central densities and temperatures high enough to fuse helium into heavier elements in their core, following a different evolutionary path. For stars more massive than this threshold (but with initial masses still below $\sim 11 M_{\odot}$), their final fate will be WDs made out of mixtures of carbon, oxygen, and neon. As the mass of the star increases, so does the fraction of heavier elements, and among these more massive WDs we can distinguish between COWDs and oxygen-neon white dwarfs (ONeWDs).

But there is a limit to how massive WDs can get. As no nuclear burning is

taking place in their interior, the force that has to challenge the gravitational collapse is the one exerted by electron degeneracy pressure. The conditions in the plasma forming WDs are so extreme that quantum mechanical effects become dominant. This happens when the average distance between particles is on the order of the de Broglie wavelength. For the densities and temperatures found inside WDs, the electrons in the gas satisfy this condition, and therefore their behavior begins to be dominated by quantum effects. The main one being that the distribution of their kinetic energy can no longer follow the Maxwell distribution, as they now must obey Pauli's exclusion principle, stating that no more than one particle can occupy each individual quantum state. Under these conditions, the equation of state (EoS) of the electron gas is decoupled from the temperature and takes the form

$$P_e = \frac{1}{20} \left(\frac{3}{\pi}\right)^{2/3} \frac{h^2}{m_e m_u^{5/3}} \left(\frac{\rho}{\mu_e}\right)^{5/3} = 1.0036 \times 10^{13} \left(\frac{\rho}{\mu_e}\right)^{5/3} \text{ (cgs)} \quad (1.1)$$

in the non-relativistic case, and

$$P_e = \frac{1}{8} \left(\frac{3}{\pi}\right)^{1/3} \frac{hc}{m_u^{4/3}} \left(\frac{\rho}{\mu_e}\right)^{4/3} = 1.2435 \times 10^{15} \left(\frac{\rho}{\mu_e}\right)^{4/3} \text{ (cgs)} \quad (1.2)$$

in the relativistic case (the derivation of these relationships and the ones that follow in this section can be found in textbooks such as [Kippenhahn et al., 2012](#)). With P_e being the pressure of the electron gas, ρ being the density of the gas, μ_e the mean molecular weight per free electron, m_u the atomic mass unit, m_e the electron mass, h the Planck constant, and c being the speed of light in vacuum. In a state of complete electron degeneracy, the pressure of the ionized gas (P_{ion}) is negligible with respect to P_e and therefore, the gas pressure is $P = P_{\text{ion}} + P_e \sim P_e$. This means that the structure of WDs can be approximated with polytropic models.

Polytropic relations take the form

$$P = K\rho^{1+1/n}, \quad (1.3)$$

where K is a constant and n is the polytropic index. It is straightforward to see that Eq. (1.1) and Eq. (1.2) satisfy this relation for $n = 3/2$ and $n = 3$ respectively. Assuming hydrostatic equilibrium and applying Eq. (1.3) to the Poisson equation, one arrives at the Lane-Emden equation:

$$\frac{1}{z^2} \frac{d}{dz} \left(z^2 \frac{dw}{dz} \right) + w^n = 0, \quad (1.4)$$

which can be used to obtain the following relationship between the mass and the radius of a polytropic stellar model

$$R \propto M^{\frac{1-n}{3-n}}. \quad (1.5)$$

A step-by-step derivation of the Lane-Emden equation and the mass-radius relationship can also be found in [Kippenhahn et al. \(2012\)](#). For the non-relativistic degenerate gas ($n = 3/2$) this results in an interesting

$$R \propto M^{-1/3}, \quad (1.6)$$

implying that the size of the star will decrease as its mass increases. This means that the more massive the WD gets, the higher its density and compactness, and the more important the relativistic effects become. However, as it can be seen from Eq. (1.5), for a fully relativistic WD ($n = 3$) this mass-radius relationship will break down. As WDs become more relativistic with increasing mass, one would expect that, physically, there should be a smooth transition between the solutions of Eq. (1.4) for $n = 3/2$ and $n = 3$. Nonetheless, for $n = 3$ the central density results to be independent of the total mass of the star, and in fact there is only one possible solution for the mass of a relativistic degenerate polytrope. This mass was first derived in Chandrasekhar (1931), and hence receiving the name of Chandrasekhar mass:

$$M_{\text{Ch}} = \frac{5.836}{\mu_e^2} M_{\odot}. \quad (1.7)$$

This is therefore the maximum mass attainable by a WD supported by electron degeneracy pressure, as, at this mass, the polytropic relations state that the central density will grow to infinity as the radius approaches zero.

As stated previously, the nuclear composition of WDs consists mainly of He, C, O, or Ne, and therefore $\mu_e \sim 2$. This gives a value for the Chandrasekhar mass of $M_{\text{Ch}} = 1.46 M_{\odot}$. For masses larger than this value, the electron degeneracy pressure will not be able to counteract gravity, and the star will collapse. It is important to notice that this limit is derived just from electron degeneracy pressure, and does not take into account additional physics such as magnetic fields, rotation, or nuclear reactions. In fact, nuclear reactions may onset before reaching M_{Ch} . As the mass of a WD increases, its radius decreases, and therefore the central density grows to ever-higher values, where nuclear reactions can occur. Under degenerate conditions, nuclear burning takes place on extremely short timescales, and it can result in a thermonuclear runaway process that completely unbinds the star. This is thought to be the process responsible for Type Ia supernova (SN) (Arnett, 1969), which are believed to be caused by the ignition of ^{12}C in the center of COWDs. The importance of Type Ia SNe for astronomy and the search of their progenitors has been extensively discussed in the literature (e.g. Taubenberger, 2017; Röpke and Sim, 2018; Ruiter, 2019; Liu et al., 2023), and will be further discussed in Sec. 3.2. Here, we would just like to draw attention to the fact that the now commonly accepted progenitor systems for this type of transient are those in which a COWD *interacts* with another star, either by receiving mass and increasing its central density until the conditions for C burning are met at masses close to M_{Ch} , or by being perturbed in such a way that its center is compressed to the point where a C ignition takes place (e.g. double-detonation scenario Woosley and Weaver, 1994), even at masses substantially below M_{Ch} .

WDs therefore have the potential to generate extremely energetic transients, since when the conditions for nuclear burning are met inside the degenerate gas, the outcome can be a thermonuclear explosion. These conditions seem to be met almost exclusively through binary stellar interactions. Binary interaction is a broad and complex topic, and in Sec. 1.2 we will only give a brief introduction to it. For a comprehensive description of the topic, the reader is referred to specialized textbooks like Eggleton (2006), Benacquista (2013), or Tauris and van den Heuvel (2023).

1.2. Binary stars

The situation of our Sun as an isolated celestial body is not the universal norm. Binarity is a frequent phenomenon in stellar systems. In fact, most *massive* stars in the Universe are not born as single stars, but rather they are formed in systems containing two or more stars (Mason et al., 2009; Sana and Evans, 2011; Chini et al., 2012; Moe and Di Stefano, 2017; Almeida et al., 2017) held together by gravitational attraction.

Stars that are born in binaries can experience lives effectively identical to the ones of those born in isolation, as long as they are far enough from their respective companion. But that is not the case for the large majority of massive stars. Sana et al. (2012) claims that 71% of the stars born with masses larger than $15 M_{\odot}$ will interact with a companion over the course of their lifetimes.

These interactions can completely alter the evolution of the stars that forming the binary by transferring mass and angular momentum between the stars, modifying their structure and chemical composition, inducing enhanced mixing in their interior, or even directly leading to a merger between the stars. A modern review on the topic of binary evolution and interactions between stars in massive binaries can be found in Marchant and Bodensteiner (2023).

There are multiple types of binary interactions, acting on different timescales. In stellar evolution, the main timescales considered are the *nuclear*, *thermal* and *dynamical* timescales (see e.g. Kippenhahn et al., 2012). These represent estimates of how quickly stars react to changes caused by different processes. The nuclear timescale describes how quickly a star changes due to the nuclear reactions taking place in its interior, which is the timescale that dictates the changes in the evolutionary stage of unperturbed stars. It can be approximated as the time the star needs to radiate away all the energy that can be released by nuclear reactions in its current state

$$t_n \approx \frac{E_n}{L}, \quad (1.8)$$

where E_n is the available nuclear energy budget of the star, and L is the luminosity. The thermal timescale, or Kelvin-Helmholtz timescale, is defined as the timescale required for a star to radiate away its gravitational potential energy. This gives estimates for how quickly a star readjusts its thermal structure, which normally governs contraction and expansion of stars. It can be approximated as

$$t_{\text{KH}} \approx \frac{GM^2}{2RL}, \quad (1.9)$$

where G is the gravitational constant, M is the mass of the star and R its radius. Dynamical timescale is usually the smallest among the considered timescales, and it represents the timescale for the star to react to a perturbation of its hydrostatic equilibrium. It is usually estimated as the free-fall timescale

$$t_{\text{dyn}} = \sqrt{\frac{R^3}{GM}}. \quad (1.10)$$

In binary systems there are additional timescales to consider that are often much more difficult to define, such as the timescale for tidal interaction (e.g. Damiani,

C. and Lanza, A. F., 2015)

$$t_{\text{tid}} \approx \frac{h}{\tau}, \quad (1.11)$$

where h is the orbital angular momentum and τ is the tidal torque, or the timescale for orbital decay due to GW emission

$$t_{\text{GW}} \approx \frac{5c^5(1+q)^2a^4}{256G^3M^3q}, \quad (1.12)$$

where q is the ratio between the masses of the binary ($q = m_2/m_1 \leq 1$) and a is the orbital separation (e.g. Peters, 1964; Zwick et al., 2020).

The focus of Chapter 2 is on modeling interactions that take place on dynamical timescales. In binaries, these interactions normally occur as a result of processes acting on longer timescales that reduce the distance between the stars. One of the most frequent mechanisms to initiate a dynamical stellar interaction is not actually a change in the orbital separation between the stars, but rather the change in the mass or radius of one of them due to reaching a new evolutionary stage. This usually happens on nuclear timescales, for example, when a star depletes its core of hydrogen, leaving the main-sequence, it enters a giant stage, with their outer layers greatly expanding and potentially getting close enough so that its companion can make its presence felt.

Other physical processes do, in fact, change the orbital parameters of the binary system and can bring the stars closer to each other. As an example, the gravitational pull of an external third body can dramatically alter the orbit of the binary and make its component interact. This can happen on an extremely short timescale, as is the case in globular clusters, where the number of stellar objects is so large that three-body interactions are frequent and can lead to very close encounters between stars. Alternatively, it can also occur over longer periods of time, as in the case of hierarchical triples, stable stellar systems formed by an inner binary in relative proximity and a distant third body. In these hierarchical triples, the outer object can induce perturbations in the orbit of the inner binary, such as the Lidov-Kozai mechanism (Lidov, 1962), which over thousands of years will bring the inner binary to a more eccentric orbit, decreasing the minimum orbital separation and forcing an interaction between the components.

On the much longer t_{GW} timescale, acting over millions of years, gravitational radiation will effectively shrink the orbit of every binary system, as it loses energy in the form of GWs. Due to the weakness of this effect at large orbital separations (the time for a binary system to merge due to GW radiation is proportional to the fourth power of its orbital separation Peters, 1964; Zwick et al., 2020), this mechanism is more apparent in binary systems that already have very tight orbits. It is also important in old binary systems, whose components have already reached their final evolutionary stages, potentially having experienced interactions in the past. Over a period of time comparable to the age of the Universe, these systems will lose energy and angular momentum due to GW emission, causing their orbital separation to shrink, which can eventually lead to faster-paced interactions.

1.3. Stellar interactions

1.3.1. Tidal interaction

The global effect of tides in binary systems is mainly the transfer of orbital angular momentum into the rotational angular momentum of the stars. The exact interplay between the orbital motions and the effects they have on the stars is very complex, and we refer the reader to [Eggleton \(2006\)](#) for a comprehensive depiction of them. In a simplified picture, whenever the stars in a binary have their rotational plane misaligned with their orbital plane, have a noncircular orbit, or are out of corotation, the binary will be out of *tidal equilibrium* ([Darwin, 1879](#); [Hut, 1980](#)). In a binary out of tidal equilibrium, the bulges caused in the stars by the tidal forces will be misaligned, effectively producing a torque that results in the aforementioned exchange between orbital and rotational angular momentum. The torque attempts to restore tidal equilibrium, trying to induce the circularization of the orbit, tidal synchronization, and the alignment of the rotational spins ([Hut, 1981](#)). This results in a transfer of angular momentum, modifying the orbital parameters until a state of equilibrium is reached. If, as a result of these changes, the orbital separation decreases past a certain point, a mass-transfer episode will be induced (Sec. 1.3.2). It is important to note that it is not always possible to restore tidal equilibrium. If a star is rotating faster than a critical value for a given eccentricity, the torque will actually induce an increase in orbital eccentricity ([Eggleton, 2006](#)). The same will happen in an initially circular orbit if the angular momentum of the orbit is lower than three times the sum of the rotational angular momentum of the stars in the binary ([Hut, 1980](#)). This is the so-called *Darwin instability* ([Darwin, 1879](#)), and it can induce stellar mergers on relatively short timescales.

Tides can also alter the evolution of the stars in a binary, even without originating mass-transfer episodes or mergers. If a binary is in tidal equilibrium, tidal synchronization implies that the rotational period of the stars matches the orbital period of the binary. At sufficiently short orbital separations, this can result in the rotation of the stars being fast enough to induce an enhanced rotational mixing inside of them that can even prevent the buildup of a chemical gradient between the core and envelope ([de Mink et al., 2008](#)). This can make stars born at short orbital separations skip the giant stage altogether, resulting in a completely different type of stellar evolution ([Maeder, 1987](#)).

1.3.2. Mass transfer

Mass transfer takes place when part of the gas belonging to one of the components of a binary system is no longer gravitationally bound to its parent star but rather to its companion, with the mass-losing star being referred to as the donor and the receiving star as the accretor. A commonly used approximation to understand the behavior of mass transfer is through the concept of the *Roche potential*. The following descriptions of the Roche potential and criteria for mass transfer stability are loosely adapted from [Eggleton \(2006\)](#). This potential is computed by treating

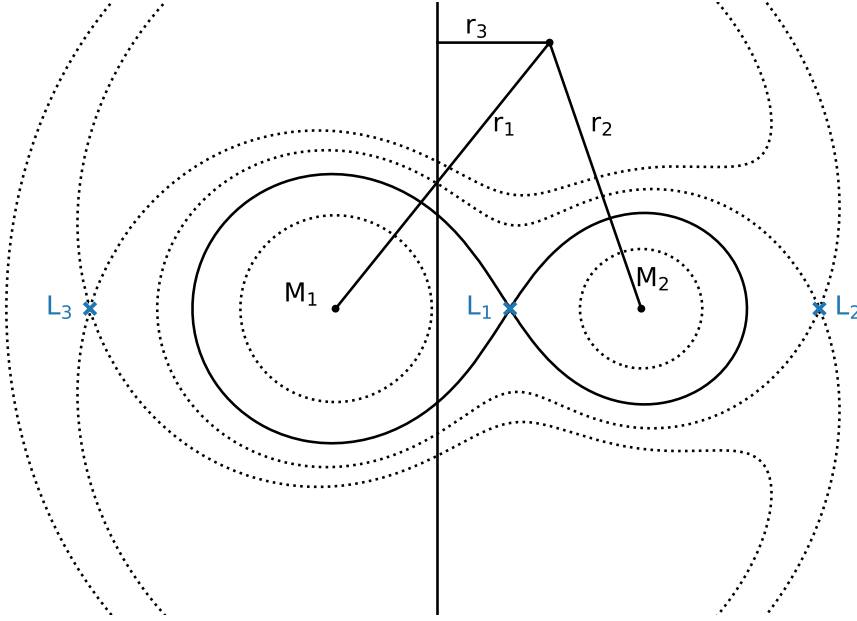


Figure 1.1: Geometry of the Roche potential for a mass ratio $M_1/M_2 = 2$. The dotted lines show selected equipotential surfaces. The vertical line shows the rotation axis of the system. The Roche lobe is the surface marked as the plain line surrounding both stars. The Lagrange points L_1 , L_2 and L_3 are indicated in blue.

the stars in a binary as point masses and taking into account the motion of the stars around each other. Under the assumption of a circular orbit, the Roche potential takes the shape

$$\Phi = -\frac{GM_1}{r_1} - \frac{GM_2}{r_2} - \frac{\omega^2 r_3^2}{2}, \quad (1.13)$$

where r_1 and r_2 are the distances to the center of the stars with masses M_1 and M_2 , r_3 is the distance to the rotation axis of the binary and ω is the angular velocity of the binary. An example of the shape of this potential for the case $M_1 = 2M_2$ is shown in Fig. 1.1. The two Roche lobes are defined as the two separate volumes confined within the equipotential line that crosses through the internal Lagrange point L_1 . The Roche lobes are evidently non-spherical. Despite this, it is useful to define an average Roche lobe radius as the one of a sphere with the same volume as the Roche lobe. This can be done by computing their volume numerically, but a more straightforward way is to take the following approximation from [Eggleton \(1983\)](#), which is correct to a 1%:

$$R_L = \frac{0.49a}{0.6 + q^{-2/3} \ln(1 + q^{1/3})}, \quad (1.14)$$

where $q \equiv M_1/M_2$ and a is the orbital separation. The material contained within the Roche lobe of a star will be gravitationally bound to that star. If a star is in hydrostatic equilibrium, its surface will correspond to an equipotential surface.

Therefore, if at any point a star reaches the size of the Roche lobe, the material on its surface can be transferred to the other star through the L_1 point, and a *mass-transfer* episode will ensue. This can happen as a result of a decrease in the orbital separation or due to a star expanding (or, on occasions, due to both stars expanding). The topic of mass transfer is complex, and here we will only briefly introduce some idealized scenarios. We refer the reader to specialized textbooks (e.g. Eggleton, 2006; Benacquista, 2013; Tauris and van den Heuvel, 2023) for a more comprehensive description.

The evolution of a mass transfer episode when one of the stars has reached the point of Roche Lobe Overflow (RLOF) depends mainly on three factors: how the orbit evolves, how the radius of the donor star reacts to the mass loss, and how the accretor reacts to the mass gain.

In an ideal scenario, if the mass and orbital angular momentum of the binary are conserved during the mass transfer, the reaction of the orbital separation to the change in mass distribution is to shrink the orbit if the mass of the donor (M_d) is larger than the mass of the accretor (M_a) and to widen it if $M_d < M_a$. This conservation of total mass and orbital angular momentum does not hold true in the majority of the cases. We have already mentioned how tides exchange orbital angular momentum into rotational angular momentum, but this is not the only scenario. For example, the accretor may not be able to accept mass at the rate that the donor is losing it and some mass can be ejected in the form of stellar winds or jets. It can also occur that part of the donated mass reaches the L_2 point and forms a circumbinary disk, carrying away angular momentum from the binary. In these cases, where the angular momentum and the total mass of the binary are not conserved, the mass transfer is considered *non-conservative* and the change in orbital separation due to the mass transfer is much more complicated to model. A detailed description of the different types of non-conservative mass transfer modes can be found in Soberman et al. (1997). Some of them prove to be almost impossible to accurately model with simple analytic or semi-analytic prescriptions.

Regarding the evolution of the donor star to the mass loss, it is important to note that whenever a star loses mass, its hydrostatic and thermal equilibrium are momentarily perturbed. The star will then readjust itself, attempting to restore a state of equilibrium, which results in a change in its radius. But the loss of mass also changes the size of the Roche lobe. Depending on how the slope of the mass-radius relationship of the star compares to that of its R_L , and how quickly hydrostatic and thermal equilibrium are restored, we can distinguish between three different modes of mass transfer.

For simplicity, and again following Eggleton (2006), we can introduce ξ_L , ξ_{ad} and ξ_{eq} as the slope

$$\xi \equiv \frac{d \log R}{d \log M} \quad (1.15)$$

of the mass-radius relationship for the Roche lobe radius, for the star restoring hydrostatic equilibrium (on a dynamical timescale) and for the star restoring thermal equilibrium (on a Kelvin-Helmholtz timescale), respectively. Generally speaking, $\xi_{ad} > \xi_{eq}$ will hold because the dynamical timescale of a star is much

shorter than the Kelvin-Helmholtz timescale and due to this the restoration of hydrostatic equilibrium is considered to be an almost adiabatic process.

If $\xi_L \leq \xi_{\text{ad}}$ and $\xi_L \leq \xi_{\text{eq}}$, the mass transfer is considered stable. The size of the Roche lobe decreases slower than the radius of the star, and the mass transfer will proceed on the timescale of whatever process triggered the RLOF (e.g. the expansion of the star on a nuclear timescale, a loss of angular momentum caused by tides, GW emission or even the non-conservative nature of mass transfer itself).

If $\xi_{\text{ad}} > \xi_L > \xi_{\text{eq}}$, the adiabatic response of the star to the mass loss keeps the stellar radius smaller than the Roche lobe radius, but mass transfer will proceed on a thermal timescale as the star attempts to restore thermal equilibrium. This is normally referred to as self-regulating mass transfer.

Finally, if $\xi_L > \xi_{\text{ad}} > \xi_{\text{eq}}$ the mass transfer is dynamically unstable. The Roche lobe radius decreases faster than the star can readjust, and the mass-transfer rate increases in a runaway process. A dynamically unstable mass transfer will almost inevitably lead to a transient event such as a stellar merger (events that will be studied in Sec. 2.2 and Sec. 2.3) or a common-envelope (CE) event (which is the main scenario studied in Sec. 2.1), depending on the properties and the evolutionary stage of both donor and accretor.

As mentioned in the last paragraphs, even using the approximate model of the Roche potential, mass transfer is very challenging to model analytically. Furthermore, real scenarios can differ on a substantial degree from this simplified approach. The mass of the stars is not concentrated in a single point, orbits will not be perfectly circular, and the use of an average R_L is inaccurate as the lobes are not spherical, among other limitations. On top of this, the interaction of mass transfer with tides adds another layer of complexity that makes analytic modeling of these interactions increasingly difficult. As a result, the only consistent method to accurately model these processes will be the use of numerical simulations.

Understanding the outcome of these interactions is crucial for binary evolution and the formation of the progenitors of astronomical transients. Many observed transients are the direct outcome of binary interactions, but in some cases, even the formation of the progenitors of these events results difficult to understand without a complicated interplay between two stars over the course of their evolution. This is specially highlighted in the case of binaries formed by two compact-objects in a tight orbital configuration. Compact objects (WDs, NSs and BHs) are remnants of increasingly more massive stars, and these stars cannot be born too close to one another, as during their lives they will go through evolutionary stages where their radii are several orders of magnitude larger than the observed orbital separation of some of these systems. Therefore, the stars in these binary systems must have been formed at a substantially larger separation between them and interacted with each other in such a way that the end result is in a tight orbit. There are many proposed formation channels involving different interactions between the binaries at different evolutionary stages. A good overview of the evolutionary channels to form double-compact-object systems can be found in [Tauris and van den Heuvel \(2023\)](#). In the last years, this topic has received copious amounts of attention (e.g. [Kalogera et al., 2007](#); [Belczynski et al., 2016](#); [Kruckow et al., 2018](#); [van Son et al., 2020](#)) in an attempt to explain the formation of the progenitor systems

of the merging BHs and NSs detected with GW observatories. These formation channels often invoke a CE event as the responsible for the orbital shortening, as it is one of the few interactions that can significantly reduce orbital separations in very short timescales. However, the difficulty in modeling this stage makes it one of the largest uncertainties for the binary evolution channels (Ivanova et al., 2013; Vigna-Gómez et al., 2018). A detailed description of the CE phase, its implications on astrophysics and the current state of its modeling is out of the scope of this thesis, but can be found in reviews such as Ivanova et al. (2013); Röpke and De Marco (2023). What follows is a brief introduction to this stage, and to some of the challenges involved in its modeling.

Common-envelope evolution

The term *common-envelope event* (Paczynski, 1976) is used to describe the stage of a binary system in which a companion star and the core of a giant star orbit each other inside the envelope of the giant. This phase is commonly accepted to be the result of an unstable mass transfer, originated when a star in a binary enters a giant stage. As the outer layers or *envelope* of the giant star expand on a short timescale, a mass transfer episode onsets. If the accretor cannot keep up with the rate at which mass is being fed to it, this mass transfer will result in the engulfment of the accreting companion by the envelope. From this point on, the companion and the core of the star will orbit around the center of mass of the system, surrounded by the dense medium formed by the envelope. Dynamical friction with the envelope will transfer orbital energy and angular momentum, heating it up while reducing the orbital separation between the core and the companion. The process will come to an end when either enough energy has been injected into the envelope to completely unbind it from the system, ejecting it, or when the orbital separation has decreased so much that it leads to a merger between the core and the companion. This is what makes CE one of the few astrophysical processes capable of dramatically changing the orbital parameters of a binary system on very short timescales, playing a fundamental role in several evolutionary channels that lead to the formation of GW progenitors.

The modeling of this stage is very challenging, mainly due to the broad range of spatial scales involved as two small cores orbit inside an extended envelope, and due to the amount of physics that dictate the evolution. Several approaches are used while attempting to explain the observations of post-CE systems. The simplest ones being fully parametric (Webbink, 1984; de Kool et al., 1987; Nelemans et al., 2000; Hirai and Mandel, 2022), and relate the energy or angular momentum required to eject the envelope with the final orbital separation of the binary. But these models do not capture the underlying physics and are unable to reliably predict the outcome of the CE event. The same applies to 1D simulations, that must parametrize the drag force, and despite this parametrization being physically motivated, it is not self-consistent. Furthermore, 1D simulations must assume symmetry in the problem while this type of interaction is inherently 3D, and ultimately, these 1D simulations will have a limited use and must be combined with more accurate representations of the event. The only approach that

can self-consistently model the interaction between the cores and the envelope is 3D simulations. These simulations are substantially more expensive and also come with a set of challenges, which will be briefly discussed in Sec. 1.4. Despite the progress that these simulations have made, even the most accurate simulations of CE events currently available (e.g. [Moreno et al., 2022](#); [Ondratschek et al., 2022](#); [Lau et al., 2022](#)) still struggle to accurately reproduce the measured orbital separations of observed post-CE binaries for all the types of systems ([Röpke and De Marco, 2023](#)).

The final orbital separation after the ejection of the envelope is a key parameter for binary evolution. It is the current consensus that the double-compact-object binaries that result in the mergers detected by GW observatories must have gone through at least one CE stage if their progenitor system formed as an isolated binary. Due to the steepness of the dependence of the orbital decay rate caused by GWs with respect to the orbital separation ([Peters, 1964](#)), if the result of a CE is a distance too large between the components, a merger cannot take place within a Hubble time. This argument applies to the formation of all interacting binaries containing at least one compact object, like the ones studied in this thesis. The NS–WD binary studied in Sec. 2.2 must have undergone a CE phase during its evolution ([Toonen et al., 2018](#)), and the WD–WD binary merger shown in Sec. 2.3 is presumed to have experienced at least two mass transfer episodes (potentially two CE events) and even the merger itself could take place during a CE, depending on the outcome of it. In order to contribute to the elucidation of this enigmatic phase of binary evolution, in Sec. 2.1 we studied the feasibility of detecting GW signals from CE events, which would effectively track the orbital evolution of the core and companion inside the envelope, revealing crucial information for understanding the processes involved in CE events.

1.3.3. Gravitational waves

The last type of stellar interaction that will be discussed in this thesis is the release of GWs. These waves arise as a direct consequence of general relativity. The Einstein field equations ([Einstein, 1915](#)) take the form:

$$R_{\mu\nu} - \frac{1}{2}g_{\mu\nu}R = \frac{8\pi G}{c^4}T_{\mu\nu}, \quad (1.16)$$

with $R_{\mu\nu}$ being the Ricci tensor, R the Ricci scalar, $g_{\mu\nu}$ being the spacetime metric and $T_{\mu\nu}$ the stress-energy tensor of the matter. These equations describe how gravitational fields are generated by the mass of matter. The origin of GWs can be derived from Eq. (1.16) by assuming a weak gravitational field (see [Maggiore, 2007](#); [Creighton and Anderson, 2011](#), for a step by step derivation). In this scenario, the spacetime metric can be written as a flat spacetime plus a perturbation:

$$g_{\mu\nu} = \eta_{\mu\nu} + h_{\mu\nu}, \quad (1.17)$$

with $\eta_{\mu\nu}$ being the flat Minkowski spacetime and $h_{\mu\nu}$ being the perturbed metric. This is called the linearized gravity approximation. Applying it to Eq. (1.16) and

defining the *trace-reversed metric perturbation*,

$$\bar{h}_{\mu\nu} = h_{\mu\nu} - \frac{1}{2}\eta_{\mu\nu}\eta^{\alpha\beta}h_{\alpha\beta}, \quad (1.18)$$

one obtains

$$\square\bar{h}_{\mu\nu} + \eta_{\mu\nu}\partial^\rho\partial^\sigma\bar{h}_{\rho\sigma} - \partial^\rho\partial_\nu\bar{h}_{\mu\rho} - \partial^\rho\partial_\mu\bar{h}_{\nu\rho} = -\frac{16\pi G}{c^4}T_{\mu\nu}, \quad (1.19)$$

where \square is the d'Alembertian operator $\square = \partial^\mu\partial_\mu$. Choosing the Lorentz gauge ($\partial^\nu\bar{h}_{\mu\nu} = 0$) this becomes a simple wave equation:

$$\square\bar{h}_{\mu\nu} = -\frac{16\pi G}{c^4}T_{\mu\nu}, \quad (1.20)$$

with the matter stress-energy tensor providing a source term. This means that in vacuum, where the right-hand side of Eq. (1.20) becomes zero, the metric perturbation solutions will be waves that propagate at the speed of light, and matter can generate them. The release of GWs plays a very important role in binary dynamics, especially for stellar remnants, as they carry away energy and angular momentum. The first indirect evidence of their existence came in 1974 with the detection of the Hulse-Taylor binary pulsar (Hulse and Taylor, 1975), and the subsequent observations that showed that its orbital period was declining at a rate consistent with the release of GWs predicted by general relativity (Weisberg et al., 1981). Gravitational waves were detected directly for the first time on September 14th, 2015 (Abbott et al., 2016b), when the two detectors of the Laser Interferometer Gravitational-Wave Observatory (LIGO) simultaneously observed the signal arising from a merger between two BHs. This signal, named GW150914, meant direct confirmation of yet another prediction of general relativity, and also opened a new window for the exploration of the cosmos. We are no longer restricted to its study by means of detecting electromagnetic (EM) signals or particles like cosmic rays and neutrinos. We could now start to observe the Universe using this new type of radiation that carries additional information about its source.

The frequency of the gravitational waves released by a source depends on its ability to generate oscillations in its quadrupole moment. In the case of orbiting binaries, since half a rotation around the center of mass translates into a full rotation of the mass quadrupole moment, the frequency of the released GWs is twice the orbital frequency of the system ($f_{\text{GW}} = 2f_{\text{orb}}$), with additional power being radiated at frequencies that are harmonics of the orbital frequency in the case of eccentric orbits (Peters and Mathews, 1963). This radiation of GWs takes energy and angular momentum away from the binary, shrinking the orbit and increasing the orbital frequency (and therefore the GW frequency as well). The amount of energy radiated in the form of GWs is very small in most cases, but it is inversely proportional to the fifth power of the orbital separation (Peters, 1964). Therefore, the orbit-shrinking effect of GWs is very weak for wide binaries, but it accelerates over time as the binaries come to ever-tighter orbits, becoming dominant in short period compact-object binaries.

Gravitational waves stretch spacetime itself as they propagate. The method devised for their detection is to measure the relative change in distance between

two points in space caused by this stretching. This is by no means an easy task, and the current state-of-the-art detectors LIGO (Aasi et al., 2015), Virgo (Acernese et al., 2014) and KAGRA (Akutsu et al., 2021) are designed to be able to measure changes in the length of the arms of the detectors as small as $\sim 10^{-16}$ cm. As of today, we only have observatories that can “listen” to GWs in two frequency bands: between ~ 10 – 1000 Hz with the aforementioned detectors, and, with much lower sensitivity, between ~ 1 – 100 nHz by measuring perturbations in the travel time of the signal of known pulsars. Despite the engineering feat that GW observatories represent, the technique employed for the detection of signals means that the physical size of the detectors constrains the range of GW frequencies that can be observed. The detectors of the LIGO-Virgo-KAGRA (LVK) Collaboration operate in the Hz–kHz band as they measure the change in travel time of a laser signal across their detector arms with lengths on the order of a couple kilometers. The longer the arms, the lower the frequencies that the detectors can potentially be sensitive to. These observatories use Fabry-Perot cavities to bounce back and forth hundreds of times the laser signal, effectively increasing the length of the detector arms by as many times as the signal is reflected. On the other hand, the detectors of the International Pulsar Timing Array (IPTA) collaboration (Manchester, 2013) measure perturbations in the arrival time of the signal from Galactic pulsars, therefore having “detector arms” with sizes on the order of thousands of light years, making them able to detect GWs on the frequency range of nHz, albeit with a much lower sensitivity than the kHz detectors.

While the search for GWs on the nHz frequency band is recently showing promising progress (EPTA Collaboration et al., 2023a,c,b; The International Pulsar Timing Array Collaboration et al., 2023; Agazie et al., 2023), the observations in the ~ 10 – 1000 Hz band have already produced groundbreaking advances in astronomy. This band of the GW spectrum is populated by signals originated by the mergers of compact objects, and since the beginning of their search for these signals, the LVK Collaboration has already detected almost a hundred events. The vast majority of these being binary BH (BBH) mergers, but a small fraction of these events have been BH–NS and binary NS (BNS) mergers. With our current detectors, the coalescence of BNS or BH–NS systems results more challenging to detect than BBH mergers, as they release GW with frequencies higher than the observatories can currently detect. Nonetheless, they provide a unique opportunity for astronomy, as BNS mergers (and BH–NS mergers if the BH is not large enough to engulf the NS before its disruption) are the progenitors of some of the most energetic EM transients known (Nakar, 2007; Metzger et al., 2010; Metzger, 2017; Nakar, 2020). This means that EM counterparts can arise from these events, opening the window for *multi-messenger astronomy*. GW170817 (Abbott et al., 2017; Abbott et al., 2017) provided the first detection of a binary NS merger, and it was detected alongside a short gamma-ray burst (sGRB) (Goldstein et al., 2017; Savchenko et al., 2017) and a kilonova (Troja et al., 2017; Alexander et al., 2017), confirming BNS mergers as progenitors of these types of transients.

In the coming decades, if the technical challenges involved are overcome, a new generation of ambitious space and lunar-based GW observatories (Seto et al., 2001; Harry et al., 2006; Robson et al., 2019; Harms et al., 2021) will make it possible

to detect signals from wider binaries with frequencies in between the currently existing kHz and nHz detectors. These observatories could additionally target systems and events that are not necessarily driven by GW release, but that rather release them due to the change in mass distribution as a result of other types of interaction, such as mass transfer or tidal effects. Detections of such systems would provide valuable insight into processes normally not accessible to EM astronomy. One example already presented is the identification of the progenitors of bright transients, but GW signals could also help to shed light on not-yet fully understood astrophysical processes such as the CE phase. As the frequency of the GWs tracks the orbital frequency of their progenitor binary, they provide information about the orbital parameters and their evolution. In Sec. 2.1 we show how the GW signals released during these events passively trace the orbital evolution inside the envelope of the core of the giant star and the companion during these events. This information would normally be hidden, as the EM signals from the CE interior would be shielded by the envelope. The same principle applies for the GW signals that originate in SNeIa (e.g. [Seitenzahl et al., 2015](#)) or in core-collapse SNe (e.g. [Kotake and Kuroda, 2017](#); [Mezzacappa and Zanolin, 2024](#)), where detections could help improve our understanding of the mechanisms at play during the explosions. These signals could even be used to obtain information about nuclear physics and how matter behaves at the densities found inside NSs.

1.4. Numerical modeling in astrophysics

Real life scenarios often depart from the idealized pictures and approximations required for analytical models. Although the fundamental physical processes involved in most of the astrophysical phenomena may be known, the interplay between them can add exponential layers of complexity.

The power of numerical modeling becomes evident when considering all the different physics participating in astrophysical processes. The stability of stars involves, among other physical processes, gravitational forces, nuclear reactions, radiative transfer or magnetic fields. As mentioned in earlier sections, analytic approximations frequently fall short in representing stellar interactions beyond a few idealized scenarios. For the rest of the cases, hydrodynamical simulations are often the most accurate modeling technique and have become a fundamental part of modern astrophysics. Hydrodynamic simulations have been used to improve our understanding of an innumerable amount of astrophysical phenomena such as stellar evolution (e.g. [Eggenberger et al., 2008](#); [Paxton et al., 2011](#)), stellar convection (e.g. [Horst et al., 2021](#); [Leidi et al., 2023](#)), SNe (e.g. [Powell et al., 2023](#); [Gronow et al., 2020](#)), stellar mergers (e.g. [Schneider et al., 2019](#)), mass transfer (e.g. [Bobrick et al., 2017](#)) and many more. Despite the invaluable insights provided by simulations, they face limitations imposed by the specific numerical techniques employed and the availability of computational power. As a result, the physics that will be included in a simulation, and their accuracy, have to be carefully considered for the individual scenario and the temporal and spatial scales that are aimed to be simulated. Another aspect that must be taken into account when

simulating astrophysical phenomena is the dimensionality of the problem. Certain scenarios can be assumed to have spherical symmetry, and this allows them to be recreated using 1D simulations with a comparatively low computational cost. This has traditionally been the case of stellar evolution for single stars (Heger et al., 2000; Paxton et al., 2011, 2013, 2015; Paxton et al., 2019). However, some physical processes are inherently multi-dimensional, such as magnetic fields or convection, and they must be approximated via simplified prescriptions in order to model them in 1D simulations (Buldgen, 2019). Precise modeling of non-spherically symmetric processes requires treating them with 2D or 3D simulations, which are increasingly more expensive but provide the most accurate modeling of complex astrophysical phenomena.

The physical conditions inside stars span many orders of magnitude in temperature, density and pressure, resulting in a broad range of characteristic length scales and timescales in their interior. This results in a challenging setup for hydrodynamical simulations. Ensuring numerical stability of the models requires an increasingly higher spatial and temporal resolution as the gradients in density and pressure become steeper. This makes simulating the entire structure of stars highly complex due to the simultaneous action of processes across several spatial and temporal scales. In order to overcome these challenges, techniques such as adaptive mesh refinement (AMR, Berger and Olinger, 1984) have been employed to optimize the consumption of computational resources. These techniques allow the use of different spatial resolutions in the simulation domain, and therefore resolution can be concentrated exclusively where it is required. But there is a fundamental issue that cannot be easily overcome. As only a finite number of temporal steps can be realistically simulated, the maximum timescale that can be effectively modeled becomes unavoidably limited by the smallest temporal scale that needs to be resolved in the simulation. Furthermore, numerical stability criteria such as the CFL condition (Courant et al., 1928) constrain the relationship between spatial and temporal resolutions, indirectly imposing a limit on the spatial resolution that can be employed. This is one of the main challenges in hydrodynamic simulations.

When attempting to simulate more than one star simultaneously, another level of complexity is added, as the different scales of both stars and the timescale of the interactions between them need to be resolved, and they can differ by several orders of magnitude. In this thesis, we study two scenarios that represent some of the most extreme examples of this challenge: the CE phase and NS–WD mergers, which will be discussed in Sec.2.1 and Sec.2.2 respectively. Both cases face the same fundamental challenge; one of the stars is substantially larger than its companion.

The issues of simulating giant stars and the CE stage in hydrodynamic simulations and what can be done to address them are thoroughly discussed in Ohlmann (2016). The CE stage takes place over timescales of years, whereas the dynamical timescale inside the core of the giant star or the companion can be on the order of a fraction of a second. To be able to successfully simulate a system with such a disparity in timescales, approximations must be made. As the timescale of the event is still much shorter than the nuclear timescale in the core, nuclear reactions

can be in principle disregarded. Additionally, to limit the minimum resolvable timescales, the core of the giant star and the companion can be replaced by point masses that only interact gravitationally with the rest of the simulation. Combined with a softened gravitational potential for the point masses, this greatly reduces the computational cost, allowing for the simulation of several dynamical timescales of the CE interaction.

NS–WD mergers present similar challenges regarding the broadness of the temporal and spatial scales that need to be covered, with the added difficulty of steeper density and pressure gradients and the necessity of modeling additional physical processes, as this time nuclear reactions or neutrino emission may play a role in shaping the dynamics of the event. In the same way as in [Ohlmann \(2016\)](#), we have tackled these challenges with the use of the AREPO code, which is the main numerical tool used to perform the simulations shown in Chapter 2, with detailed descriptions of the methods being given in each respective paper.

1.4.1. The AREPO code

AREPO ([Springel, 2010](#); [Pakmor et al., 2011, 2016](#); [Weinberger et al., 2020](#)), is a 3D MHD code that uses an unstructured, moving, Voronoi mesh that moves along with the local flow velocity. This allows the code to combine some of the benefits of both Lagrangian and Eulerian AMR formulations of hydrodynamics. Eulerian grid codes allow for better resolving shocks and fluid instabilities than Lagrangian Smoothed-particle hydrodynamics (SPH) simulations, but in turn, they do not inherently conserve angular momentum, and advection errors can rapidly accumulate in setups with large bulk velocities such as binaries or accretion disks. On the other hand, Lagrangian schemes conserve angular momentum but cannot accurately resolve hydrodynamic instabilities nor low-density material. The moving mesh of AREPO makes it behave as a quasi-Lagrangian code, providing a great conservation of angular momentum while retaining the accuracy and highly adaptive resolution of Eulerian grid codes, and allows for the use of local time steps instead of global time stepping.

On top of these fundamental advantages of the code, AREPO is in constant development and has received a large set of feature updates such as the inclusion of nuclear reactions ([Pakmor et al., 2013](#)) or general relativity ([Lioutas et al., 2024](#)). This makes the code extremely flexible, and despite the fact that it was initially developed for cosmological simulations ([Vogelsberger et al., 2014](#); [Sijacki et al., 2015](#)), it performs exceptionally well in modeling any astrophysical phenomena that require covering a large range of spatial and temporal scales. The code is currently being used to produce state-of-the-art simulations of several types of events, ranging from cosmology and galaxy formation (e.g. [Grand et al., 2017](#); [Marinacci et al., 2018](#); [Naiman et al., 2018](#); [Springel et al., 2018](#); [Pillepich et al., 2018](#); [Nelson et al., 2019](#); [Pakmor et al., 2023](#); [Ferlito et al., 2023](#)) to Type Ia SNe and thermonuclear explosions (e.g. [Gronow et al., 2021](#); [Pakmor et al., 2021](#); [Glanz et al., 2023](#); [Burmester et al., 2023](#)), tidal disruption events (e.g. [Goicovic et al., 2019](#); [Vynatheya et al., 2023](#); [Ryu et al., 2024](#)), compact-object mergers (e.g. [Zhu et al., 2015](#); [Lioutas et al., 2024](#)) or CE events (e.g. [Ohlmann et al., 2017](#);

[Sand et al., 2020](#); [Ondratschek et al., 2022](#); [Moreno et al., 2022](#)). The simulations presented in this thesis are only possible thanks to the flexibility and angular momentum conservation of the AREPO code. The resolution achieved for these processes would have been computationally unattainable with other codes.

For this research, we have further improved the capabilities of the code by adding new physics. In order to compute GW signals, we implemented the calculation of the quadrupole radiation from Newtonian gravity, following the same approach as [Seitenzahl et al. \(2015\)](#). This is described in detail in the methods section of Sec. 2.1. We have also implemented cooling via the release of thermal neutrinos, which is important in the regimes of high density and temperature found in Sec. 2.2 and Sec. 2.3.

2. Results

This chapter presents the main results of the thesis. It comprises three articles that have been accepted for publication in the peer-reviewed journal *Astronomy & Astrophysics*¹. The arrangement of sections follows the chronological order of acceptance dates by the journal. As of the writing of this thesis, the first and second articles are already published, whereas the third is still in the production stage by the journal and will be published in the coming months. Each article is prefaced by a brief introduction providing additional context.

¹<https://www.aanda.org/>

2.1. Publication I: GW emission from dynamical stellar interactions

This article studies the GW signals released by three types of stellar interactions between the components of a binary system, taking place on dynamical timescales. The first one is a merger between two main-sequence stars, the second one being a successful CE ejection, and the third one a core merger resulting from a failed CE ejection. The primary motivation for this study stemmed from recent publications ([Ginat et al., 2020](#); [Renzo et al., 2021](#)), which suggested that GW signals released during CE events could be detectable by the future space-based observatory LISA. As described in Sec. 1.3.2 and Sec. 1.4, the CE stage is extremely challenging to model, and previous works had to rely on semi-analytical methods to estimate the shape and frequency of the GW signals released during these events. This publication aims to corroborate the findings from the previous works by the means of 3D MHD simulations, which provide the most accurate modeling of this stage of binary evolution.

Publication Information

Title Gravitational wave emission from dynamical stellar interactions.

Authors J. Morán-Fraile, F. R. N. Schneider, F. K. Röpke, S. T. Ohlmann, R. Pakmor, T. Soultanis, A. Bauswein.

Status Published on A&A on March 23rd, 2023.

Digital Object Identifier <https://doi.org/10.1051/0004-6361/202245109>

Credit Moran-Fraile et al. A&A, 672, A9, 2023, reproduced with permission ©ESO.

Author's contribution

JMF is the principal author of this article. JMF performed all the simulations, analyzed the results, wrote the manuscript and produced all the figures. All authors actively contributed, discussing the methods and results during several stages of the project. The idea originated while discussing with FRNS, who also contributed with the initial model for the main-sequence star merger that was later recomputed by JMF. FRNS also provided several suggestions implemented by JMF, such as including a toy model to estimate the GW signal during the earlier stages of the CE merger. STO additionally contributed with the initial model for the successful common-envelope ejection. In collaboration with RP, JMF implemented the computation of the GW signal in AREPO. TS and AB counseled during the analysis of the GW signals, pointing to the relevant literature.

Gravitational wave emission from dynamical stellar interactions

Javier Morán-Fraile¹, Fabian R. N. Schneider^{1,2}, Friedrich K. Röpke^{1,3}, Sebastian T. Ohlmann⁴,
Rüdiger Pakmor⁸, Theodoros Soultanis^{5,1,6}, and Andreas Bauswein^{5,7}

¹ Heidelberger Institut für Theoretische Studien (HITS), Schloss-Wolfsbrunnenweg 35, 69118 Heidelberg, Germany
e-mail: javier.moranfraile@h-its.org

² Zentrum für Astronomie der Universität Heidelberg, Astronomisches Rechen-Institut, Mönchhofstr. 12-14,
69120 Heidelberg, Germany

³ Zentrum für Astronomie der Universität Heidelberg, Institut für Theoretische Astrophysik, Philosophenweg 12,
69120 Heidelberg, Germany

⁴ Max Planck Computing and Data Facility, Gießenbachstraße 2, 85748 Garching, Germany

⁵ GSI Helmholtzzentrum für Schwerionenforschung, Planckstraße 1, 64291 Darmstadt, Germany

⁶ Max-Planck-Institut für Astronomie, Königstuhl 17, 69117 Heidelberg, Germany

⁷ Helmholtz Research Academy Hesse for FAIR (HFHF), GSI Helmholtz Center for Heavy Ion Research, Planckstraße 1,
64291 Darmstadt, Germany

⁸ Max-Planck-Institut für Astrophysik, Karl-Schwarzschild-Str. 1, 85748 Garching, Germany

Received 30 September 2022 / Accepted 16 February 2023

ABSTRACT

We are witnessing the dawn of gravitational wave (GW) astronomy. With currently available detectors, observations are restricted to GW frequencies in the range between ~ 10 Hz and 10 kHz, which covers the signals from mergers of compact objects. The launch of the space observatory LISA will open up a new frequency band for the detection of stellar interactions at lower frequencies. In this work, we predict the shape and strength of the GW signals associated with common-envelope interaction and merger events in binary stars, and we discuss their detectability. Previous studies estimated these characteristics based on semi-analytical models. In contrast, we used detailed three-dimensional magnetohydrodynamic simulations to compute the GW signals. We show that for the studied models, the dynamical phase of common-envelope events and mergers between main-sequence stars lies outside of the detectability band of the LISA mission. We find, however, that the final stages of common-envelope interactions leading to mergers of the stellar cores fall into the frequency band in which the sensitivity of LISA peaks, making them promising candidates for detection. These detections can constrain the enigmatic common-envelope dynamics. Furthermore, future decihertz observatories such as DECIGO or BBO would also be able to observe this final stage and the post-merger signal, through which we might be able to detect the formation of Thorne-Żytkow objects.

Key words. binaries: close – gravitational waves – magnetohydrodynamics (MHD)

1. Introduction

Mass transfer between stars in binary systems can lead to many different outcomes. Some of these outcomes can dramatically change the systems (Langer 2012; De Marco & Izzard 2017). Whenever the stars that form a binary get close enough to each other so that one of them fills its Roche lobe (because of either a change in the evolution stage of the stars or in the orbital parameters), mass transfer will start. Unstable mass transfer can become dynamical and lead to a common-envelope (CE) event or even a full stellar merger. In a CE event, the accretor is engulfed in the envelope of the giant donor (Paczynski 1976) and the stellar cores transfer orbital energy to the envelope. This shrinks the orbital separation. The energy injected in the envelope can lead to its ejection (successful CE event). As a result, the orbit will cease shrinking, and the outcome of the interaction is a binary system in a tighter orbit (Ivanova et al. 2013). In contrast, if the companion fails to eject the envelope of the giant star, it will continue to inspiral and ultimately result in a merger of the core of the giant star and the companion (CE merger).

With the upcoming launch of the Laser Interferometer Space Antenna (LISA; Baker et al. 2019), we may have a new tool for the study of these dynamical phases of CE events and stel-

lar mergers, as they are promising sources for gravitational wave (GW) signals (Ginat et al. 2020; Renzo et al. 2021). Compared to the detectors of the LIGO¹-Virgo-KAGRA² network (Aasi et al. 2015; Acernese et al. 2014; Akutsu et al. 2021), which operates in a frequency band centered on hundreds of Hz, LISA will have a peak sensitivity centered at ~ 4 mHz. The gap in between those frequency bands is proposed to be covered in the future with decihertz observatories such as the DECi-hertz Interferometer Gravitational wave Observatory (DECIGO; Seto et al. 2001) or the Big Bang Observer (BBO; Phinney 2003). The frequency range of LISA will allow it to detect signals from wider binary systems (the frequency of the GWs released by a binary system is twice the orbital frequency: $f_{\text{GW}} = 2 \times f_{\text{orb}}$). Similarly to the case of compact object mergers, the GWs produced by a stellar binary system shift to higher frequencies as the orbit shrinks. In the case of stellar mergers and CE events, the rate at which the orbital separation decreases is generally not governed by the emission of GW radiation, but is mainly driven by mass transfer and drag forces. Although not dynamically

¹ Laser Interferometer Gravitational-Wave Observatory.

² Kamioka Gravitational Wave Detector.

Table 1. Summary of the simulations.

Model	M_1 (total) [M_\odot]	M_1 (core) [M_\odot]	M_2 [M_\odot]	a_0 [R_\odot]	$f_{\text{GW},0}$ [Hz]	a_{final} [R_\odot]	$f_{\text{GW},\text{final}}$ [Hz]
MS-merger	9	–	8	6.2	5.3×10^{-5}	5.0	7.3×10^{-5}
CE-merger	0.63	–	0.42	0.047	2.0×10^{-2}	0.039	2.5×10^{-2}
Successful CE	2	0.37	0.99	49	6.8×10^{-7}	3.9	3.0×10^{-5}

Notes. a_0 is the initial orbital separation, a_{final} is defined as the separation between the stars right before disruption in the case of the MS star merger and the CE merger. In the case of the successful CE, as the orbit is eccentric, a_{final} is defined as the semi-major axis of the orbital separation between the core and the companion at the end of the simulation. $f_{\text{GW},0}$ and $f_{\text{GW},\text{final}}$ are computed as twice the orbital frequency assuming a Keplerian orbit and separation equal to a_0 and a_{final} , respectively. In the case of the successful CE ejection, only the mass of the core and the companion are considered for the calculation of the Keplerian frequency.

dominant, GWs provide an interesting opportunity for observing such short-lived and elusive events.

Three-dimensional hydrodynamic (3D HD) or magneto-hydrodynamic (3D MHD) simulations are one of the most reliable (albeit expensive) ways of modeling CE events (see Ricker & Taam 2012; Ohlmann et al. 2016; Staff et al. 2016; Prust & Chang 2019; Reichardt et al. 2019; Sand et al. 2020; Chamandy et al. 2020; Reichardt et al. 2020; Moreno et al. 2022; Glanz & Perets 2021; Lau et al. 2022a,b; Zou et al. 2022; Ondratschek et al. 2022, for some recent examples) and mergers between different types of stars, such as main-sequence (MS) stars (Schneider et al. 2019) and white dwarfs (Munson et al. 2021; Dan et al. 2012; Zhu et al. 2015). In setups in which general relativity (GR) is dynamically not relevant, these methods provide the most consistent predictions of the merger process, and GWs can be derived from these simulations, but this has rarely been done. In the case of white dwarf mergers, predictions of the GWs that are released were obtained using smoothed particle hydrodynamics (Rasio & Shapiro 1994; Lorén-Aguilar et al. 2005), as they are a known target for LISA (Baker et al. 2019). Most of the research done has focused on the GWs that are emitted during the inspiral phase rather than during the merger, however. There are predictions of the GWs emitted during CE events (Ginat et al. 2020; Renzo et al. 2021), but because it is difficult to fully model them, all of the research so far has been based on analytic or semi-analytical models. The reliability of these predictions is limited by the fact that the interaction between the inspiraling companion and the envelope is not modeled in a self-consistent 3D MHD approach. Consequently, they ignore the contribution of the envelope itself to the production of GWs and employ an approximate drag force that drives the inspiral.

For neutron-star mergers, however, 3D HD simulations accounting for GR effects are common (Baiotti & Rezzolla 2017; Bauswein & Stergioulas 2019; Dietrich et al. 2021; Shibata 2015). This has broadly been applied for the study of GW signals that are produced by neutron-star mergers as they can be detected by the LIGO-Virgo-KAGRA network.

In this work, we fill the gap and derive GW signals from up to date 3D MHD simulations of binary interactions for which GR is not dynamically relevant. We revisit an already published simulation of a main-sequence star merger (Schneider et al. 2019) and run two new simulations of a successful CE ejection and a CE merger.

In Sect. 2 we briefly describe the methods we used for the different simulations and how we computed the GW signals. In Sect. 3 we explain the outcome of the simulations and discuss the GW signals. We discuss the detectability of these events in Sect. 4, and we summarize our main findings in Sect. 5.

2. Methods

All simulations were carried out with the code AREPO (Springel 2010; Pakmor et al. 2011), which is a 3D MHD code that uses an unstructured moving Voronoi mesh with a second-order finite-volume approach. Gravity is Newtonian and was computed using a tree-based algorithm. The energy loss by GWs is negligible and was therefore not taken into account. For the successful CE ejection simulation, we included the impact of recombination energy by using the OPAL (Rogers et al. 1996, 2002) equation of state (EoS). We also used the OPAL EoS for the main-sequence star merger, whereas for the CE merger, in which we consider only the stellar cores, for which ionization effects are irrelevant, we used the Helmholtz EoS (Timmes et al. 2000). The initial models of the main-sequence stars as well as the giant star were created using the one-dimensional stellar evolution code MESA (Paxton et al. 2011, 2013, 2015). The setups of the different simulations are summarised in Table 1.

2.1. Setups

2.1.1. Main-sequence star merger

For the merger between main-sequence stars, we used the simulation described in Schneider et al. (2019), involving two early main-sequence stars with masses of $8 M_\odot$ and $9 M_\odot$ with radii of $1.7 R_\odot$ and $1.9 R_\odot$, respectively. It is computationally not feasible to simulate the merger from the point of Roche-lobe overflow until the merger, so the merging process was sped up artificially for 1.5 orbits, and only then was the evolution of the merger followed by the simulation.

2.1.2. Successful CE ejection

In giant stars, the dynamical timescale of the outer parts of the envelope is orders of magnitude longer than in the core. Accurately resolving the core requires that the simulation uses time steps on the order of milliseconds, whereas dynamical processes involving the envelope will occur on a timescale of days. For this reason, the computational cost of simulating the common-envelope phase with a fully resolved core and companion becomes too expensive, and therefore, approximations are necessary.

For the successful CE ejection, we used one of the models described in Ohlmann (2016) as primary star. We took a model with a zero-age main-sequence (ZAMS) mass of $2 M_\odot$, evolved with MESA until the red giant (RG) stage, at which point it had a radius of $49 R_\odot$. This model was mapped onto an AREPO grid. For this simulation, we used a version of AREPO with the

same methods and the OPAL EoS as in Sand et al. (2020). We replaced the core of the giant star and the companion with a gravitation-only particle to limit the range in timescales, resolving their softening lengths with a minimum of 20 cells following Ohlmann (2016). The softening length of both particles was initially set to $2.47 R_{\odot}$, and this value was reduced during the simulation to ensure that it remained below 40% of the separation between the core and the companion. We did not include magnetic fields in this simulation. The masses of the core and companion were $0.37 M_{\odot}$ and $0.99 M_{\odot}$, respectively. This stellar model was then relaxed to re-establish hydrostatic equilibrium (Ohlmann et al. 2017). For the relaxation process, we placed the star in a box with a size of 7×10^{13} cm and a uniform background density of $\rho = 10^{-13}$ g cm $^{-3}$ and evolved it for ten dynamical timescales (8.2×10^6 s). During the first half of the relaxation, we applied a damping force to remove spurious velocities; during the second half, the star was let free to evolve on its own, and we verified that the model remained hydrostatically stable. We then simulated the common-envelope phase by placing the star and its companion in a box with a side length of 1.6×10^{15} cm ($2.35 \times 10^4 R_{\odot}$) at an initial separation of $49 R_{\odot}$, which corresponds to the surface of the RG, with a corotation fraction of 95%.

2.1.3. CE merger

As we cannot simulate the entire common-envelope phase with a fully resolved core and companion, we set up an entirely new simulation to study the GW signals released by a CE merger in which we considered only the part that generates the loudest highest-frequency GWs during the event: the merger of the red giant core and its companion. To ensure that the companion was not disrupted too far from the RG core, we chose a compact object; in particular, we took a $0.6 M_{\odot}$ white dwarf (WD) as a companion for which 50% of the mass was carbon and 50% oxygen, and whose initial radius was $0.012 R_{\odot}$. As first-order approximation, we modeled the RG core as a $0.4 M_{\odot}$ WD made entirely of helium with a radius of $0.016 R_{\odot}$. The methods and setup of the white dwarfs in this simulation are similar to those of Pakmor et al. (2021). The stellar models were constructed as simple hydrostatic equilibrium configurations assuming a uniform temperature of 2×10^7 K for the RG core and 10^6 K for the companion. We obtained their density profiles following the Helmholtz equation of state, and then we gave the AREPO cells the appropriate masses. Both stars were given a seed magnetic field set up in a dipole configuration with a polar surface field strength of 10 G. The stars were relaxed separately to ensure hydrostatic equilibrium because mapping the initial 1D models to 3D can lead to discretization errors in the hydrostatic equilibrium. The relaxation process was the same for both stars: They were placed in a box of 10^{10} cm with a static, uniform background grid density of $\rho = 10^{-5}$ g cm $^{-3}$. During the first half of the relaxation, we applied a damping force that reduced potential spurious velocities from discretization errors. During the second half of the relaxation, the stars were left to evolve on their own (without the damping force), and we verified that the density profiles were stable. The duration of the relaxation was chosen to be ten times the dynamical timescale of each star, that is, 20 s for the $0.6 M_{\odot}$ WD and 63 s for the $0.4 M_{\odot}$ RG core. After the relaxation, we placed the two relaxed stars into the same box with a box size of 7.3×10^{11} cm with a static, uniform background grid with $\rho = 10^{-5}$ g cm $^{-3}$. This background density was chosen to resemble the denser regions of a stellar envelope, but it has very little effect on the dynamics of the merger because at this

stage, it will be driven by the mass transfer and tidal interaction between the core and the companion. The mass resolution of the simulation was $m_{\text{cell}} \approx 5 \times 10^{-7} M_{\odot}$. The initial distance between the WDs was chosen to be three times the separation at the point of Roche-lobe overflow, and then we artificially shrank the orbit until the onset of a steady mass transfer in a similar fashion as for the main-sequence star merger. This occurred at an orbital separation of 3.25×10^9 cm. At this point, we started the unmodified simulation of the merger.

2.2. Computing the gravitational waves

To compute the gravitational wave signal, we calculated the approximate quadrupole radiation from Newtonian gravity. We followed the same approach as in Seitzzahl et al. (2015) and used the method by Blanchet et al. (1990) and Nakamura & Oohara (1989) to compute the second derivative of the quadrupole moment. In this way, the gravitational quadrupole radiation field in the transverse-traceless gauge h^{TT} takes the form

$$h_{ij}^{\text{TT}}(\mathbf{x}, t) = \frac{2G}{c^4 R} P_{ijkl}(\mathbf{n}) \int d^3x \rho (2v_k v_l - x_k \partial_l \Phi - x_l \partial_k \Phi). \quad (1)$$

Here, \mathbf{P} is the transverse-traceless projection operator,

$$P_{ijkl}(\mathbf{n}) = (\delta_{ij} - n_i n_j)(\delta_{kl} - n_k n_l) - \frac{1}{2}(\delta_{ij} - n_i n_j)(\delta_{kl} - n_k n_l), \quad (2)$$

with the normalized position vector $\mathbf{n} = \mathbf{x}/R$ and the distance to the source $R = |\mathbf{x}|$. As usual, G is the gravitational constant, c is the speed of light, ρ is the density, \mathbf{v} is the velocity, ∂_i represents a partial derivative with respect to the spatial coordinate i , and Φ is the Newtonian gravitational potential.

The amplitude of the GW radiation field can be written in terms of the two unit linear polarization tensors e_+ and e_{\times} , and when a line of sight is chosen, the amplitude of the GWs takes the form

$$h_{ij}^{\text{TT}}(\mathbf{x}, t) = \frac{1}{R}(A_+ e_{ij}^+ + A_{\times} e_{ij}^{\times}), \quad (3)$$

where A_+ and A_{\times} are the amplitudes of the two polarizations as a function of time. We worked in Cartesian coordinates and considered as line of sight the z -direction, corresponding to the initial axis of rotation of our binary systems. In this line of sight, the GW emission is strongest and therefore provides the most optimistic scenario in terms of detectability of the signal. Along this axis, the polarization amplitudes take the form

$$A_+^z = A_{xx} - A_{yy} \quad (4a)$$

$$A_{\times}^z = 2A_{xy}, \quad (4b)$$

with A_{ij} defined as

$$A_{ij} = \frac{G}{c^4} \int d^3x \rho (2v_i v_j - x_i \partial_j \Phi - x_j \partial_i \Phi). \quad (5)$$

We implemented the computation of the terms A_{xx} , A_{xy} , A_{xz} , A_{yy} , A_{yz} , and A_{zz} in AREPO following Eq. (5) in order to output the emitted GW signal on the fly during the simulations.

The characteristic strain of a GW signal is defined as $h_c(f) = 2f \tilde{h}(f)$, where \tilde{h} is the Fourier transform of the time-domain amplitude of the GW,

$$\tilde{h}(f) = \frac{1}{R} \sqrt{|\tilde{A}_+(f)|^2 + |\tilde{A}_{\times}(f)|^2}, \quad (6)$$

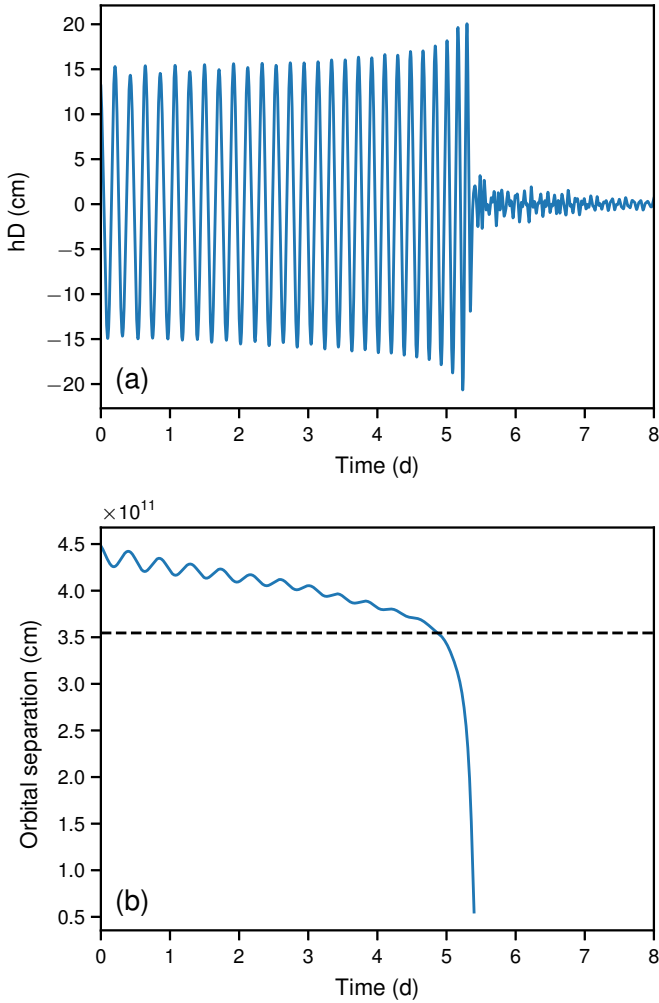


Fig. 1. Evolution of the main-sequence star merger. Top (a): Strain of the GW signal h over time (+ polarization in the z -direction, $h = A_z^2/D$). The amplitude is shown for an observer situated at a distance D . Bottom (b): Orbital separation over time. The dashed black line indicates the last stable orbital separation before disruption at 3.5×10^{11} cm.

with

$$\tilde{A}(f) = \int_{-\infty}^{\infty} e^{-2\pi ift} A(t) dt, \quad (7)$$

where $A(t)$ is the amplitude of each polarization over time. We calculated these values using a discrete fast Fourier transform and a Tukey window (Abbott et al. 2016). To capture the main features of the signal at its start and end, we used an asymmetric Tukey window in the case of the successful CE ejection. The signal-to-noise ratio (SNR) of a signal then takes the form (e.g., Moore et al. 2015)

$$(\text{SNR})^2 = 4 \int_0^{\infty} \frac{|\tilde{h}(f)|^2}{S_n(f)} df, \quad (8)$$

where S_n is the noise power spectrum density of the detector. We took the approximate values for LISA from Robson et al. (2019).

3. Results

3.1. Main-sequence star merger

A full description of the hydrodynamic outcome of the merger between the main-sequence stars can be found in Schneider et al.

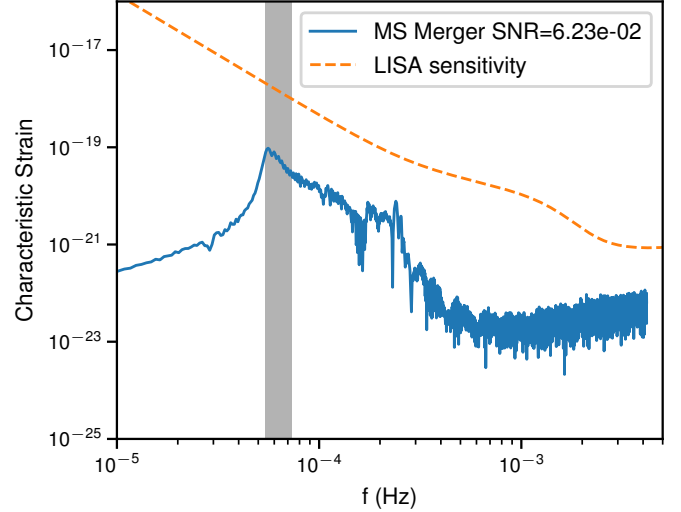


Fig. 2. Characteristic strain of the GW signal released by the merger of two main-sequence stars (in blue) assuming a distance of 1 kpc to the source along the polar axis. The LISA sensitivity from Robson et al. (2019) is shown by the dashed orange line. The region shaded in gray represents the frequency range spanning between twice the orbital frequency at the beginning of the simulation and twice the orbital frequency at the moment the star is disrupted (assuming the orbits to be perfectly circular and Keplerian).

(2019). The initially more massive (primary) star transfers mass to the initially less massive (secondary) star for a few days, draining angular momentum and shrinking the orbit. By the time the orbital separation reaches the tidal disruption radius of the primary star, commonly approximated as

$$r_t = \left(\frac{M_2}{M_1} \right)^{1/3} R_1, \quad (9)$$

where M_1 and M_2 are the masses of the primary and the secondary stars and R_1 is the radius of the disrupted star (primary), it is disrupted, and its central material merges with that of the secondary star. The resulting remnant consists of a $\sim 14 M_\odot$ central core with a $3 M_\odot$ torus surrounding it. The gravitational waves determined from the 3D MHD simulation of the merger event are shown in Fig. 1.

The amplitude of the strain increases as the orbital separation shrinks, and it peaks at the moment of the disruption of the primary star. Immediately after the merger takes place, the emission ceases. This decline in signal strength is expected as the remnant rapidly evolves to a mostly axisymmetric configuration. The characteristic strain of the GWs is shown in Fig. 2 assuming a distance of 1 kpc between source and detector. For this distance, we obtain an SNR of 0.062 with LISA. The peak of the characteristic strain is found at a frequency of about 5.4×10^{-5} Hz, which corresponds to an orbital frequency of 2.7×10^{-5} Hz.

The Keplerian orbital separation for a system orbiting at this frequency is 4.3×10^{11} cm. This value is very similar to the separation between the stars at the beginning of our computations. The characteristic strain integrates the signal over the observation time, so that the longer the system spends at a certain orbital frequency, the higher the associated characteristic strain for that frequency. In our simulation, the binary system only evolves through a small range of orbital separations before the disruption between 4.3×10^{11} cm and 3.5×10^{11} cm, which corresponds to a narrow GW frequency range from 5.4×10^{-5} Hz to 7.3×10^{-5} Hz (shaded in gray in Fig. 2). Theoretically, we

expect most of the GWs produced in our simulation to be within this frequency range. We lack simulation data at larger separations, which explains the cutoff at frequencies below this range. We could also have lower frequencies from ejected material after the disruption, so the characteristic strain is not zero. The signal at higher frequencies (smaller separations) originates from the phase after disruption of the primary star, and hence, we see a drop-off in the characteristic strain at frequencies higher than the frequency corresponding to the separation equal to the tidal disruption radius of the star. The characteristic strain at these higher frequencies ($f_{\text{GW}} > 10^{-4}$ Hz) comes from the weak post-merger signal.

It is difficult to compute the tidal disruption radii in noncompact interacting systems. The usual approximation for the tidal disruption radius, shown in Eq. (9), is obtained by equating the self-gravity force of the disrupted star with the gravitational pull that it experiences from the companion object and assuming that the radius of the star is much smaller than the separation between the stars. Therefore, this approximation does not hold true when the tidal disruption radius is on the order of magnitude of the radius of the star.

To obtain a better approximation, we calculated the tidal force across the disrupted star. First, we computed the gravitational acceleration at the points of the star that are closest and farthest from the companion:

$$a_{\text{grav}} = \frac{GM_1}{(d \pm R_2)^2}, \quad (10)$$

where d is the distance to the companion. To obtain the tidal acceleration, we subtracted the contribution from the acceleration on the near point from the contribution from the point far out,

$$\begin{aligned} a_{\text{tidal}} &= GM_1 \left[\frac{1}{(d - R_2)^2} - \frac{1}{(d + R_2)^2} \right] \\ &= GM_1 \frac{4dR_2}{(d^2 - R_2^2)^2}. \end{aligned} \quad (11)$$

The acceleration due to self-gravity is

$$a_{\text{self}} = \frac{GM_2}{R_2^2}. \quad (12)$$

At the point of tidal disruption, $d = r_t$ and $a_{\text{tidal}} = a_{\text{self}}$. Therefore, equating Eqs. (11) and (12), we obtain

$$\frac{M_2}{M_1} = \frac{4R_2^3 r_t}{(r_t^2 - R_2^2)^2}. \quad (13)$$

Solving Eq. (13) numerically for the tidal disruption radius, we obtain a better approximation of its value. In the following, we define the tidal disruption radius as the solution of Eq. (13) unless stated otherwise.

Another source of uncertainty is the fact that the stellar radius is difficult to define during ongoing mass transfer. For example, using the original radius of the star from the MESA models, we obtain a tidal disruption radius of 5.5×10^{11} cm, which is larger than the initial separation of our system. When we consider as the stellar radius the distance from the center in which 99% of the stellar mass is contained, we obtain a more sensible value for the tidal disruption radius of 3.5×10^{11} cm. Figure 1 shows that the latter value matches the actual point of disruption well. With this, we aim to show that the tidal disruption radius of a star in a binary system can give us a rough estimate of the highest frequency of the GWs that the merger would release during the inspiral phase.

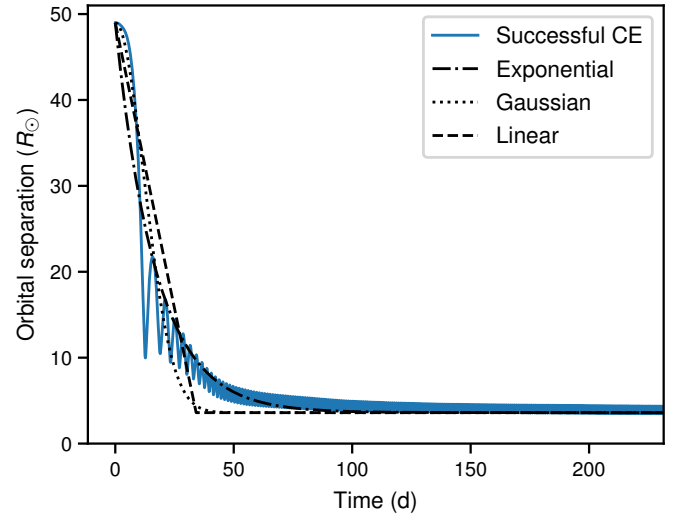


Fig. 3. Time evolution of the orbital separation during the successful CE ejection. In blue we show the data from the AREPO simulation. The black lines show the fit to these data with an exponential, a Gaussian, and a linear orbital decrease.

3.2. Successful common-envelope ejection

The initial separation between the core of a giant star and its companion is generally too large for the detection of the system with LISA. The frequencies of the associated GWs are too low because the radii of giant stars are on the order of 10 to 100 R_\odot . In order for these events to be detectable, the orbit must shrink to a separation at which the orbital frequency is in the appropriate frequency band for LISA. The evolution of our simulation of a successful CE ejection is very similar to that of Sand et al. (2020), but with an RG instead of an asymptotic giant branch (AGB) star, and the whole interaction occurs on a shorter timescale.

As soon as the simulation starts, the companion plunges into the envelope and its orbit shrinks for a few hundred days, until it ejects most of the envelope mass. From this point on, there is little orbital evolution on the simulated timescale, and the binary remains on an eccentric orbit with a semi-major axis of $3.6 R_\odot$ after 200 days. The evolution of the orbital separation is shown in Fig. 3. At this final separation, the companion orbits the core of the RG with a frequency of 0.017 mHz. In contrast to the other two simulations, the GW signal is not shut down. Instead, the main component of the signal evolves from low to higher frequencies. The characteristic strain of this simulation is shown in Fig. 4. It peaks at a frequency of 3.4×10^{-5} Hz, which corresponds to exactly twice the orbital frequency after the envelope has been ejected. The final orbit is not perfectly circular; it has an eccentricity of 0.1. Keplerian elliptic orbits emit GWs at multiple harmonics (frequencies that are integer multiples) of the orbital frequency (Maggiore 2008). We observe this in the characteristic strain of the signal as further peaks located at frequencies equal to the harmonics of the final orbital frequency. The frequency of maximum strain is also still too far from the peak sensitivity of LISA to be detectable; we obtain an SNR of 4.28×10^{-4} .

A common approximation used for calculating the GWs generated by CEs is to only consider the core of the RG and the companion as point-mass particles and neglect the effect of the envelope on the GW signal (Ginat et al. 2020; Renzo et al. 2021). With our simulation, we can test how accurate this treatment is. Figure 5 shows the difference in the characteristic strain

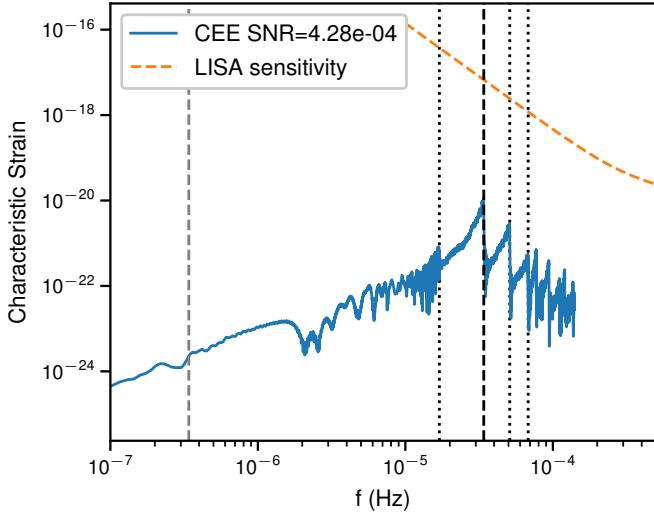


Fig. 4. Characteristic strain of the GW signal released by the successful common-envelope ejection (in blue) assuming a distance of 1 kpc to the source. The LISA sensitivity from Robson et al. (2019) is shown by the dashed orange line. The vertical dashed gray line represents twice the orbital frequency at the beginning of the CE (assuming a perfectly circular and Keplerian motion). The dashed black line represents twice the orbital frequency after the ejection of the envelope. The dotted black lines represent the first four harmonics of the final orbital frequency ($f_n = n \cdot f_{\text{orb,final}}$).

of the GWs released by the entire system and the strain resulting from the cores alone. The characteristic strain differs slightly at the lowest frequencies, but is essentially the same at frequencies higher than 3×10^{-6} Hz. As most of the envelope mass is ejected early on in the simulation when the orbital frequency of the system increases rapidly, the envelope is not expected to contribute significantly at GW frequencies much higher than twice the initial orbital frequency. As the system moves to higher orbital frequencies by ejecting the envelope, the contribution to the GW signal from the envelope necessarily decreases at higher frequencies. The difference between the two characteristic strains should therefore mostly be present at GW frequencies close to the one corresponding to the initial orbital frequency. In any case, the magnitude of this discrepancy is very small, therefore we can safely state that the approximation holds true for these systems in regard to their detectability with LISA. It is not clear whether this also applies to a CE evolution that leads to a merger. If the envelope is not completely ejected, it may contribute to the GW signal at higher frequencies. Furthermore, while there is no significant direct contribution of the envelope to the formation of the GW signal, an accurate representation of the core-envelope interaction in the simulations is still necessary to reliably determine the rate of inspiral and the final orbital separation between the cores that ultimately shape the GW signal.

3.3. Common-envelope merger

The hydrodynamical evolution of the CE merger is summarized in Fig. 6. From the beginning of the simulation, the less massive, less dense core of the RG primary star transfers mass onto the more massive and more compact companion. The orbit shrinks for a few hundred seconds due to this mass transfer until it reaches the point of tidal disruption and the RG core is disrupted around the inspiraling WD companion. The companion accretes a fraction of the mass of the former RG core, approxi-

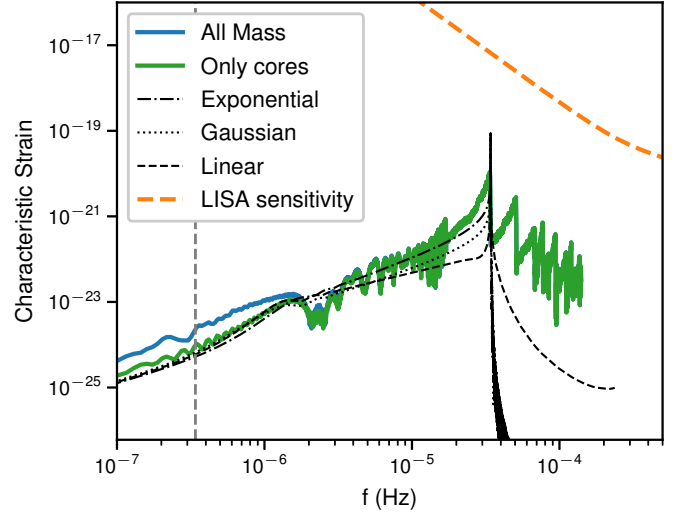


Fig. 5. Characteristic strain of the successful CE ejection. The characteristic strain of the GWs released by the entire simulation (the core of the RG, its envelope, and the companion) is shown in blue. In green we show the characteristic strain of the GW signal produced by only the core of the RG and the companion. The dashed gray line represents twice the orbital frequency at the beginning of the simulation. The black lines show the characteristic strain produced by toy models (see Sect. 3.4). The LISA sensitivity from Robson et al. (2019) is shown by the dashed orange line.

mately $0.11 M_{\odot}$. The remaining mass forms a disk-like structure around the remnant. This structure is not axisymmetric immediately after disruption, but it becomes so after a few hundred seconds.

The strain of the GWs (Fig. 6, bottom) is quite similar to the emission of the merger between MS stars, with a few differences. For the WDs, the merger occurs on a shorter timescale (hundreds of seconds instead of days). The amplitude of the GWs does not noticeably increase immediately before the merger, but its maximum value rather remains mostly constant until the disruption. Moreover, the post-merger signal is initially more pronounced than in the case of the MS star merger. The explanation for this stronger post-merger signal is the initial lack of axial symmetry in the remnant. As the disk homogenizes, the signal declines.

There is again a narrow range of orbital separations before the binary is disrupted. Our initial separation is 3.25×10^9 cm, which corresponds to a GW frequency of 2×10^{-2} Hz. No significant contribution to the signal is expected at frequencies lower than this value in our simulation. The computation of the tidal disruption radius for this simulation is even more challenging than in the case of the MS star merger because the disrupted star is a WD. This means that its radius will increase as it loses mass. Eq. (13) shows that the tidal disruption radius increases with the stellar radius. Therefore, the tidal disruption radius is underestimated when the initial value of the radius of the RG core is used. When the distance from the center in which 99% of the stellar mass is contained is used as the radius, we find $r_t = 2.4 \times 10^9$ cm following Eq. (13), which corresponds to a GW frequency of 3.17×10^{-2} Hz, assuming the orbit to be perfectly circular and Keplerian. The top panel of Fig. 6 shows that this value matches the point of disruption well.

Computing the characteristic strain (Fig. 7), we find that it peaks at a frequency of 2×10^{-2} Hz, which matches twice the orbital frequency at the beginning of the simulation. This is expected because this is the largest orbital separation that we

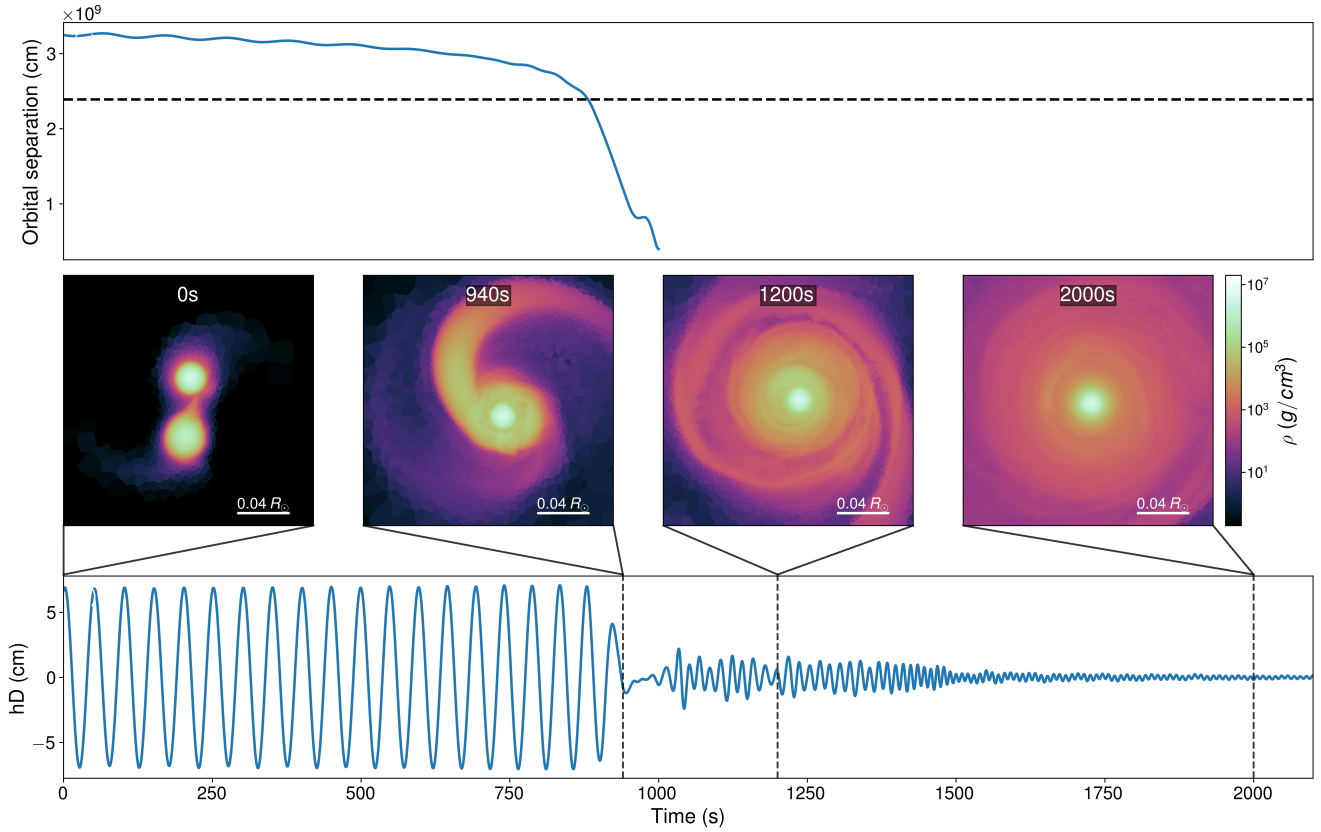


Fig. 6. Evolution of the CE merger. Top: Orbital separation over time. The dashed black line indicates the computed tidal disruption radius at 2.4×10^9 cm. Middle: Hydrodynamical evolution of the core merger resulting from a CE merger. The density is color-coded. The computation of the gravitational waves starts at the onset of steady mass transfer. The more massive companion shreds mass from the less massive, less dense core of the RG. The separation between the two objects slowly decreases until it reaches the point of tidal disruption at ~ 840 s. The companion accretes a fraction of the mass from the former RG core ($\sim 0.11 M_{\odot}$), while the remaining mass forms a disk-like structure around it. Bottom: Strain of the GW signal over time released by the CE merger (cross-polarization in the z -direction, $h = A_{+}^z/D$).

simulated, therefore we do not predict any significant GW signal at lower frequency. In this frequency range, LISA is far more sensitive than in the case of the MS star merger. For this reason, the characteristic strain of the CE merger ejection peaks above the sensitivity curve of LISA for a signal that lasts only a few minutes, generating an SNR of 6.6 at a distance of 1 kpc. The post-merger signal also contributes some high-frequency components to the characteristic strain. There is some relatively high strain up to frequencies close to 0.1 Hz. These higher frequencies are in the correct range for future decihertz GW observatories such as DECIGO or BBO. We computed the SNR for the CE merger simulation with DECIGO and BBO using the sensitivity curves described in Yagi & Seto (2011), and we obtained values of 896 and 1865, respectively, at a distance of 1 kpc. If designed according to current plans, these instruments would be able to detect the final disruption of CE-mergers with a much higher SNR due to the increase in sensitivity and the higher frequency band.

The computed value of the tidal disruption radius has been underestimated and thus overestimates the highest frequencies released by the binary before the merger (end of the region shaded in gray in Fig. 7). It is still within a factor of two from the peak frequency, however, and can be used as an upper bound.

3.4. Toy model for CE inspiral

Based on our successful CE ejection simulation, we modeled the plunge-in of the companion inside the red giant envelope with

simple analytical formulae in order to determine how the characteristic strain obtained from them compares with the strain of our simulation. We used three functional forms to model the orbital decay: an exponential, a Gaussian, and a linear function, defined as

$$a_{\text{exp}}(t) = (a_0 - a_{\text{final}}) e^{-\frac{t}{\tau}} + a_{\text{final}}, \quad (14a)$$

$$a_{\text{gauss}}(t) = (a_0 - a_{\text{final}}) e^{-\left(\frac{t}{\tau}\right)^2} + a_{\text{final}}, \quad (14b)$$

$$a_{\text{lin}}(t) = \begin{cases} (a_0 - a_{\text{final}}) \left(1 - \frac{t}{\tau}\right) + a_{\text{final}} & t \leq \tau, \\ a_{\text{final}} & t > \tau. \end{cases} \quad (14c)$$

Here a_0 and a_{final} have the values specified in Table 1, and τ in each formula was chosen to be the timescale of the orbital decay such that it fits the rate observed in our successful CE simulation. We find $\tau = 1.47 \times 10^6$ s for the exponential and Gaussian models, and $\tau = 2.94 \times 10^6$ s for the linear model. We followed these models for a time equal to the longest time in our simulation. Figure 3 shows that the Gaussian model captures the early part of the plunge-in best, whereas the exponential model matches it better at a later stage. In these simple models, we assumed no eccentricity, such that there is a smooth decrease of the orbital separation. We can then compute the GWs that would be released by two point-masses following the orbital evolution as described in Creighton & Anderson (2011),

$$A_{+}(t) = \frac{4G\mu}{c^2} \left(\frac{v(t)}{c}\right)^2 \cos\phi(t) \quad (15a)$$

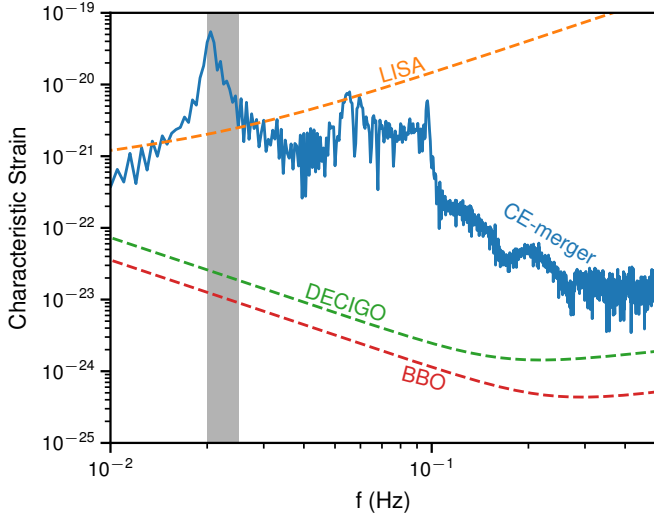


Fig. 7. Characteristic strain of the GW signal of the CE merger (in blue) assuming a polar distance of 1 kpc to the source. The sensitivities of LISA (Robson et al. 2019), DECIGO, and BBO (Yagi & Seto 2011) are shown as dashed orange, green, and red lines, respectively. The region shaded in gray represents the frequency range spanning between twice the orbital frequency at the beginning of the simulation and twice the orbital frequency at the moment when the star is disrupted.

$$A_{\times}(t) = \frac{4G\mu}{c^2} \left(\frac{v(t)}{c} \right)^2 \sin \phi(t), \quad (15b)$$

where μ is the reduced mass, $v(t)$ is defined as $\sqrt{\frac{GM_{\text{total}}}{a(t)}}$ and $\phi(t)$ is the phase of the GWs, which we obtained by numerically solving $\dot{\phi} = 2\pi f_{\text{GW}}(t) = 4\pi f_{\text{orb}}(t)$. For these toy models, we assumed that the point-masses are always on a Keplerian circular orbit in order to obtain the instantaneous value of the orbital frequency. We calculated the characteristic strain of these toy models and compare it with the data from our simulations in Fig. 5. As we explicitly specified a final orbit, we have a sharp peak at twice the final orbital frequency of the system, and no features at its harmonics as there is no eccentricity. In general, the shape of the strain of the toy model GWs reasonably matches the strain of the AREPO simulation. For the lowest frequencies produced by our simulation, the three toy models give the same value for the GW strain as in the hydro simulation when only the core masses were taken into account. For frequencies greater than 3×10^{-6} Hz, the exponential model reproduces the shape of the strain in the simulation best. The three toy models produce an SNR similar to the SNR in the simulation (4.00×10^{-4} for the exponential, 4.16×10^{-4} for the Gaussian model, and 4.17×10^{-4} for the linear model). We conclude from this that the models capture the strain of the GWs in the specified frequency range moderately well and can be used as simple toy models for the inspiral of our CE simulation.

Assuming that this approach also holds valid in a CE merger scenario, we applied it to the phase leading up to our CE merger simulation in order to estimate the GW signal produced during its inspiral phase. Disregarding any potential signal from the envelope, we took two point mass particles with the masses of our WD and the core of the RG to compute the reduced mass in Eqs. (15a) and (15b) and shrank the orbit according to Eq. (14) at a rate that resembles what we observe in our accurate simulation of the successful CE ejection ($\tau = 1.47 \times 10^6$ s in the exponential and Gaussian models, and $\tau = 2.94 \times 10^6$ s for the linear model). However, instead of stopping the inspiral at a distance of $3.6 R_{\odot}$,

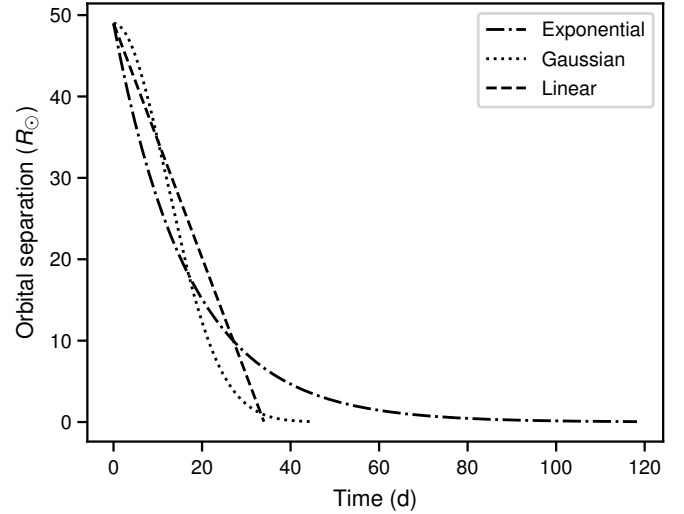


Fig. 8. Time evolution of the orbital separation of our toy models. The orbit shrinks from the initial orbital separation of the successful CE simulation to the initial orbital separation of the CE merger.

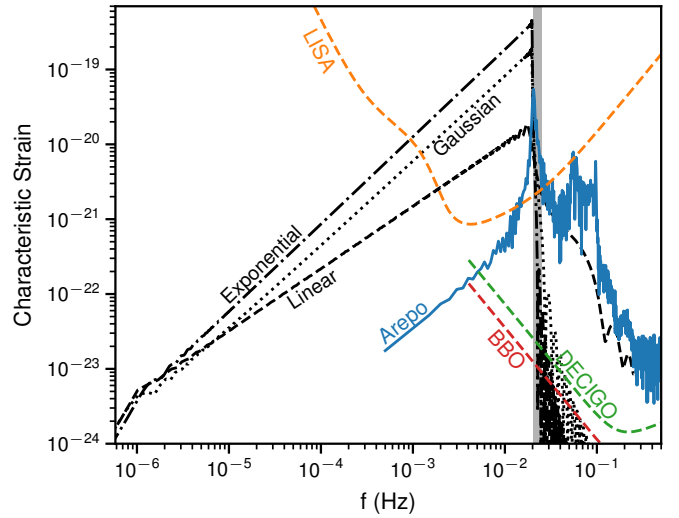


Fig. 9. Characteristic strain of the GW signal released by the CE merger (in blue) assuming a distance of 1 kpc to the source along the polar axis. The sensitivities of LISA (Robson et al. 2019), DECIGO, and BBO (Yagi & Seto 2011) are shown as dashed orange, green and red lines, respectively. The region shaded in gray represents the frequency range spanning between twice the orbital frequency at the beginning of the simulation and twice the orbital frequency at the moment when the star is disrupted (assuming the orbits to be perfectly circular and Keplerian). The black lines show the characteristic strain produced by our toy models.

we let the orbit shrink to a separation of $a_{\text{final}} = 3.25 \times 10^9$ cm, equal to the initial orbit used in our simulation of the CE merger. With these toy models, we obtained an estimate of the characteristic strain of the GWs released during the earlier stages of a CE merger ejection. The orbital evolution of our toy models is shown in Fig. 8.

As observed in our previous simulations, the orbital frequency shifts from lower values up to the initial values of the CE merger simulation, while the strength of the GWs increases. The duration of this inspiral phase differs between our toy models, as we stopped them the moment they reached a separation equal to the initial orbital separation in our core merger simulation.

The more time the system spends orbiting at a certain orbital frequency, the greater the strain of the GWs associated with that frequency. The exponential model has the highest value for the characteristic strain at high frequencies because it spends more time at orbital separations close to the desired final orbit, and the linear model has the lowest SNR because it reaches its final orbit faster. The signal during this stage crosses the peak sensitivity of LISA, and therefore, most of the SNR for this observatory could actually come from this phase depending on the exact rate of the orbital decay. With the chosen toy models, we indeed obtain SNR values for the inspiral phase of 191.1 for the exponential model, 84.5 for the Gaussian, and 10.5 for the linear model (to compute the SNR in these toy models, we ignored the characteristic strain at frequencies higher than twice the orbital frequency at the final orbital separation because this part of the characteristic strain is just numerical noise introduced by the fast Fourier transform on nonperiodic data). The final part of the inspiral phase begins to enter the frequency range of DECIGO and BBO, and because of the planned increase in sensitivity with respect to LISA, they would be even better able to measure this final stage of the CE merger, obtaining DECIGO SNRs of 6784, 2961, and 299 and BBO obtaining SNRs of 13957, 6092, and 616 for the exponential, Gaussian, and linear models, respectively.

4. Discussion

We computed the SNRs for all our simulations following Eq. (8), and assuming a polar distance to the source of 1 kpc. This distance is small and provides a best-case scenario for the detection of these events. The SNR is inversely proportional to the distance between detector and source, that is, if the event were to take place at 10 kpc rather than 1 kpc, the SNR would be ten times lower.

In the case of the merger between two MS stars, we obtain an SNR of 0.062, which suggests that these events are not suitable candidates for LISA sources. In Fig. 2 we show that the characteristic frequency of the GWs of this type of mergers is too far from the peak sensitivity of LISA. We started the simulation only a few days prior to the merger, whereas LISA could theoretically observe such a system for a few years before the disruption takes place, building up more signal and producing a higher SNR, but the frequency of these GWs will still be in the low-sensitivity band. The strength of the produced signal would increase in the case of a more massive merger (GW amplitude $\propto M_{\text{chirp}}^{5/4}$; Creighton & Anderson 2011), where M_{chirp} is the chirp mass of the binary,

$$M_{\text{chirp}} = \frac{(m_1 m_2)^{3/5}}{(m_1 + m_2)^{1/5}}. \quad (16)$$

However, it would also likely mean a larger tidal disruption radius, leading to lower GW frequencies and a decreased LISA sensitivity. The maximum frequency of GWs released by these systems before disruption can be estimated as twice the orbital frequency at the point where the separation between the stars equals the tidal disruption radius. We conclude that even at higher masses or longer observing times, the mismatch between the frequency of the GWs and the peak sensitivity of LISA makes main-sequence star mergers an unlikely GW source for this observatory.

Figure 4 shows that in our simulation of a successful CE ejection, the final orbit reached is not tight enough to produce GWs in a frequency that LISA can detect even at an optimistic distance of 1 kpc. As indicated by Renzo et al. (2021), the final

orbit resulting from a CE ejection has to shrink below one solar radius to be in a frequency range where LISA has a chance to detect them. Unfortunately, we do not observe a sufficient orbital shrinkage in this simulation or in any of the other simulations resulting in successful CE ejection that we analyzed (Sand et al. 2020; Ondratschek et al. 2022; Moreno et al. 2022). Therefore, we do not obtain any detectable GW signal from the dynamical phase of successful CE ejections for the LISA mission. Our final orbital separations are in line with those from Iaconi & de Marco (2019), showing that most simulations of successful CE ejections produce final orbits larger than $1 R_{\odot}$.

Different setups might shrink the orbit further. All our setups involved giant stars with loosely bound envelopes that require less energy to be transferred from the binary orbit to eject them. It is possible that CE events in which the giant star has a more strongly bound envelope might result in tighter final orbits. There are some indications that the final orbits reached in our simulations are too large compared to observations (Iaconi & de Marco 2019). Many of the close binaries used as LISA verification targets (Stroeer & Vecchio 2006; Kupfer et al. 2018) will have evolved through a successful CE phase. It is not clear whether their orbits shrink to the current tight orbits after the CE or in the dynamical phase of the CE. This further shrinking stage after the dynamical plunge-in could be due to a self-regulated inspiral, as suggested by Ivanova et al. (2013) or other mechanism draining angular momentum from the binary orbit (e.g., a circumbinary disk) such that the GWs are in the frequency band of LISA.

Figure 7 showed that the frequencies of the GWs in our CE-merger simulation are in a band in which LISA is more sensitive than in the case of the merger between two main-sequence stars. Computing the SNR, we obtain a value of 6.6, even though the total simulated time in this case is only a few thousand seconds. The frequency of the post-merger signal of this simulation is close to the optimal frequency range of decihertz GW observatories such as DECIGO and BBO, and the signal from our merger would produce SNRs of 896 and 1865, much higher than LISA due to the much higher planned sensitivity of the detectors, and because their frequency bands are able to best detect the post-merger signal. In Fig. 9 we showed that a large fraction of the GW signal is likely to be produced during the inspiral phase: As the orbital separation decreases, the frequency of the GWs will move from low frequencies (where LISA is not very sensitive) up to higher frequencies, crossing the peak sensitivity of LISA. The exact rate of the orbital decay strongly impacts the SNR, and at the same time, the dynamical plunge-in is one of the lesser known stages of the CE phase. A detection of such an event could provide information about stellar interiors in RG stars and the drag forces that the companion experiences while spiraling into the envelope. For example, different density profiles of the star lead to differences in the temporal evolution of the drag forces, causing very different waveforms and SNRs. Even if we were to observe the electromagnetic counterpart but do not detect the GW signal, a slow inspiral might be ruled out and a rapid plunge-in through the envelope might be indicated. Therefore, accurate models for this inspiral stage are required for generating waveform templates and estimating the detection rates. In turn, future observations may reveal binary dynamics.

Using semi-analytical models and smoothed particle hydrodynamics simulations, Ginat et al. (2020) computed the waveform and characteristic strain of the inspiral phase of CE mergers. Their simulations covered the initial phase of the CE stage, but their models were stopped at larger orbital separations than the initial separation in our simulation, and a core merger

was assumed to take place. The authors showed that the GWs released until that point might be observable by LISA. In our 3D models, we followed the final disruption in detail, probing down to shorter orbital separation (higher frequencies), and our findings confirm that statement. The disruption on its own already produces a strong signal that could be detected if the source were close enough to LISA. Although we did not compute a detailed model of the late inspiral phase, our estimates using toy models of the inspiral point in the same direction as those of [Ginat et al. \(2020\)](#). With SNRs ranging between approximately 10 and 191 (depending on the model), the signal from the entire CE event could be strong enough for a detection with LISA. We also computed the SNR for the signals of these toy models with DECIGO and BBO. If their final design achieves the planned sensitivity, they might be able to detect the final phase of the inspiral in CE mergers with a much higher SNR than LISA, ranging between approximately 300 and 7000 for DECIGO and between 600 and 14 000 for BBO, allowing them to be found at much larger distances.

Our findings about the detectability of these events with both LISA and the decihertz observatories are expected to hold for different masses for the core of the giant and also the inspiraling companion. Depending on the exact masses, we might enter a regime in which the CE merger of two white dwarfs leads to runaway thermonuclear burning and to an explosive event ([Pakmor et al. 2021](#)), which, in contrast to type Ia supernovae, is expected to contain substantial amounts of H and He in its ejecta (this corresponds to the so-called core degenerate supernova scenario of [Soker 2011](#)). However, we did not include nuclear burning here. In the event that one of the stars explodes, the GW signal will diverge from our results from that point on. The explosion could release a strong GW signal ([Seitenzahl et al. 2015](#)) and the emission would cease immediately thereafter. If the explosion occurred during or after the disruption of the core, mainly the high-frequency components of the GWs will be affected, which does not alter the SNR significantly, and makes the system an interesting candidate for a multimessenger detection.

Changing the mass of the companion changes the tidal disruption radius of the core, and thus the highest GW frequency reached by the system before the disruption. A higher-mass companion such as a neutron star will disrupt the core at a larger distance and will also produce a stronger signal because the GW amplitude is proportional to $M_{\text{chirp}}^{5/4}$, but the maximum frequency is more sensitive to the core radius and mass than to the companion mass.

If the companion were to be a neutron star, the formation of a Thorne-Żytkow object might be observed ([Thorne et al. 1977](#); [Hirai & Podsiadlowski 2022](#)) because the strength and frequency of the GW signal during the inspiral and merger would not sensibly differ from the one we computed here. In particular, these objects are predicted to show high-frequency features in the post-merger signal, for whose detection decihertz observatories would be very well suited.

5. Conclusions

We have computed the GW signal released during the merger between two MS stars, a successful CE ejection, and a CE merger in order to study their detectability with LISA. The simulations were carried out with the 3D MHD code AREPO.

The GWs from mergers between main-sequence stars are found to be outside the sensitivity range of LISA at distances

equal to or larger than 1 kpc. This result holds true for every merger between main-sequence stars, regardless of their masses. The tidal disruption radii of stars in binary systems can be used to approximate the cutoff frequency of the GWs released by these systems during their mergers.

From our simulation of a successful CE ejection, we find that the final separation between the core of the giant star and the companion is too large to release GWs in the frequency range where LISA could detect them. This result applies to all successful CEs that we simulated, but observations seem to suggest smaller final orbits, which would move the final systems closer to the frequency range of LISA. We also find that during successful CE ejections, the GWs emitted by the envelope contribute to the whole signal mostly in the lowest frequency range. This plays a very small role for the detection of such a system, and thus the signal associated with the envelope can safely be ignored.

Computing the GWs originating from the last stage of a CE-merger in 3D HD simulations of the interaction of the core of a giant star with a WD companion, we find their frequency inside the frequency range of LISA. They might therefore be detectable depending on the distance. We also used toy models to estimate the contribution to the GW signal from the inspiral phase and showed that it further increases the chances of detecting these systems. Such a detection would help to better understand the CE stage. The time evolution of the GWs gives an accurate depiction of how the orbital frequency changes as the companion inspirals through the envelope. GWs could serve as probes to study the interior of giant stars, helping us model the drag forces experienced by the companion and the density profile of the star. The exact conditions required for a successful ejection of the envelope or those leading to a merger are not fully known; detections of these events would place constraints on these cases. These events would probably have a detectable electromagnetic counterpart that could make them a suitable target for multimessenger astronomy.

Acknowledgements. T.S. and J.M-F. are fellows of the International Max Planck Research School for Astronomy and Cosmic Physics at the University of Heidelberg (IMPRS-HD) and acknowledge financial support from IMPRS-HD. This work acknowledges support by the European Research Council (ERC) under the European Union's Horizon 2020 research and innovation programme under grant agreement No. 759253 and 945806, the Klaus Tschira Foundation, and the High Performance and Cloud Computing Group at the Zentrum für Datenverarbeitung of the University of Tübingen, the state of Baden-Württemberg through bwHPC and the German Research Foundation (DFG) through grant no INST 37/935-1 FUGG. T.S. and A.B. acknowledge support by the State of Hesse within the Cluster Project ELEMENTS. A.B. also acknowledges support by Deutsche Forschungsgemeinschaft (DFG, German Research Foundation) – Project-ID 279384907 – SFB 1245. F.R. and A.B. acknowledge support by DFG through Project-ID 138713538 – SFB 881 (“The Milky Way System”, subproject A10).

References

- Aasi, J., Abbott, B. P., Abbott, R., et al. 2015, *CQG*, **32**, 074001
- Abbott, B. P., Abbott, R., Abbott, T. D., et al. 2016, *Phys. Rev. D*, **93**, 122003
- Acernese, F., Agathos, M., Agatsuma, K., et al. 2014, *CQG*, **32**, 024001
- Akutsu, T., Ando, M., Arai, K., et al. 2021, *Prog. Theor. Exp. Phys.*, **2021**, 49
- Baiotti, L., & Rezzolla, L. 2017, *Rep. Prog. Phys.*, **80**, 096901
- Baker, J., Bellovary, J., Bender, P. L., et al. 2019, *BAAS*, **51**, 77
- Bauswein, A., & Stergioulas, N. 2019, *J. Phys. G: Nucl. Part. Phys.*, **46**, 113002
- Blanchet, L., Damour, T., & Schäfer, G. 1990, *MNRAS*, **242**, 289
- Chamandy, L., Blackman, E. G., Frank, A., Carroll-Nellenback, J., & Tu, Y. 2020, *MNRAS*, **495**, 4028
- Creighton, J. D., & Anderson, W. G. 2011, *Gravitational-Wave Physics and Astronomy. An Introduction to Theory, Experiment and Data Analysis*, 86
- Dan, M., Rosswog, S., Guillochon, J., & Ramirez-Ruiz, E. 2012, *MNRAS*, **422**, 2417
- De Marco, O., & Izzard, R. G. 2017, *PASA*, **34**, 35

- Dietrich, T., Hinderer, T., & Samajdar, A. 2021, *General Relativ. Gravitation*, **53**, 1
- Ginat, Y. B., Glanz, H., Perets, H. B., Grishin, E., & Desjacques, V. 2020, *MNRAS*, **493**, 4861
- Glanz, H., & Perets, H. B. 2021, *MNRAS*, **507**, 2659
- Hirai, R., & Podsiadlowski, P. 2022, *MNRAS*, **517**, 4544
- Iaconi, R., & de Marco, O. 2019, *MNRAS*, **490**, 2550
- Ivanova, N., Justham, S., Chen, X., et al. 2013, *A&ARv.*, **21**, 1
- Kupfer, T., Korol, V., Shah, S., et al. 2018, *MNRAS*, **480**, 302
- Langer, N. 2012, *ARA&A*, **50**, 107
- Lau, M. Y. M., Hirai, R., Price, D. J., et al. 2022a, *MNRAS*, **516**, 4669
- Lau, M. Y., Hirai, R., González-Bolívar, M., et al. 2022b, *MNRAS*, **512**, 5462
- Lorén-Aguilar, P., Guerrero, J., Isern, J., et al. 2005, *MNRAS*, **356**, 627
- Maggiore, M. 2008, *Gravitational Waves: Volume 1: Theory and Experiments* (Oxford University Press)
- Moore, C. J., Cole, R. H., & Berry, C. P. 2015, *CQG*, **32**, 015014
- Moreno, M. M., Schneider, F. R. N., Röpke, F. K., et al. 2022, *A&A*, **667**, A72
- Munson, B., Chatzopoulos, E., Frank, J., et al. 2021, *ApJ*, **911**, 103
- Nakamura, T., & Oohara, K.-I. 1989, *Prog. Theor. Phys.*, **82**, 1066
- Ohlmann, S. T. 2016, PhDT, Heidelberg University
- Ohlmann, S. T., Roepke, F. K., Pakmor, R., & Springel, V. 2016, *ApJ*, **816**, L9
- Ohlmann, S. T., Röpke, F. K., Pakmor, R., & Springel, V. 2017, *A&A*, **599**, 5
- Ondratschek, P. A., Röpke, F. K., Schneider, F. R., et al. 2022, *A&A*, **660**, L8
- Paczynski, B. 1976, *IAUS*, **73**, 75
- Pakmor, R., Bauer, A., & Springel, V. 2011, *MNRAS*, **418**, 1392
- Pakmor, R., Zenati, Y., Perets, H. B., & Toonen, S. 2021, *MNRAS*, **503**, 4734
- Paxton, B., Bildsten, L., Dotter, A., et al. 2011, *ApJ*, **192**, 3
- Paxton, B., Cantiello, M., Arras, P., et al. 2013, *ApJS*, **208**, 4
- Paxton, B., Marchant, P., Schwab, J., et al. 2015, *ApJS*, **220**, 15
- Phinney, E. S. 2003, *Big Bang Observer Mission Concept Study*
- Prust, L. J., & Chang, P. 2019, *MNRAS*, **486**, 5809
- Rasio, F. A., & Shapiro, S. L. 1994, *ApJ*, **438**, 887
- Reichardt, T. A., De Marco, O., Iaconi, R., Tout, C. A., & Price, D. J. 2019, *MNRAS*, **484**, 631
- Reichardt, T. A., De Marco, O., Iaconi, R., Chamandy, L., & Price, D. J. 2020, *MNRAS*, **494**, 5333
- Renzo, M., Callister, T., Chatziioannou, K., et al. 2021, *ApJ*, **919**, 128
- Ricker, P. M., & Taam, R. E. 2012, *ApJ*, **746**, 74
- Robson, T., Cornish, N. J., & Liu, C. 2019, *CQG*, **36**, 105011
- Rogers, F. J., Swenson, F. J., & Iglesias, C. A. 1996, *ApJ*, **456**, 902
- Rogers, F. J., Nayfonov, A., Rogers, F. J., & Nayfonov, A. 2002, *ApJ*, **576**, 1064
- Sand, C., Ohlmann, S. T., Schneider, F. R., Pakmor, R., & Röpke, F. K. 2020, *A&A*, **644**, A60
- Schneider, F. R., Ohlmann, S. T., Podsiadlowski, P., et al. 2019, *Nature*, **574**, 211
- Seitenzahl, I. R., Herzog, M., Rüter, A. J., et al. 2015, *Phys. Rev. D*, **92**, 124013
- Seto, N., Kawamura, S., & Nakamura, T. 2001, *Phys. Rev. Lett.*, **87**, 221103
- Shibata, M. 2015, *Numerical Relativity. 100 years of General Relativity* (World Scientific), 1, 844
- Soker, N. 2011, ArXiv eprints [arXiv:1109.4652]
- Springel, V. 2010, *MNRAS*, **401**, 791
- Staff, J. E., De Marco, O., Macdonald, D., et al. 2016, *MNRAS*, **455**, 3511
- Stroeer, A., & Vecchio, A. 2006, *CQG*, **23**, S809
- Thorne, K. S., Zytow, A. N., Thorne, K. S., & Zytow, A. N. 1977, *ApJ*, **212**, 832
- Timmes, F. X., Swesty, F. D., Timmes, F. X., & Swesty, F. D. 2000, *ApJS*, **126**, 501
- Yagi, K., & Seto, N. 2011, *Phys. Rev. D*, **83**, 044011
- Zhu, C., Pakmor, R., Kerkwijk, M. H., & Chang, P. 2015, *ApJ*, **806**, L1
- Zou, Y., Chamandy, L., Carroll-Nellenback, J., Blackman, E. G., & Frank, A. 2022, *MNRAS*, **514**, 3041

2.2. Publication II: Self-consistent MHD simulation of jet launching in a NS–WD merger

Mergers between compact objects are extremely energetic events and the most likely progenitors of several of the brightest EM transients. The first detection of GW signals from binary BH and binary NS mergers (Abbott et al., 2016a, 2017) sparked a renewed interest in these types of events, and since then, their EM counterparts have been thoroughly studied (e.g. Narayan et al., 1992; Metzger et al., 2010; Metzger, 2017; Nakar, 2020). Massive binary WD mergers have been studied in depth as promising candidates for the origin of Type Ia SNe (Soker, 2018; Ruiter, 2019). The second most frequent type of compact-object merger, following WD mergers, are the mergers between NSs and WDs (Nelemans et al., 2001; Toonen et al., 2018). Despite being forecasted to be much more frequent, NS–WD mergers have been studied in substantially less detail than those between BBHs, BNSs and BH–NS.

The reason for this disparity is two-fold. In the first place, the aforementioned GW detections have motivated the scientific community to look for a better understanding of the observed mergers. Secondly, the most accurate technique for modelling these events is 3D MHD simulations. And although at first glance mergers between NS and WD could seem easier to model, as the effects of general relativity (GR) are less relevant than in the other presented cases, they provide a unique challenge that is not present in any other kind of double compact object merger: the disparity in scale.

The radius of NSs is comparable to that of the Schwarzschild radius of stellar mass BHs, on the order of tens of kilometers (Abbott et al., 2018; Lattimer, 2021). In comparison, the radius of WDs lies on the order of thousands of kilometers (Shipman and L., 1979; Carvalho et al., 2016). This difference in size means that modeling mergers between WDs and NSs or BHs requires covering a much broader range of spatial scales than those between WD–WD, NS–NS, BH–BH or BH–NS. This has historically placed NS–WD mergers out of reach of 3D simulations. There have been attempts to model them by scaling down the size of the WD (e.g. Paschalidis et al., 2009, 2011) or by reducing the problem to two dimensions (e.g. Fernández and Metzger, 2013; Fernández et al., 2019; Zenati et al., 2019). In recent years, with the increasing availability of computational power and improvements in computational techniques, the first 3D simulations of these mergers have been performed by employing relatively low resolution with SPH methods (e.g. Bobrick et al., 2017; Zenati et al., 2020; Bobrick et al., 2022).

The following paper makes use of the angular momentum conservation and unparalleled capabilities of the AREPO code (Springel, 2010; Pakmor et al., 2011, 2016; Weinberger et al., 2020), which excels in resolving a broad range of spatial and temporal scales, to perform the first high-resolution 3D MHD simulation of a NS–WD merger.

Publication Information

Title Self-consistent magnetohydrodynamic simulation of jet launching in a neutron star – white dwarf merger.

Authors J. Morán-Fraile, F. K. Röpke, R. Pakmor, M. A. Aloy, S. T. Ohlmann, F. R. N. Schneider, G. Leidi, G. Lioutas.

Status Published on A&A on January 5th, 2024.

Digital Object Identifier <https://doi.org/10.1051/0004-6361/202347555>

Credit Moran-Fraile et al. A&A, 681, A41, 2024, reproduced with permission ©ESO.

Author's contribution

JMF is the principal author of this article. JMF performed all the simulations, analyzed the results, wrote the manuscript and produced all the figures. The original idea was proposed by FKR as the main project for the PhD of JMF. RP and STO helped JMF with many of the numerical issues that originated during the development of the project. MAA and G. Leidi suggested most of the tests performed by JMF to analyze the jets and the magnetic field amplification, respectively. In collaboration with G. Lioutas, JMF implemented the neutrino cooling routines into the 3D MHD code. All the authors actively contributed, discussing the methods and results during several stages of the project.

Self-consistent magnetohydrodynamic simulation of jet launching in a neutron star – white dwarf merger[★]

Javier Morán-Fraile¹, Friedrich K. Röpke^{1,2}, Rüdiger Pakmor³, Miguel A. Aloy^{4,5}, Sebastian T. Ohlmann⁶, Fabian R. N. Schneider^{1,7}, Giovanni Leidi¹, and Georgios Lioutas^{8,9}

¹ Heidelberger Institut für Theoretische Studien (HITS), Schloss-Wolfsbrunnenweg 35, 69118 Heidelberg, Germany
e-mail: javier.moranfraile@h-its.org

² Zentrum für Astronomie der Universität Heidelberg, Institut für Theoretische Astrophysik, Philosophenweg 12, 69120 Heidelberg, Germany

³ Max-Planck-Institut für Astrophysik, Karl-Schwarzschild-Str. 1, 85748 Garching, Germany

⁴ Departament d'Astronomia i Astrofísica, Universitat de València, 46100 Burjassot, València, Spain

⁵ Observatori Astronòmic, Universitat de València, 46980 Paterna, Spain

⁶ Max Planck Computing and Data Facility, Gießenbachstraße 2, 85748 Garching, Germany

⁷ Zentrum für Astronomie der Universität Heidelberg, Astronomisches Rechen-Institut, Mönchhofstr. 12-14, 69120 Heidelberg, Germany

⁸ GSI Helmholtzzentrum für Schwerionenforschung, Planckstraße 1, 64291 Darmstadt, Germany

⁹ Department of Physics and Astronomy, Ruprecht-Karls-Universität Heidelberg, Im Neuenheimer Feld 226, 69120 Heidelberg, Germany

Received 25 July 2023 / Accepted 20 September 2023

ABSTRACT

The merger of a white dwarf (WD) and a neutron star (NS) is a relatively common event that produces an observable electromagnetic signal. Furthermore, the compactness of these stellar objects makes them an interesting candidate for gravitational wave (GW) astronomy, potentially being in the frequency range of LISA and other missions. To date, three-dimensional simulations of these mergers have not fully modeled the WD disruption or have used lower resolutions and have not included magnetic fields even though they potentially shape the evolution of the merger remnant. In this work, we simulated the merger of a $1.4 M_{\odot}$ NS with a $1 M_{\odot}$ carbon oxygen WD in the magnetohydrodynamic moving mesh code AREPO. We find that the disruption of the WD forms an accretion disk around the NS, and the subsequent accretion by the NS powers the launch of strongly magnetized, mildly relativistic jets perpendicular to the orbital plane. Although the exact properties of the jets could be altered by unresolved physics around the NS, the event could result in a transient with a larger luminosity than kilonovae. We discuss possible connections to fast blue optical transients (FBOTs) and long-duration gamma-ray bursts. We find that the frequency of GWs released during the merger is too high to be detectable by the LISA mission, but suitable for deci-hertz observatories such as LGWA, BBO, or DECIGO.

Key words. stars: jets – white dwarfs – magnetohydrodynamics (MHD) – stars: neutron – gravitational waves – magnetic fields

1. Introduction

Binary systems formed by a neutron star (NS) and a white dwarf (WD) are one of the most abundant double compact object systems in the Galaxy (Nelemans et al. 2001), second only to WD-WD systems. If the two compact objects are born with a short orbital separation, the release of energy in the form of gravitational waves (GWs) can make the binary system merge on timescales shorter than the age of the Universe. This process can be accelerated if the binary has undergone a common-envelope (CE) phase, where the drag in the envelope drives the orbital shrinking and may even lead to a prompt merger. When the orbit has decreased to the point where the WD fills its Roche lobe, a mass transfer episode commences. The stability of this mass transfer depends primarily on the mass of the WD. For sufficiently low-mass WDs, the mass transfer will be stable, and the system can be observed as an ultra-compact X-ray binary (Nelson et al. 1986). If the WD mass is above a critical value

of $M_{\text{WD}} = 0.2 M_{\odot}$ (Bobrick et al. 2017), the mass transfer will be unstable and the system will merge on a dynamical timescale, leading to a variety of electromagnetic transients (Metzger 2012; Fernández et al. 2019; Zenati et al. 2019, 2020; Bobrick et al. 2022; Kaltenborn et al. 2023) and a burst of GWs, similar to the ones released by binary black hole (BH) mergers (Abbott et al. 2016) and binary NS mergers (Abbott et al. 2017) that have been detected by the LIGO¹-Virgo-KAGRA² (LVK) Collaboration (Aasi et al. 2015; Acernese et al. 2014; Akutsu et al. 2021), albeit in a different frequency range.

The GWs released by these systems prior to the merger make these binaries a likely source (van Zeist et al. 2023; Abdusalam et al. 2020) for the LISA³ mission (Robson et al. 2019). The GWs released by the merger itself will have higher frequency and will be better captured by proposed deci-hertz observatories such as space-based DECIGO⁴ (Seto et al. 2001)

¹ Laser Interferometer Gravitational-Wave Observatory.

² Kamioka Gravitational Wave Detector.

³ Laser Interferometer Space Antenna.

⁴ DECI-hertz Interferometer Gravitational wave Observatory.

[★] Movies associated with Fig. 1 are available at <https://zenodo.org/records/8284075>

and BBO⁵ (Harry et al. 2006) or the Moon-based LGWA⁶ (Harms et al. 2021). The post-merger signal which could originate as accretion onto the NS excites oscillation modes of the NS (Schutz 2008), would be in the frequency range of the LVK network (Aasi et al. 2015; Acernese et al. 2014; Akutsu et al. 2021).

The electromagnetic signal released during these mergers has been proposed to explain several fast-evolving transients such as AT2018kzr (Gillanders et al. 2020) or AT2018cow (Metzger 2022), as well as long gamma-ray bursts (GRBs) such as GRB 211211A (Yang et al. 2022; Zhong et al. 2023) or GRB 060614 (King et al. 2007). NS-WD mergers are also predicted to result in magnetars, and were suggested to cause some fast radio bursts (FRBs) such as FRB 190824 and FRB 180916.J0158+65 (Zhong & Dai 2020).

In this work, we aim to study such a merger by the means of magnetohydrodynamic (MHD) simulations. Previous studies have looked into several different aspects of these mergers. Fernández et al. (2019) and Zenati et al. (2019) used two-dimensional (2D) hydrodynamic simulations to study the accretion disk resulting from the disruption of the WD and the nuclear reactions that would take place on it. Paschalidis et al. (2011) performed the first fully general relativistic simulations of mergers between NSs and scaled-down “pseudo-WDs” and studied whether the remnant would collapse into a BH. Zenati et al. (2020) and Bobrick et al. (2022) ran three-dimensional (3D) simulations of NS-WD mergers using smooth particle hydrodynamics (SPH) starting from realistic initial conditions. The enormous range of scales required for this simulations, spanning over ten orders of magnitude in density, forced previous works to revert to two-dimensional models or a relatively low resolution when simulating these events. Furthermore, none of the existing hydro simulations have yet included magnetic fields, which could be decisive in shaping the merger and post-merger dynamics (Zhong & Dai 2020). In this paper, we study the dynamics of the disruption and present the first high-resolution, 3D MHD simulation of a NS-WD merger.

2. Methods

For our simulations, we use the AREPO code (Springel 2010; Pakmor et al. 2011, 2016; Weinberger et al. 2020). AREPO uses the finite volume method to solve the 3D, fully compressible equations of ideal MHD with gravity:

$$\frac{\partial \rho}{\partial t} + \nabla \cdot (\rho \mathbf{u}) = 0, \quad (1)$$

$$\frac{\partial (\rho \mathbf{u})}{\partial t} + \nabla \cdot (\rho \mathbf{u} \otimes \mathbf{u} + p_{\text{tot}} \mathbb{I} - \mathbf{B} \otimes \mathbf{B}) = \rho \mathbf{g}, \quad (2)$$

$$\frac{\partial E}{\partial t} + \nabla \cdot [(E + p_{\text{tot}}) \mathbf{u} - \mathbf{B}(\mathbf{B} \cdot \mathbf{u})] = \rho(\mathbf{g} \cdot \mathbf{u}), \quad (3)$$

$$\frac{\partial \mathbf{B}}{\partial t} + \nabla \cdot (\mathbf{u} \otimes \mathbf{B} - \mathbf{B} \otimes \mathbf{u}) = \mathbf{0}, \quad (4)$$

where ρ denotes the density, \mathbf{u} the velocity, \mathbf{B} the magnetic field⁷, $p_{\text{tot}} = p + |\mathbf{B}|^2/2$ the total pressure, p the gas pressure, E the total energy density per unit volume, and \mathbf{g} the gravitational acceleration. Equations (1)–(4) are discretized on an unstructured, moving, Voronoi mesh as described in Pakmor et al. (2016). The boundary conditions are periodic for all variables except

the gravitational potential, which we compute by assuming that the density outside of the box domain is 0. Hyperbolic fluxes are computed at cell interfaces using the five-wave HLLD solver of Miyoshi & Kusano (2005), and the strength of magnetic monopoles is kept under control using the Powell scheme (Powell et al. 1999). The grid is generated at each timestep from a set of mesh-generating points that move with the local velocity of the fluid with small corrections to keep the mesh regular, leading to a nearly Lagrangian scheme. The resolution of the simulation can be changed locally by refining or de-refining the mesh following a set of criteria. The main criterion enforces the same mass for all cells within a factor of two of a chosen target mass and a maximum volume ratio between neighboring cells of a factor of five. On top of these criteria, we employed additional refinement criteria which are described in detail in Sects. 2.1 and 2.2. Self-gravity is included with a tree-based algorithm for the gas cells, and via exact force computation for the NS. We performed these simulations using Newtonian gravity, as the processes and dynamics that we aim to resolve are sufficiently distant from the NS. The equation of state (EoS) used in our simulations is the Helmholtz EoS (Timmes et al. 2000). We assume that the simulation takes place in a regime where the gas is completely transparent to neutrinos, and they leave the system without interactions. Therefore, neutrino transport simplifies to a cooling process. We take into account thermal neutrino cooling by implementing⁸ the fits from Itoh et al. (1996). The energy lost to GW is negligible and not taken into account, as it is not dynamically relevant for the part of the merger that we simulate. We computed the GWs in the same way as Morán-Fraile et al. (2023) by calculating the approximate quadrupole radiation from Newtonian gravity. We did not use a nuclear network as nuclear processes are predicted to play a minor role in the dynamical evolution of the disruption (Zenati et al. 2019).

2.1. Stellar setup

We took a $1.4 M_{\odot}$ NS as a primary star in our binary system, and for the companion we took a $1 M_{\odot}$ WD composed of an equal-by-mass mixture of carbon and oxygen with a central density of $\rho_c = 3.4 \times 10^7 \text{ g cm}^{-3}$ and an initial radius of $5.3 \times 10^8 \text{ cm}$ (defined as the radius containing 99.9% of the stellar mass). The WD model was generated with a uniform initial temperature of $5 \times 10^7 \text{ K}$. We then obtained the density profile by assuming hydrostatic equilibrium and mapped it into 3D using a healpix-based algorithm following Pakmor et al. (2012) and Ohlmann et al. (2017). We used the Helmholtz EoS to compute the values of the internal energy for the AREPO cells given the temperature. We added an initial dipole magnetic field with a polar surface value of 10^5 G to the WD. The magnetic dipole field is set up along the z -axis, and we imposed a cutoff radius in the center of the star with a size equal to two times the radius of the smallest AREPO cell to avoid an arbitrarily large value for the magnetic field in the center of the WD.

This WD is relaxed in isolation to ensure hydrostatic equilibrium, as deviations from equilibrium could appear due to discretization errors when mapping the one-dimensional profiles to the unstructured 3D mesh of AREPO. For the relaxation we place the star in a box of 10^{10} cm side length with a uniform background grid of density $\rho = 10^{-5} \text{ g cm}^{-3}$. The total relaxation time is chosen to be ten times the dynamical timescale of the star, corresponding to 11 s. During the first half of this time we apply a

⁵ Big Bang Observer.

⁶ Lunar Gravitational-Wave Antenna.

⁷ Here we use the Lorentz-Heaviside notation, $\mathbf{B} = \mathbf{b}/\sqrt{4\pi}$.

⁸ Adapting Frank Timmes’ scripts which can be found in: https://cococubed.com/code_pages/nuloss.shtml

damping force to reduce the spurious velocities that could have arisen during the mapping. During the second half of the relaxation, the star is left to evolve on its own (with no damping force being applied), and we check that the density, pressure, and internal energy profiles remain stable.

Due to the difference in the dynamical timescales of a NS and a WD, it is computationally unachievable to resolve the hydrodynamic evolution of both the NS and the WD in one simulation. We therefore model the NS as a gravitation-only point particle with a mass of $1.4 M_{\odot}$. To limit the pressure gradient next to our point mass NS, we used a softened gravitational potential. We found that low-resolution inside the softening length produces issues with energy conservation from the beginning of the simulation. At the same time, increasing the resolution close to the NS becomes prohibitively expensive for small values of the softening length. Experimentally, we increased the resolution while decreasing the size of the softening length, and we found a good compromise between computational expense and energy conservation by using a softening length of 8.4×10^7 cm and enforce a minimum of 40 cells per dimension within the softening length.

The gravitational potential inside the volume enclosed by the softening length deviates from a Newtonian potential. Therefore, we consider this region unresolved, and we report the values obtained by the simulation within this volume solely as a reference as they may deviate from realistic ones. As a point mass, the only characteristic for a NS that we assume is its mass and we do not model any other physical property. Thus, we cannot give it a magnetic field with the current implementation of MHD in AREPO. We could set a dipole configuration in the background around it, but as the mass contained in the background is so small compared with the one of the WD, as soon as accretion onto the NS starts, the initial magnetic field around the NS will become dynamically irrelevant. Therefore, we did not establish an initial magnetic field around the NS.

2.2. Binary setup

The target mass resolution of our simulation is $m_{\text{cell}} = 5 \times 10^{-7} M_{\odot}$, which results in $\sim 2 \times 10^6$ AREPO cells before further refinement. Due to the extreme pressure and density gradients in the neighborhood of the NS, we further increased the resolution in a disk-like region around the NS where a large fraction of the gas ends up after the disruption of the WD. We define this region as a cylinder centered on the NS with a radius of 6×10^8 cm (approximately half of the tidal disruption radius of the WD) and a height of 5×10^7 cm. In this region, we imposed the same refinement and derefinement conditions as within the softening length of the NS, which in turn means ensuring a minimum of ~ 6 million particles in this region. We allowed for further refinement if the mass of the cells inside this region exceeds our target m_{cell} . With this setup, the typical total number of cells in the simulation is ~ 8.1 million.

At the beginning of the simulation, the stars were placed in a Keplerian circular orbit at a distance of 2.27×10^9 cm, which corresponds to 1.5 times the separation at Roche-lobe overflow (RLOF, Eggleton 1983). The WD is initially set to solid-body rotation in co-rotation with the NS at the point of RLOF. The orbit is then artificially shrunk on a timescale longer than the dynamical timescale of the WD so that potential tidal effects can still take place. This is done using the scheme described by Pakmor et al. (2021) that removes angular momentum from the binary system. We stopped shrinking the orbit at the point of RLOF (corresponding to an orbital separation of 1.52×10^9 cm), when a steady mass transfer sets in. At this point, the system

has a total angular momentum of $L = 8.3 \times 10^{50} \text{ g cm}^2 \text{ s}^{-1}$. From here on, the system was left to evolve on its own and the WD disruption takes place on a few dynamical timescales. As the outer layers of the WD cannot be fully resolved, there is some numerical mass loss during the orbit-shrinking stage. Part of this mass will be accreted by the NS before the onset of the steady accretion stream. Furthermore, as explained in Bobrick et al. (2017), the tidal force exerted by the NS deforms the WD making it not completely spherical and its gravitational potential not perfectly Keplerian. This results in our initial orbit having a small eccentricity (~ 0.001), which also contributes to a small amount of mass transfer before the end of the orbit shrinking process. The amount of mass accreted into the softening length at the time that we stop the orbit shrinking is $10^{-4} M_{\odot}$. This initial mass transfer is dynamically irrelevant, but during this stage the amplification of the magnetic fields around the NS already begins. Table 1 shows the initial parameters and important timescales of the numerical setup for easy reference.

3. Results

The hydrodynamical evolution of the merger is summarized in Fig. 1⁹, and the temperature is shown in Fig. 2. After the end of the artificial orbital shrinkage ($t = 0$ s), a steady mass transfer developed. Moreover, during this stage, a small fraction of mass from the WD left the binary through the Lagrange point, L_2 . The transfer of mass and angular momentum makes the orbit shrink further, and after four complete orbits ($t = 80$ s, Fig. 1b) the WD becomes closer to the NS than its tidal disruption radius and is torn apart at an orbital separation of 1.14×10^9 cm. By this point, $0.005 M_{\odot}$ of gas has been unbound. This takes place mainly through the L_2 point, with a smaller fraction of the gas being also ejected along the polar axis of the NS. The disruption unbinds another $0.01 M_{\odot}$ of material. The disrupted stellar material initially forms a spiral arm and then starts to be accreted onto the NS (Fig. 1d).

The infalling material intersects itself while accreting, developing shear instabilities and shocks that heat the gas and transport angular momentum outwards. In this transient process, the orbit of the disrupted material circularises and a disk is formed due to the tidal interaction of the turbulent, infalling material with the NS (Figs. 1e,f). The temperature in the shocks reaches values up to $T = 9 \times 10^8$ K (Fig. 2), but the hottest regions of the shocks remain at rather low densities of $< 10^6 \text{ g cm}^{-3}$. Therefore, only minor nuclear burning is expected to take place in these shocks. The regions close to the NS heat up rapidly, reaching temperatures of 10^{10} K inside the softening length. In this region, nuclear reactions are essentially unavoidable. By $t \approx 160$ s, the disrupted material has formed a disk-like structure around the NS. As the NS does not have a surface and its gravitational potential is softened, the accreted mass accumulates inside the volume of the softening length. In our simulation, any ‘‘accretion’’ is not onto the NS, but into this volume. During the 150 s following the disruption of the WD ($t < 230$ s), $0.056 M_{\odot}$ of material is accreted into the gravitationally softened volume at an average rate of $3.7 \times 10^{-4} M_{\odot} \text{ s}^{-1}$. The density inside this region keeps increasing as material is accreted. At the time of the WD disruption, the maximum density is $\rho = 2 \times 10^7 \text{ g cm}^{-3}$, and at the end of the simulation it has reached a value of $\rho = 1.4 \times 10^9 \text{ g cm}^{-3}$. As we did not model nor resolve the physical processes around

⁹ Additional movies are available in <https://doi.org/10.5281/zenodo.8073873> and in <https://jmoran2611.github.io/publications/nswd2023/>

Table 1. Mass of the NS (M_{NS}), mass of the WD (M_{WD}), orbital separation after the end of the artificial orbital shrinkage (a_0), orbital separation at which the WD is tidally disrupted ($a_{\text{disruption}}$), time elapsed until the disruption of the WD ($t_{\text{disruption}}$), jet launching ($t_{\text{jet, launch}}$), and end of the simulation (t_{fin}); total magnetic energy ($E_{\text{B},0}$) and average magnetic field strength ($\langle B_0 \rangle$) at the beginning of the simulation and the value of the dipole magnetic field seed at the equator of the WD (B_{seed}).

M_{NS} [M_{\odot}]	M_{WD} [M_{\odot}]	a_0 [cm]	$a_{\text{disruption}}$ [cm]	$t_{\text{disruption}}$ [s]	$t_{\text{jet, launch}}$ [s]	t_{fin} [s]	$E_{\text{B},0}$ [erg]	$\langle B_0 \rangle$ [G]	B_{seed} [G]
1.4	1	1.52×10^9	1.14×10^9	~ 80	~ 140	242	2×10^{41}	2.5×10^7	10^5

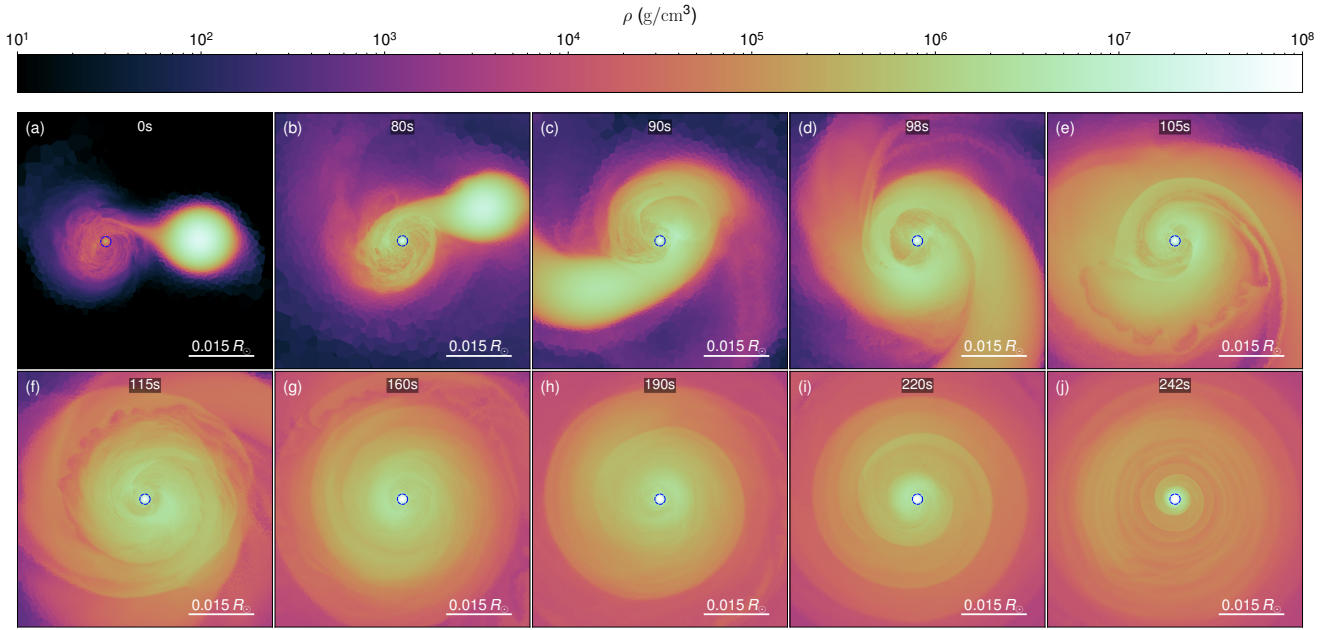


Fig. 1. Hydrodynamical evolution of merger. The panels show density slices in the orbital plane from the beginning of the simulation (panel a) until we stop it at $t = 242$ s (panel j). The region with a softened gravitational potential is shown in a blue dashed line.

and at the NS, we observe an artificial accumulation of material inside the softened volume. Part of this material should be accreted onto the NS, potentially through an accretion disk. During several stages of the simulation the combination of temperatures and densities inside the softened volume are suitable for a strong nuclear burning, which would also impact the density and temperature profiles in the neighborhood of the softening length.

The tidal interaction of the NS with the nonuniform accretion disk generates shocks, producing spiral density waves (Figs. 1i,j) that transfer angular momentum (Fig. 3a). The heat dissipation produced by the shocks speeds up the transfer of angular momentum, increasing the accretion rate (Fig. 3c). This culminates in a rapid accretion event at $t = 242$ s, where we observe a peak accretion rate of $3 \times 10^{-3} M_{\odot} \text{ s}^{-1}$. At this point, $0.077 M_{\odot}$ of gas has been accreted into the gravitationally softened volume. Inside the gravitationally softened volume, the gas rotates as a solid body and transitions to a quasi-Keplerian rotation in the accretion disk. The distribution of angular momentum and mass during the simulation can be seen in Figs. 3a,b. Most of the mass and angular momentum after the disruption of the WD is concentrated at a distance from the NS equal to the tidal disruption radius of the WD. It is initially slowly pushed out of this region by the turbulent motions and the shocks. When the spiral waves are developed they transport momentum outwards very efficiently, as can be seen by the rapid change in the angular momentum distribution between $t = 180$ s and $t = 242$ s.

At $t = 242$ s we stop the simulation as we cannot resolve the accretion and energy errors start accumulating in the simulation. Considering every AREPO cell with a total energy larger than zero as unbound material, by the time we end the simulation, $0.94 M_{\odot}$ of gas remain gravitationally bounded when only taking into account potential and kinetic energy. This number decreases to $0.93 M_{\odot}$ when also including magnetic and internal energy in the total energy.

3.1. Magnetic field amplification

The evolution of the magnetic energy in the simulation is shown in Fig. 4. As explained in Sect. 2.1, the WD is given an initial magnetic field seed with a value of 10^5 G at the equator. As soon as mass transfer begins, shear within the accretion stream amplifies the magnetic field around the NS, while compression of the magnetic field lines amplifies it in the shocked regions. The amplification process is complex and involves a combination of several mechanisms including magneto-rotational instability (MRI; discussed in more detail in Appendix A); Kelvin-Helmholtz instabilities and dynamo processes, similar to what is observed in 3D simulations of common-envelope evolution (Ondratschek et al. 2022); main-sequence star mergers (Schneider et al. 2019); binary white dwarf mergers (Zhu et al. 2015); or binary neutron star mergers (Obergaullinger et al. 2010; Kiuchi et al. 2015; Aguilera-Miret et al. 2020). This amplification process begins as soon as we start the simulation,

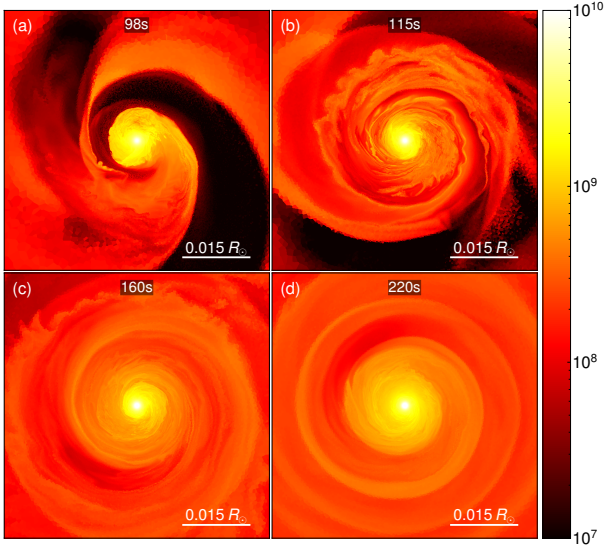


Fig. 2. Slice through orbital plane showing the temperature at selected times.

and the NS begins to accrete the pseudo-vacuum surrounding it as well as part of the mass lost by the WD during this stage. By the time the artificial orbital shrinking phase finishes, the magnetic energy (E_B) of the system has increased from an initial value of 2×10^{41} erg up to a value of 7.0×10^{45} erg, with the fields reaching values of up to 5.6×10^{11} G inside the gravitationally softened volume around the NS.

This initial amplification of the magnetic energy due to the NS accreting the pseudovacuum is unavoidable. To ensure that the amplification is not boosted by our artificial orbit shrinkage, we have performed two more simulations. In both of them we have placed the stars at a distance of 1.1 times the distance of RLOF. In the first one, we let the stars evolve freely (keeping constant orbital separation), and in the second one we shrank the orbit further down to the distance of RLOF before letting it evolve freely. At this initial distance of 1.1 times the separation at RLOF, the accretion of mass lost from the WD by numerical effects is the main source of magnetic amplification rather than the accretion of the pseudo-vacuum. In both simulations, the total magnetic energy is amplified to values of $\sim 1 \times 10^{46}$ erg on a timescale of 25 s, matching the magnetic energy generated in our fiducial simulation at this separation, but generating it on a shorter timescale. The simulation left to evolve freely at a separation equal to 1.1 of the separation at RLOF remains at a constant orbital separation, and after this initial fast amplification the growth of the magnetic energy slows down and plateaus at around 2×10^{46} erg. In contrast, in the simulation where we shrank the orbit down to the point of RLOF, a steady mass transfer set in and the magnetic fields continued to be amplified with the evolution of the total magnetic energy matching the one of our fiducial simulation. Hence, we conclude that this initial phase of magnetic amplification previous to the start of our simulation is self-consistent and independent of the artificial orbital shrinking.

The amplification of the magnetic field takes place dominantly in a toroidal direction around the NS, following the accretion stream, as evidenced by the ϕ component of the magnetic energy in Fig. 4. When a steady mass transfer sets in, the amplification of the magnetic field speeds up as the NS begins to

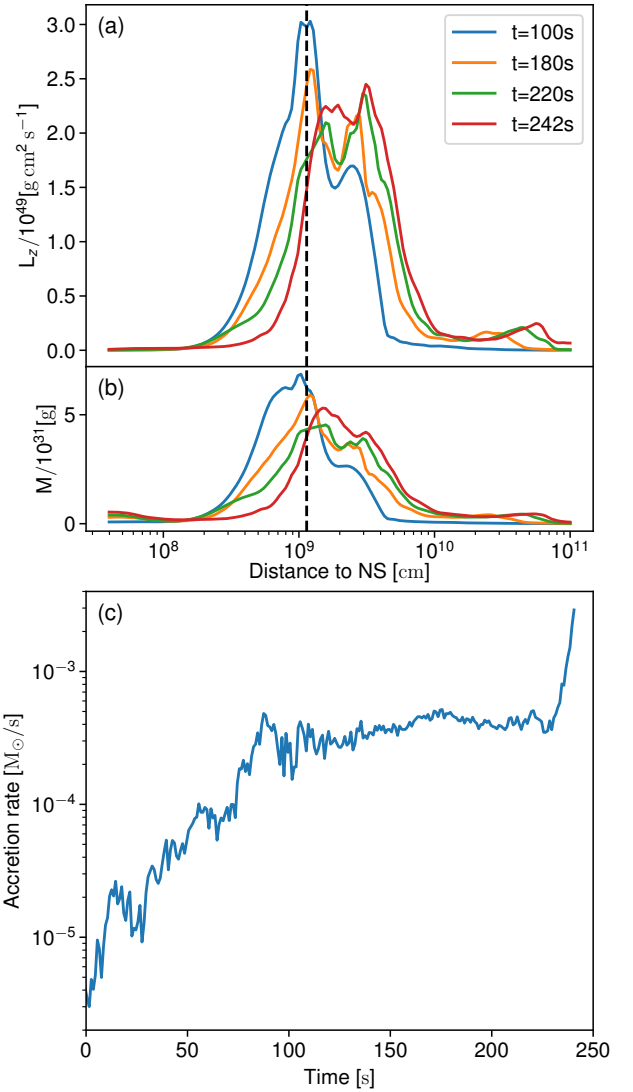


Fig. 3. Evolution of the disrupted material around the NS. Panel a: Z component of the angular momentum with respect to the distance to the NS for selected times. Panel b: distribution of gas mass with respect to the distance to the NS for selected times. The distance at which the WD is disrupted is shown by the black dashed line. Panel c: rate in $M_\odot \text{ s}^{-1}$ at which mass is accreted onto the gravitationally softened volume.

accrete the outermost layers of the WD. At this initial stage, the e -folding growth time of the magnetic energy peaks at a value of ~ 20 s. As the orbit shrinks and the mass transfer rate increases, the magnetic energy keeps steadily growing, with an abrupt increase shortly after the disruption of the WD due to the turbulent motions. At this point, the total magnetic energy has increased to 6.7×10^{47} erg, reaching maximum local values of up to 5×10^{12} G inside the gravitationally softened region around the NS. During the period of rapid accretion onto the NS driven by the spiral waves ($t \sim 240$ s), there is a second phase of fast amplification of the magnetic fields with E_B raising up to 5×10^{48} erg and reaching maximum values of 2.3×10^{13} G next to the NS.

3.2. Jet-launching

The magnetic fields generated throughout the entire event power two polar outflows launched in opposite directions (Fig. 5).

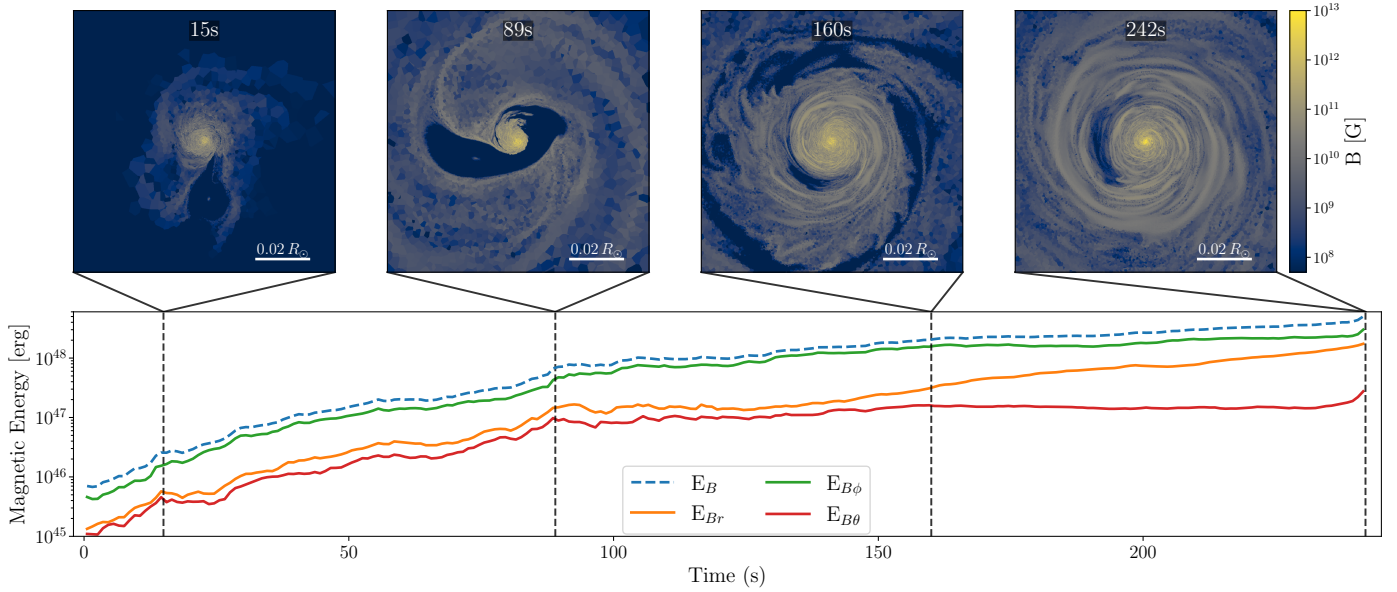


Fig. 4. Evolution of magnetic field throughout the simulation. Top: slices through orbital plane, centered on the NS, showing the absolute magnitude of the magnetic field for selected snapshots in color. Bottom: evolution of total magnetic energy over time (blue, dashed line) as well as the energy of the different components of the magnetic field in spherical coordinates (orange, green, and red for the radial, azimuthal, and polar components, respectively).

After the onset of mass transfer, regions with a magnetic-to-fluid pressure ratio (p_b/p_f) larger than one develop perpendicular to the orbital plane (third column in Fig. 5), where the magnetic pressure exceeds the dynamic pressure. In these regions, the Maxwell stresses dominate the dynamics, driving the collimated ejecta (note the white-to-blue shades in the upper panels of Fig. 6). As a result, since the beginning of the simulation, a small fraction of the accreting mass is ejected along the polar axis of the NS following the direction of the steepest magnetic pressure gradient. This outflow becomes faster and more collimated as the energy associated with the radial component of the magnetic field (E_{Br} in Fig. 4) increases. At $t \sim 140$ s (Figs. 5e–h) the outflows become distinguishable as highly magnetized, high-entropy gas ejected perpendicular to the orbital plane with velocities close to 1% of the speed of light, c . By $t \sim 170$ s (Figs. 5i–l), a bipolar jet structure has developed with characteristic velocities of $\sim 0.05c$, reaching maximum velocities of $0.08c$. In spite of the large entropy of the jets, the (relativistic) specific enthalpy, $h = 1 + \epsilon/c^2 + p_f/(\rho c^2)$ (where ϵ is the internal energy per unit mass), is very close to unity, indicating the ejection of a cold and highly magnetized jet. The computed values of h provide a proxy for the asymptotic Lorentz factor of the fluid, $\Gamma_\infty \sim 1.005\text{--}1.01$ ($\Gamma_\infty \sim h$, according to Bernoulli’s law along streamlines). Likely, this is a lower bound, since after the formation of a low-density polar funnel, matter further ejected through the jet will be accelerated to higher terminal speeds. The strength of the jets varies in time and evolves unevenly in the two directions. During the late period of accretion dominated by the spiral waves, the outflow above the orbital plane weakens, while the outflow below the orbital plane greatly increases in strength with typical velocities $v \sim 0.08c$ and a maximum velocity of $v \sim 0.1c$ at $t = 242$ s (Figs. 5q–t). The outflows are initially launched at a distance of $\sim 4.4 \times 10^8$ cm from the NS, which roughly corresponds to five times its softening length. In the ejecta, $p_b/p_f \sim 10$, and locally p_b/p_f reaching values of ~ 1000 close to the gravitationally softened volume around the NS. The energy and luminosity of the jets is shown in the upper panel of Fig. 7. There, we

measure a non-monotonically growing jet energy along with a growing luminosity, with imprinted variability timescales down to ~ 25 s (Fig. 7 bottom panel, showing the ratio jet-energy-to-jet-luminosity, which provides an idea of the timescale of changes in the jet luminosity). Likely, this timescale is an upper bound of the smallest variability timescales induced by the jet interacting with the surrounding, stratified medium, dictated by the time it takes Alfvén or sound waves to cross the jet transverse radius ($\sim 1\text{--}2$ s; see, e.g., Aloy et al. 2002; Matsumoto et al. 2017 for analogous jets propagating in stellar environments). Capturing the jet–environment interaction requires a very large numerical resolution on the jet, which we are lacking here, as outside of our disk-like region surrounding the NS the resolution criteria fall back to target a mass per cell of $m_{\text{cell}} = 5 \times 10^{-7} M_\odot$. Also, in our case, it depends on the operative definition of matter belonging to the jet. While the impact of small variations of the radial velocity threshold adopted to define the jet on its energy is negligible, the choice of the threshold may induce moderate changes for the luminosity variability timescale. Shorter timescales may be induced by the dynamics of the accretion/ejection of matter in the vicinity of the (here unresolved) NS, but likely at later times (in analogy to what is found for jets induced in collapsars Aloy et al. 2000; Matzner 2003; Morsony et al. 2010; Gottlieb et al. 2020). The jets eject material at an average rate of $\sim 3 \times 10^{-4} M_\odot \text{ s}^{-1}$ and have opening half-angles oscillating between $\sim 22^\circ$ and 25° for the top jet and between 18° and 22° for the bottom jet. As the accretion rate increases, the region of gas with the highest p_b/p_f draws closer to the gravitationally softened volume around the NS, and by $t \sim 242$ s the material is launched from the outer regions of the softened volume.

As gravity inside the softening length around the NS diverges from a realistic gravitational potential, we must be careful when interpreting processes that have an origin close to the softened volume. Also, nuclear reactions can massively change the energy budget of the central region. As the jet is initially launched at a reasonably large distance from the NS, we consider its formation a realistic physical effect rather than an artifact of the numerical

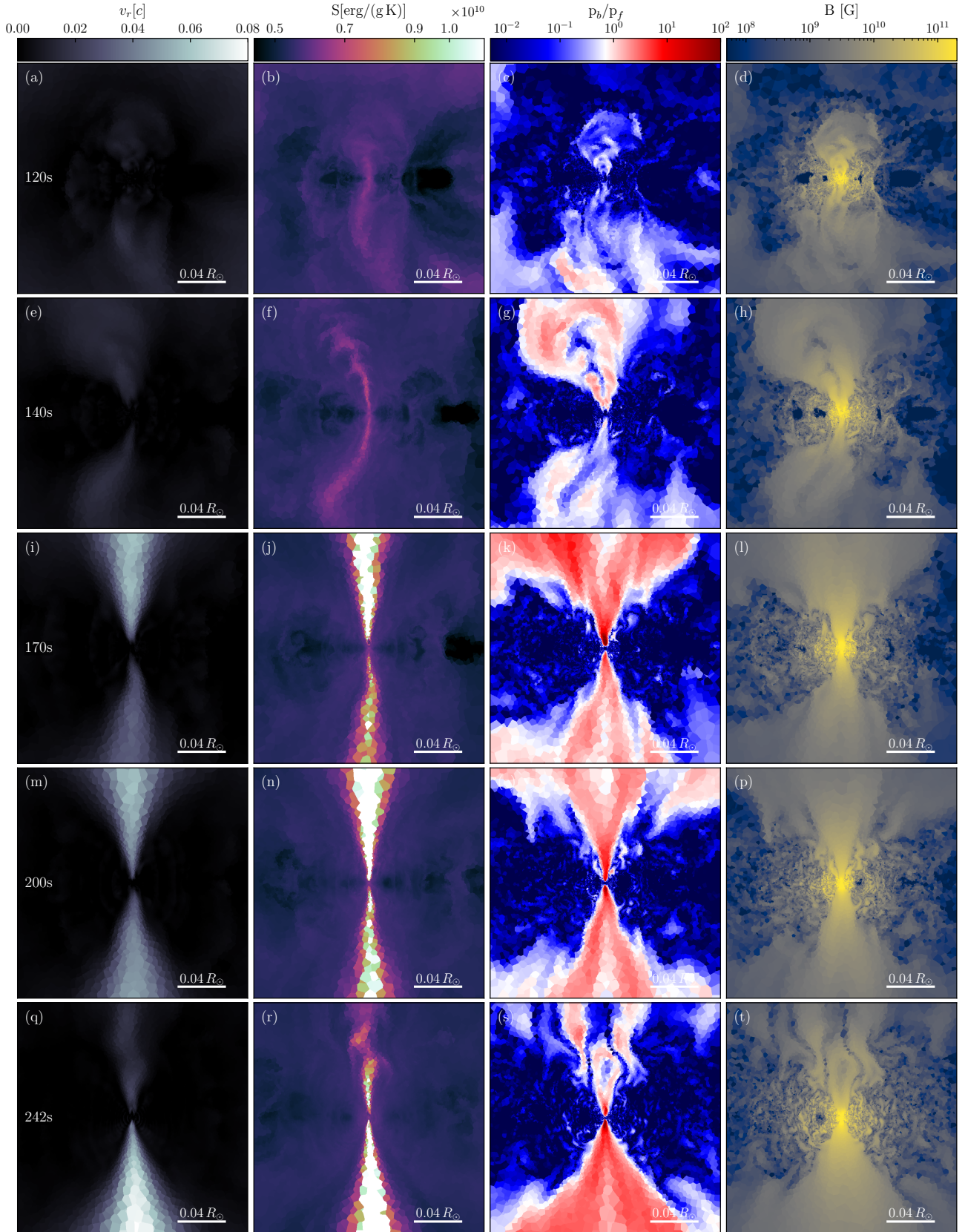


Fig. 5. Slices through midplane perpendicular to the orbital plane of the binary, centered on the NS before and after the formation of the polar outflows. The first column shows the radial velocity of the gas as a fraction of the speed of light, (v_r/c). The second column shows the entropy of the gas. The third column shows the magnetic-to-fluid pressure ratio, p_b/p_f . The fourth column shows the absolute magnitude of the magnetic field in the gas.

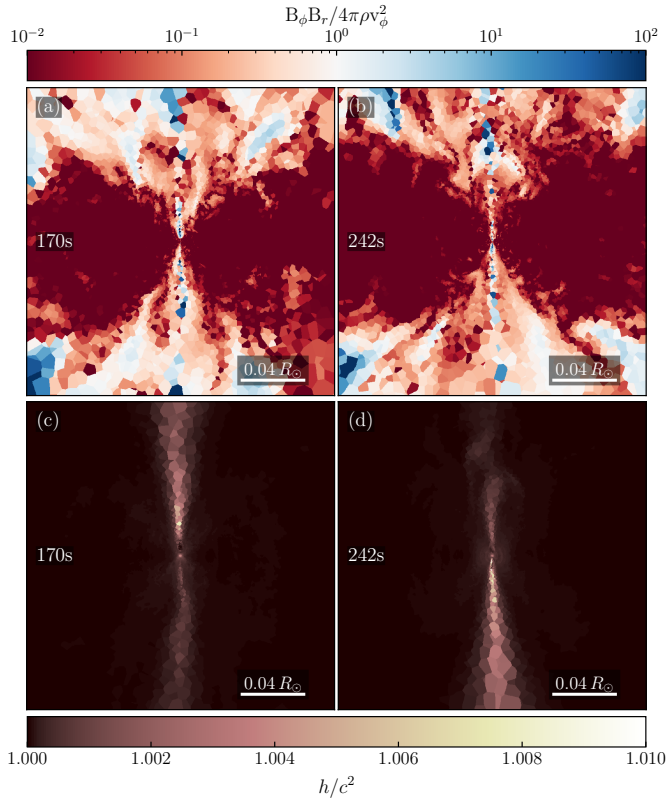


Fig. 6. Slices through midplane perpendicular to the orbital plane of the binary, centered on the NS at two times during the jet evolution. The top row shows the $r\phi$ component of the Maxwell stress tensor in the gas normalized by the centrifugal component of the Reynolds stress tensor. The bottom row shows the specific enthalpy of the gas.

model. However, as the region of acceleration draws closer to the NS, we must consider the jet-launching at later stages unresolved. Moreover, we used a nonrelativistic version of AREPO, and therefore gas moving at velocities close to $0.1c$ is no longer accurately treated, contributing to our decision to stop the simulation during the fast accretion event that takes place at $t = 242$ s.

3.3. Gravitational waves

Figure 8 shows the GWs released during the simulation as seen from the top of the orbital plane, which is the viewing angle that results in the loudest signal, providing a best-case scenario for their observation. The cross (h_{\times}) and plus (h_{+}) polarizations of the GWs have been computed using the approximate quadrupole radiation in the same way as in Morán-Fraile et al. (2023), and the characteristic strain is defined as $h_c(f) = 2f\tilde{h}(f)$, where \tilde{h} is the Fourier transform of the time-domain amplitude of the GW:

$$\tilde{h}(f) = \frac{1}{R} \sqrt{|\tilde{h}_{+}(f)|^2 + |\tilde{h}_{\times}(f)|^2}, \quad (5)$$

with

$$\tilde{h}(f) = \int_{-\infty}^{\infty} e^{-2\pi ift} h(t) dt. \quad (6)$$

During the accretion of the outer parts of the WD, the amplitude of the waves oscillates in the time domain (Fig. 8a) mainly due to the eccentricity of the binary orbit at this stage, but it does not significantly rise or fall prior to the merger, while the frequency

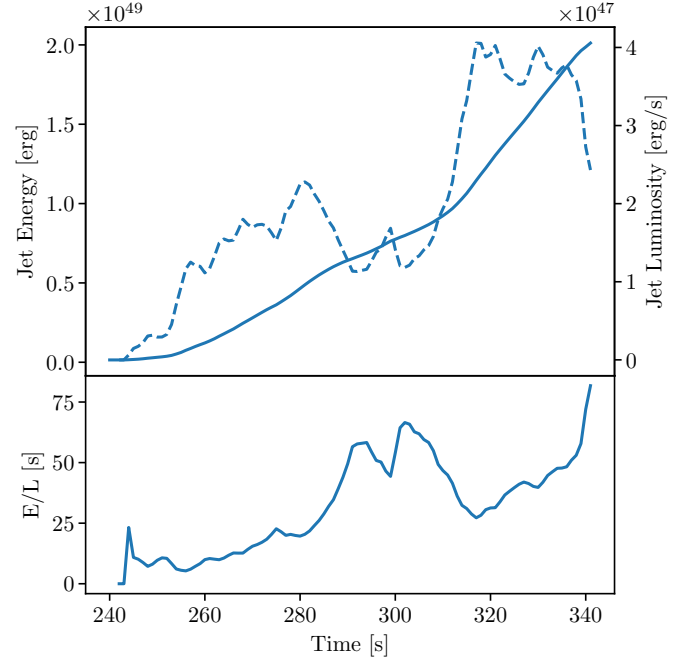


Fig. 7. Time evolution of energy and luminosity of the jets. Top: energy in the jets is shown by the plain blue line and the jets luminosity is shown in a blue dashed line. Bottom: energy divided by luminosity over time.

remains approximately constant. The emission reduces abruptly shortly after the tidal disruption of the WD. Only higher frequency components due to the lack of perfect axial symmetry of the accretion disk remain in the signal (Fig. 8a).

The characteristic strain (Fig. 8b) shows a strong peak at $f = 0.1$ Hz, which roughly corresponds to twice the orbital frequency of the binary at $t = 0$ s ($f_{\text{orb}} = 4.8 \times 10^{-2}$ Hz). As expected from binary star dynamics, the frequency of the GWs released corresponds to twice the orbital frequency of the system. This can be used to explain some of the main features seen in the characteristic strain. Because we only simulate the merger from an initial orbital frequency of ~ 0.05 Hz, we miss the GWs released during the previous stages of the evolution of the binary, which would emit GWs mainly at frequencies below the peak. NS-WD binaries are expected to release GWs below this frequency during their inspiral stage (van Zeist et al. 2023).

In our simulation, the orbital frequency of the binary does not change substantially before the tidal disruption of the WD, and the amplitude of the GWs decreases sharply after the disruption, explaining the narrow peak that we observe in the characteristic strain (Fig. 8b). The higher frequency components of the GW signal produced primarily after the disruption have a much lower amplitude than the GWs released prior to the merger. Between $f = 0.2$ Hz and $f = 0.5$ Hz, they show a mainly constant characteristic strain ~ 50 times smaller than at the peak. For higher frequencies, the strain drops down another order of magnitude, and at frequencies higher than 5 Hz we become limited by the sampling rate of our simulation. Frequencies on the order of some hertz and higher may arise from material close to and inside the softened volume, and they should therefore be considered unresolved.

The characteristic frequencies of the signal released during and after the merger make this event an ideal target for deci-hertz observatories such as BBO and DECIGO, which, for a source at a distance of 1Mpc, would produce a signal-to-noise ratio (S/N)

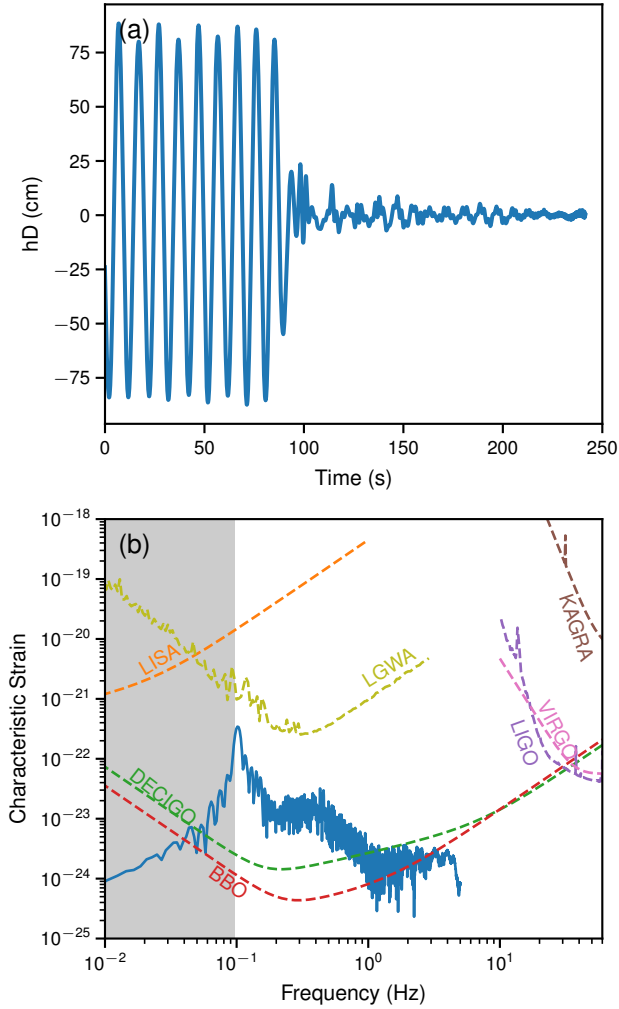


Fig. 8. Gravitational waves produced in simulation. Top: strain of GW signal h times the distance D to the source, observed from the z -direction (polar axis), over time. Bottom: characteristic strain of GW signal assuming a distance of 1Mpc to the source along the polar axis. The sensitivities of LISA (Robson et al. 2019); DECIGO and BBO (Yagi & Seto 2011); LIGO, VIRGO, and KAGRA (Abbott et al. 2020); and LGWA (Dupletsa et al. 2023) are shown as dashed orange, green, red, purple, brown, and yellow lines, respectively. The gray shaded area denotes the frequencies below two times our initial orbital frequency where signal coming from the inspiral phase of the binary is expected to be present.

of approximately 115 and 50, respectively. The S/N is defined as

$$S/N = \sqrt{4 \int_0^\infty \frac{|\tilde{h}(f)|^2}{S_n(f)} df},$$

where S_n is the noise power spectrum density of the corresponding detector given by Yagi & Seto (2011). For the moon-based LGWA, the signal is not loud enough at 1 Mpc, and the merger would have to take place significantly closer to be detected.

4. Discussion and summary

We performed the first 3D-MHD simulations of the merger between a $1 M_\odot$ COWD and a $1.4 M_\odot$ NS. We find that the disruption of the WD takes place a few dynamical timescales after reaching the separation of RLOF. The mass transfer from the

WD to the NS and the ensuing disruption of the WD amplify any pre-existing magnetic fields by several orders of magnitude, producing magnetic fields up to 10^{13} G.

The strong magnetic fields generated during the event launch two mildly relativistic jets perpendicular to the orbital plane with velocities on the order of 0.05 – $0.1c$. These values should be taken as order-of-magnitude estimates because several aspects of the final outcome of these mergers are expected to depend on the physics that are not resolved in our simulations.

As we model the NS as a point mass particle with a softened potential, not only gravity inside the softened volume deviates from a realistic gravitational potential, but we also do not provide any physical model for accretion onto the NS, which would potentially be limited by the Eddington accretion luminosity, dramatically changing the conditions in the neighborhood of the NS. As the conditions around the NS allow for nuclear burning, we have run a simulation in which we couple the MHD solver to a 13 isotope nuclear network following the same methods as in Gronow et al. (2021) and Pakmor et al. (2021). In this simulation, the production of ^{56}Ni is observed both outside and inside the softening length. While the first effect is resolved and physical, the burning inside the softening length is unresolved but may still be physical. While we must exercise caution when interpreting these results, which will be studied in more detail in follow up publications, they do provide support for the idea that mergers between NS and WD result in iron rich transients such as AT2018kzr (Gillanders et al. 2020).

As reported in Sect. 5 the jet is initially launched sufficiently far from the NS, so we consider its origin physical, but as accretion into the softened potential increases, the jet becomes faster and its acceleration region draws closer to the NS. A shorter softening length will lead to larger flow accelerations close to the NS, potentially generating stronger magnetic fields, which may alter the properties of the jet. Moreover, because the velocities of the ejected material reach up to $0.1c$, our Newtonian treatment becomes less accurate and a relativistic solver is needed at some point (e.g., Lioutas et al. 2022).

The merger of our two compact stellar remnants releases GWs in the deci-Hertz frequency range. We observe that GWs at the moment of WD disruption are released mainly at a frequency of 0.1 Hz, and the post merger releases higher frequency GWs, making these mergers an ideal target for proposed deci-Hertz observatories such as DECIGO, BBO, and LGWA. We only report GWs up to frequencies of ~ 5 Hz as higher frequency components will mainly originate from the regions of the simulation with characteristic frequencies smaller than that which correspond to the softened volume. To obtain accurate GW signals of higher frequencies, accretion on to the NS must be modeled. With a hydrodynamically resolved NS, one could excite oscillation modes that would result in GWs with frequencies up to kilohertz, which would be in the range of the LVK network (Schutz 2008).

The long-term evolution of the merger remnant is difficult to predict. At the point we ended the simulation, there was $0.94 M_\odot$ of gravitationally bound gas. If this material were to be accreted onto the NS, it could lead to an accretion-induced collapse into a BH as we approach the maximum mass for an NS depending on the EoS. The jets have steadily ejected material at a rate of $3 \times 10^{-4} M_\odot \text{ s}^{-1}$. We cannot predict the long-term evolution of this rate, as the launching region enters the unresolved volume at the end of the simulation. Additionally, the amount of mass ejected by the jet is likely dependant on unresolved or non-modeled physics. In particular, accurately modeling the

accretion onto the NS can dramatically change the outcome. The accretion would release a great amount of the gravitational energy budget that is contained on the disk that and could contribute to the heating or ejection of the material as well as the release of neutrinos.

Nuclear reactions also inject energy into the gas, reducing the amount of gravitationally bound material. Depending on the amount of mass that these non-modeled effects can unbind, the NS may survive or collapse into a BH.

Despite the limitations of our current simulations, we show that a bipolar jet is self-consistently launched. The duration of the jetted ejection is difficult to estimate from the period of time computed so far. A rough extrapolation of the mass accretion rate onto the unresolved central compact object implies that the bound mass around the unresolved NS may be swallowed on scales of few thousand seconds. We find that the variability of the jet-luminosity happens down to timescales of ~ 25 s. This is probably an upper bound induced by the moderate numerical resolution of the jets combined with the effective criteria employed to define the matter in the jet. The power at (significantly) smaller variability timescales would be induced by the changes close to the neutron star, which we cannot resolve.

The jet may be sustained for a sizeable fraction of the accretion time. The transient produced by this merger may share a number of qualitative similarities with other jetted ejections resulting from, for example, the tidal disruption of main-sequence stars by black holes (e.g., [Mimica et al. 2015](#)), with some key differences. Firstly, due to the compactness of the WD (compared to a $1 M_{\odot}$ star), the disruption takes place very close to the NS and, as a result, a large fraction of the disrupted material is still gravitationally bound. In analogy to jetted tidal disruption events (TDEs), the accretion of most of the WD mass onto the central object on scales of thousands of seconds will likely produce a very luminous transient. Secondly, the jets launched during this event may asymptotically reach velocities of the order of the escape velocity at the jet basis.

Assuming the NS does not collapse into a BH despite the accretion, we expect asymptotic jet velocities close to those observed in objects such as galactic microquasars ($\gtrsim 0.9c$, e.g., [Mirabel & Rodríguez 1998](#)), with typical Lorentz factors of two to ten. As a result, the spectrum of this event could be characterized by an initial soft X-ray or UV flash that will evolve into progressively lower frequencies. This would make this event resemble some fast blue optical transients (FBOTs; see, e.g., [Drout et al. 2014](#); [Ho et al. 2023](#); [Prentice et al. 2018](#); [Coppejans et al. 2020](#)). These transients have also been observed in the outskirts of galaxies, suggesting an origin related to old stellar populations, for which a NS-WD merger would be a good match. Depending on the properties of the interstellar medium surrounding the NS-WD merger, a bright, weeks-to-months-long radio signal may be observed (see [Mimica et al. 2015](#)). The luminosity of this transient could be larger than that of typical kilonovae ($\sim 10^{41}$ erg s^{-1} ; [Metzger 2017](#)), not only because of the larger mass and velocity of the ejecta, but also because the simulated event does not appear to harbor optimal conditions for the production of r -process yields. The presence of lanthanides in kilonovae obscures these events due to their large contribution to the opacity. If, however, the NS eventually does collapse into a BH, significantly higher (ultrarelativistic) jet speeds could be produced, resulting in some long or possibly ultra-long GRB-like transient ([Thöne et al. 2011](#); [Levan et al. 2014](#)).

We obtain an average neutrino flux of 2×10^{48} erg s^{-1} , which would put this transient one order of magnitude below the fluxes predicted for supernovae. However, we caution that in our simulations the neutrino luminosity is dominated by the unresolved conditions next to the NS.

The magnetically driven jet observed in our simulations is promising when it comes to explaining some recently discovered astrophysical transients. Therefore, a better numerical resolution of the material in the jet is desirable, and this can easily be achieved by changing the refinement criteria applied in our AREPO simulations. Future modeling work on mergers between WDs and NSs includes the addition of nuclear reactions to our simulations (for models including nuclear reactions, see [Bobrick et al. 2022](#)), paying special attention to the treatment of nuclear burning inside the unresolved regions, and a more accurate modeling of the physics around the NS, ideally including accretion onto the compact object.

Acknowledgements. The authors thank Valeriya Korol, Eva Laplace and Maryam Modjaz for their valuable input. J.M-F. is fellow of the International Max Planck Research School for Astronomy and Cosmic Physics at Heidelberg (IMPRS-HD) and acknowledges financial support from IMPRS-HD. This work was supported by the European Research Council (ERC) under the European Union's Horizon 2020 research and innovation programme under grant agreement No. 759253 and 945806, the Klaus Tschira Foundation, and the High Performance and Cloud Computing Group at the Zentrum für Datenverarbeitung of the University of Tübingen, the state of Baden-Württemberg through bwHPC and the German Research Foundation (DFG) through grant no INST 37/935-1 FUGG. M.A.A. acknowledges the support through the grant PID2021-127495NB-I00 funded by MCIN/AEI/10.13039/501100011033 and by the European Union, the Astrophysics and High Energy Physics program of the Generalitat Valenciana ASFAE/2022/026 funded by MCIN and the European Union NextGenerationEU (PRTR-C17.I1), and the grant CIPROM/2022/13 from the Generalitat Valenciana. Georgios Lioutas acknowledges support by the European Research Council (ERC) under the European Union's Horizon 2020 research and innovation programme under grant agreement No. 759253 and by the European Research Council (ERC) under the European Union's Horizon 2020 research and innovation programme (ERC Advanced Grant KILONOVA No. 885281). Georgios Lioutas also acknowledges support by the Deutsche Forschungsgemeinschaft (DFG, German Research Foundation) – Project-ID 138713538 – SFB 881 (“The Milky Way System”, subproject A10) and by the Deutsche Forschungsgemeinschaft (DFG, German Research Foundation) – MA 4248/3-1.

References

- Aasi, J., Abbott, B. P., Abbott, R., et al. 2015, *CQG*, **32**, 074001
- Abbott, B. P., Abbott, R., Abbott, T. D., et al. 2016, *Phys. Rev. Lett.*, **116**, 061102
- Abbott, B. P., Abbott, R., Abbott, T. D., et al. 2017, *Phys. Rev. Lett.*, **119**, 161101
- Abbott, B. P., Abbott, R., Abbott, T. D., et al. 2020, *Liv. Rev. Rel.*, **23**, 3
- Abdusalam, K., Ablimit, I., Hashim, P., et al. 2020, *ApJ*, **902**, 125
- Acernese, F., Agathos, M., Agatsuma, K., et al. 2014, *CQG*, **32**, 024001
- Aguilera-Miret, R., Viganò, D., Carrasco, F., Miñano, B., & Palenzuela, C. 2020, *Phys. Rev. D*, **102**, 103006
- Akutsu, T., Ando, M., Arai, K., et al. 2021, *Prog. Theor. Exp. Phys.*, **2021**, 49
- Aloy, M. A., Müller, E., Ibáñez, J. M., Martí, J. M., & MacFadyen, A. 2000, *ApJ*, **531**, L119
- Aloy, M.-A., Ibáñez, J.-M., Miralles, J.-A., & Urpin, V. 2002, *A&A*, **396**, 693
- Bobrick, A., Davies, M. B., & Church, R. P. 2017, *MNRAS*, **467**, 3556
- Bobrick, A., Zenati, Y., Perets, H. B., Davies, M. B., & Church, R. 2022, *MNRAS*, **510**, 3758
- Coppejans, D. L., Margutti, R., Terreran, G., et al. 2020, *ApJ*, **895**, L23
- Drout, M. R., Chornock, R., Soderberg, A. M., et al. 2014, *ApJ*, **794**, 23
- Dupletsa, U., Harms, J., Banerjee, B., et al. 2023, *Astron. Comput.*, **42**, 100671
- Eggleton, P. P. 1983, *ApJ*, **268**, 368
- Fernández, R., Margalit, B., & Metzger, B. D. 2019, *MNRAS*, **488**, 259
- Gillanders, J. H., Sim, S. A., & Smartt, S. J. 2020, *MNRAS*, **497**, 246
- Gottlieb, O., Levinson, A., & Nakar, E. 2020, *MNRAS*, **495**, 570
- Gronow, S., Collins, C. E., Sim, S. A., & Roepke, F. K. 2021, *A&A*, **649**, A155
- Harms, J., Ambrosino, F., Angelini, L., et al. 2021, *ApJ*, **910**, 1
- Harry, G. M., Fritschel, P., Shaddock, D. A., Folkner, W., & Phinney, E. S. 2006, *Class. Quantum Gravity*, **23**, 4887
- Ho, A. Y. Q., Perley, D. A., Gal-Yam, A., et al. 2023, *ApJ*, **949**, 120
- Itoh, N., Hayashi, H., & Nishikawa, A. 1996, *ApJS*, **102**, 411
- Kaltenborn, M. A. R., Fryer, C. L., Wollaeger, R. T., et al. 2023, *ApJ*, **956**, 71
- King, A., Olsson, E., & Davies, M. B. 2007, *MNRAS*, **374**, L34
- Kiuchi, K., Cerdá-Durán, P., Kyutoku, K., Sekiguchi, Y., & Shibata, M. 2015, *Phys. Rev. D*, **92**, 124034
- Levan, A. J., Tanvir, N. R., Starling, R. L. C., et al. 2014, *ApJ*, **781**, 13

- Lioutas, G., Bauswein, A., Souldanis, T., et al. 2022, MNRAS submitted [arXiv:2208.04267]
- Matsumoto, J., Aloy, M. A., & Perucho, M. 2017, MNRAS, 472, 1421
- Matzner, C. D. 2003, MNRAS, 345, 575
- Metzger, B. D. 2012, MNRAS, 419, 827
- Metzger, B. D. 2017, Liv. Rev. Rel., 20, 3
- Metzger, B. D. 2022, ApJ, 932, 84
- Mimica, P., Giannios, D., Metzger, B. D., & Aloy, M. A. 2015, MNRAS, 450, 2824
- Mirabel, I. F., & Rodríguez, L. F. 1998, Nature, 392, 673
- Miyoshi, T., & Kusano, K. 2005, J. Comput. Phys., 208, 315
- Morán-Fraile, J., Schneider, F. R. N., Röpke, F. K., et al. 2023, A&A, 672, A9
- Morsony, B. J., Lazzati, D., & Begelman, M. C. 2010, ApJ, 723, 267
- Nelemans, G., Yungelson, L. R., & Portegies Zwart, S. F. 2001, A&A, 375, 890
- Nelson, L. A., Rappaport, S. A., & Joss, P. C. 1986, ApJ, 304, 231
- Obergaulinger, M., Aloy, M. A., & Müller, E. 2010, A&A, 515, A30
- Ohlmann, S. T., Röpke, F. K., Pakmor, R., & Springel, V. 2017, A&A, 599, A5
- Ondratschek, P. A., Röpke, F. K., Schneider, F. R., et al. 2022, A&A, 660, L8
- Pakmor, R., Bauer, A., & Springel, V. 2011, MNRAS, 418, 1392
- Pakmor, R., Edelmann, P., Röpke, F. K., & Hillebrandt, W. 2012, MNRAS, 424, 2222
- Pakmor, R., Springel, V., Bauer, A., et al. 2016, MNRAS, 455, 1134
- Pakmor, R., Zenati, Y., Perets, H. B., & Toonen, S. 2021, MNRAS, 503, 4734
- Paschalidis, V., Liu, Y. T., Etienne, Z., & Shapiro, S. L. 2011, Phys. Rev. D, 84, 104032
- Powell, K. G., Roe, P. L., Linde, T. J., Gombosi, T. I., & De Zeeuw, D. L. 1999, J. Comput. Phys., 154, 284
- Prentice, S. J., Maguire, K., Smartt, S. J., et al. 2018, ApJ, 865, L3
- Rembiasz, T., Obergaulinger, M., Cerdá-Durán, P., Müller, E., & Aloy, M. A. 2016, MNRAS, 456, 3782
- Robson, T., Cornish, N. J., & Liu, C. 2019, CQG, 36, 105011
- Schneider, F. R., Ohlmann, S. T., Podsiadlowski, P., et al. 2019, Nature, 574, 211
- Schutz, B. F. 2008, J. Phys.: Conf. Ser., 118, 012005
- Seto, N., Kawamura, S., & Nakamura, T. 2001, Phys. Rev. Lett., 87, 221103
- Springel, V. 2010, MNRAS, 401, 791
- Thöne, C. C., de Ugarte Postigo, A., Fryer, C. L., et al. 2011, Nature, 480, 72
- Timmes, F. X., Swesty, F. D., Timmes, F. X., & Swesty, F. D. 2000, ApJS, 126, 501
- van Zeist, W. G. J., Eldridge, J. J., & Tang, P. N. 2023, MNRAS, 524, 2836
- Weinberger, R., Springel, V., & Pakmor, R. 2020, ApJS, 248, 32
- Yagi, K., & Seto, N. 2011, Phys. Rev. D - Part. Fields Grav. Cosmol., 83, 044011
- Yang, J., Ai, S., Zhang, B.-B., et al. 2022, Nature, 612, 232
- Zenati, Y., Perets, H. B., & Toonen, S. 2019, MNRAS, 486, 1805
- Zenati, Y., Bobrick, A., & Perets, H. B. 2020, MNRAS, 493, 3956
- Zhong, S.-Q., & Dai, Z.-G. 2020, ApJ, 893, 9
- Zhong, S.-Q., Li, L., & Dai, Z.-G. 2023, ApJ, 947, L21
- Zhu, C., Pakmor, R., Kerkwijk, M. H., & Chang, P. 2015, ApJ, 806, L1

Appendix A: MRI

In order to analyze how well we resolved the MRI amplification in our simulation, we computed the fastest growing mode following Rembiasz et al. (2016) and compare it to the size of

the grid cells in Fig. A.1. We find that in the regions closest to the NS, where most of the magnetic field amplification takes place (see Fig. 4), the fastest growing mode of the MRI is well resolved.

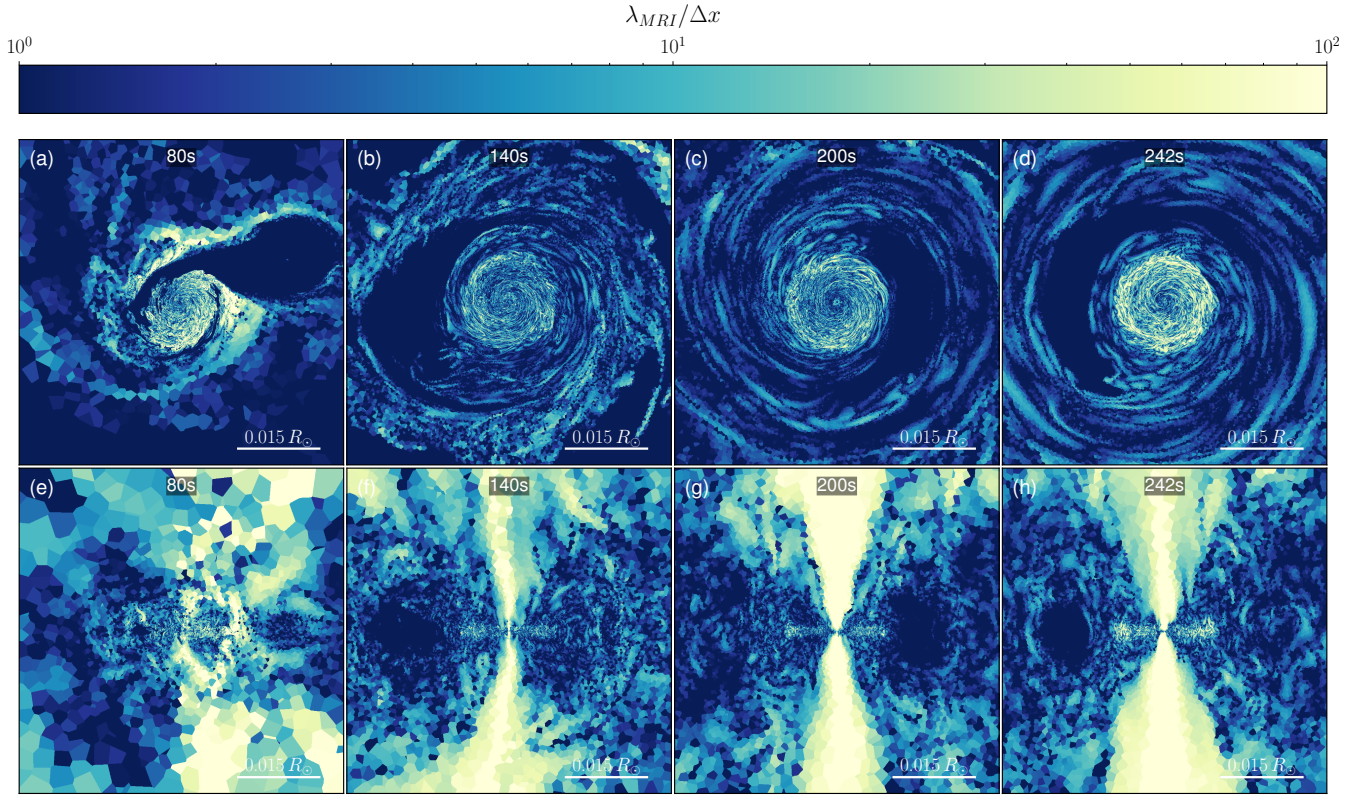


Fig. A.1. Number of cells per wavelength λ_{MRI} of the fastest growing MRI mode. *Top:* Slices through the orbital plane, centered on the NS. *Bottom:* Slices perpendicular to the orbital plane, centered on the NS.

2.3. Publication III: Faint Ca-rich transient from the double-detonation of a $0.6 M_{\odot}$ COWD

This paper presents a 3D MHD simulation of a merger between a $0.4 M_{\odot}$ HeWD and a $0.6 M_{\odot}$ COWD using the AREPO code. This setup originated as a follow-up study of the CE merger simulated in Sec. 2.1. That simulation consists of the merger of a $0.6 M_{\odot}$ COWD with a $0.4 M_{\odot}$ degenerate red giant (RG) core, but it does not include nuclear reactions, as it was not expected that nuclear burning would have a meaningful effect on the dynamics of the merger as a result of the low mass of the COWD. WD mergers are one of the leading candidates for explaining Type Ia SNe, but previous studies have shown that only COWDs with masses close to $1 M_{\odot}$ are capable of synthesizing enough ^{56}Ni to power SNeIa lightcurves, and no explosion has been found for masses below $\sim 0.8 M_{\odot}$. Despite this, in the simulation shown in Sec. 2.1 very high temperatures and densities were locally found shortly after the CE merger, warranting a more detailed inspection. This led to two new simulations where the MHD solver was coupled to a nuclear network. In first place, a re-computation of the simulation shown in Sec. 2.1, this time accounting for nuclear reactions, and secondly a new setup with a colder HeWD replacing the hot RG, core which is the main system studied in the following publication.

Publication Information

Title Faint calcium-rich transient from a double-detonation of a $0.6 M_{\odot}$ carbon-oxygen white dwarf star.

Authors J. Morán-Fraile, A. Holas, F. K. Röpke, R. Pakmor, F. R. N. Schneider.

Status Accepted for publication on A&A on December 7th, 2023.

Digital Object Identifier <https://doi.org/10.48550/arXiv.2310.19669>

Credit Moran-Fraile et al. *arXiv e-prints* art. arXiv:2310.19669, reproduced with permission ©ESO.

Author's contribution

JMF is the principal author of this article. This paper originated from JMF's further investigation of one of the simulations conducted in Sec. 2.1 of this thesis. JMF performed the hydrodynamical simulations and analyzed their results. JMF also performed the post-processing of the nuclear composition, wrote the majority of manuscript and produced the figures corresponding to the hydrodynamical simulation. AH performed the radiation transfer simulations and produced the figures for the lightcurves and spectra of the event, and wrote section 3.2 of the article as well as the paragraph corresponding to the discussion of the spectra and lightcurves in the discussion section. All the authors actively contributed, discussing the methods and results during several stages of the project.

Faint calcium-rich transient from a double-detonation of a $0.6 M_{\odot}$ carbon-oxygen white dwarf star

Javier Morán-Fraile¹, Alexander Holas^{1,2}, Friedrich K. Röpkke^{1,2}, Rüdiger Pakmor³, and Fabian R. N. Schneider^{1,4}

¹ Heidelberger Institut für Theoretische Studien (HITS), Schloss-Wolfsbrunnenweg 35, 69118 Heidelberg, Germany

² Zentrum für Astronomie der Universität Heidelberg, Institut für Theoretische Astrophysik, Philosophenweg 12, 69120 Heidelberg, Germany

³ Max-Planck-Institut für Astrophysik, Karl-Schwarzschild-Str. 1, 85748 Garching, Germany

⁴ Zentrum für Astronomie der Universität Heidelberg, Astronomisches Rechen-Institut, Mönchhofstr. 12-14, 69120 Heidelberg, Germany

November 28, 2023

ABSTRACT

We have computed a three-dimensional hydrodynamic simulation of the merger between a massive ($0.4 M_{\odot}$) helium white dwarf (He WD) and a low-mass ($0.6 M_{\odot}$) carbon-oxygen white dwarf (CO WD). Despite the low mass of the primary, the merger triggers a thermonuclear explosion as a result of a double detonation, producing a faint transient and leaving no remnant behind. This type of event could also take place during common-envelope mergers whenever the companion is a CO WD and the core of the giant star has a sufficiently large He mass. The spectra show strong Ca lines throughout the first few weeks after the explosion. The explosion only yields $< 0.01 M_{\odot}$ of ^{56}Ni , resulting in a low-luminosity SN Ia-like lightcurve that resembles the Ca-rich transients within this broad class of objects, with a peak magnitude of $M_{\text{bol}} \approx -15.7$ mag and a rather slow decline rate of $\Delta m_{15}^{\text{bol}} \approx 1.5$ mag. Both, its lightcurve-shape and spectral appearance, resemble the appearance of Ca-rich transients, suggesting such mergers as a possible progenitor scenario for this class of events.

Key words. white dwarfs, stellar merger, supernovae, hydrodynamics, radiative transfer, nucleosynthesis

1. Introduction

Binary white dwarf (WD) systems are the most common type of double compact objects in our galaxy (Nelemans et al. 2001). Consequently, their mergers are a common occurrence. These mergers can take place because gravitational wave emission (GW), common-envelope events, three-body interaction, and other processes can shrink the orbit of the binaries down to the point of Roche-lobe overflow (RLOF), giving rise to a variety of astronomical transients depending on the mass and composition of the involved WDs. These mergers have been primarily studied with the goal of finding the progenitors of Type Ia supernovae (SNe Ia, Liu et al. 2023), which are thought to be produced by thermonuclear explosions in carbon-oxygen (CO) WDs. To enhance the chance for the ignition of a thermonuclear explosion and to ensure the production of the $\sim 0.5 M_{\odot}$ of ^{56}Ni required to power the lightcurve of a normal SN Ia, most of the previous research has focused on mergers involving CO WDs with masses above $0.9 M_{\odot}$ (Sim et al. 2010; Shen et al. 2021). The exact mechanism that initiates the explosion is debated, but most of the proposed scenarios involve a so-called “double-detonation”. In this scenario, a helium (He) shell surrounding the CO WD is ignited initially. The detonation of the He shell converges near the core of the CO WD. In the convergence point, the density and temperature are greatly increased and a detonation wave is launched that propagates outwards incinerating the CO WD material. But higher-mass CO WDs are less abundant in nature than their lower-mass counterparts both among single stars (Kepler et al. 2007) as well as in binaries (Nelemans et al. 2001; Toonen et al. 2012). If low-mass CO WDs were to produce some type

of detectable transient, they could potentially be much more frequent than SNe Ia due to their ubiquity. At masses $\sim 0.6 M_{\odot}$, the central density of CO WDs is one order of magnitude below that of their $0.9 M_{\odot}$ counterparts, making the conditions for carbon ignition (Seitenzahl et al. 2009) difficult to attain, even under the double-detonation scenario. For these low-mass CO WDs to explode, a new mechanism for their detonation must be found or they must be enveloped in a very massive He shell that generates a more potent compression than in the classic double-detonation scenario, compressing the CO WD core enough to reach the conditions of carbon ignition.

Only material burned at densities over $\rho > 10^7 \text{ g cm}^{-3}$ is able to produce ^{56}Ni (see, e.g., Sim et al. 2010), and therefore any potential explosion of a low-mass CO WD would result in a very low ^{56}Ni yield. As a direct consequence of the low ^{56}Ni yield, these explosions would produce transients much fainter than SN Ia.

Here we present a three-dimensional magnetohydrodynamic (3D MHD) simulation of the merger between a $0.4 M_{\odot}$ He WD and a $0.6 M_{\odot}$ CO WD exploding in a double detonation scenario with no bound remnant. The outcome is a faint transient that shares features with Ca-rich transients (Perets et al. 2010; Waldman et al. 2011; Kasliwal et al. 2012; Taubenberger 2017; Shen et al. 2019). Throughout this paper we use the term “Ca-rich” but we note that it is debated whether a substantial amount of calcium is required to excite the Ca line in the late spectra (Shen et al. 2019; Jacobson-Galán et al. 2020).

The thermonuclear explosion takes place minutes after the disruption of the He WD as the disrupted material is accreted by the CO WD.

2. Methods

2.1. Hydrodynamic explosion simulation

The hydrodynamic simulation is carried out with the `AREPO` code (Springel 2010; Pakmor et al. 2011, 2016; Weinberger et al. 2020), which is a 3D MHD code that uses a second-order finite volume approach on an unstructured moving Voronoi mesh. In our simulation, we employ similar methods as in Pakmor et al. (2021). We use explicit refinement and de-refinement for cells that are more than a factor of two away from the target mass of the cells ($m_{\text{target}} = 5 \times 10^{-7} M_{\odot}$), which results in $\sim 2 \times 10^6$ `AREPO` cells. Self-gravity is treated as Newtonian and computed using a oct-tree based algorithm. We use the Helmholtz equation of state (Timmes & Swesty 2000) including Coulomb corrections. We also include a 55 isotope nuclear reaction network coupled to hydrodynamics (Pakmor et al. 2012a, 2021; Gronow et al. 2021) that includes the following isotopes: n, p, ^4He , ^{11}B , $^{12-13}\text{C}$, $^{13-15}\text{N}$, $^{15-17}\text{O}$, ^{18}F , $^{19-22}\text{Ne}$, $^{22-23}\text{Na}$, $^{23-26}\text{Mg}$, $^{25-27}\text{Al}$, $^{28-30}\text{Si}$, $^{29-31}\text{P}$, $^{31-33}\text{S}$, $^{33-35}\text{Cl}$, $^{36-39}\text{Ar}$, ^{39}K , ^{40}Ca , ^{43}Sc , ^{44}Ti , ^{47}V , ^{48}Cr , ^{51}Mn , $^{52,56}\text{Fe}$, ^{55}Co , and $^{56,58-59}\text{Ni}$. We use the JINA reaction rates (Cyburt et al. 2010). Nuclear reactions are computed for all cells with $T > 2 \times 10^7$ K, but we limit burning at shock front as described by Pakmor et al. (2021).

2.2. Setup

Our initial binary system consists of a $0.6 M_{\odot}$ WD with an equal-by-mass mixture of carbon and oxygen and an initial radius of $0.0121 R_{\odot}$ ¹, and a $0.4 M_{\odot}$ WD composed entirely of He with a radius of $0.0156 R_{\odot}$. Our simulation is set up similar to that of Pakmor et al. (2021). The stellar models are constructed in hydrostatic equilibrium assuming a uniform temperature of $T = 10^6$ K. We map the density profiles to a 3D mesh in `AREPO` and assign the cells the appropriate internal energy for the given temperature using the Helmholtz equation of state. The stars are first relaxed separately to ensure hydrostatic equilibrium and remove noise introduced by the mapping process. The relaxation procedure is the same for both stars: they are placed in a cubic box of 2×10^{10} cm sides, with a uniform background grid density of $\rho = 10^{-5} \text{ g cm}^{-3}$ and a thermal energy of 10^{14} erg/g ($T \sim 5 \times 10^5$ K). The duration of the relaxation is chosen to be ten times the dynamical timescale of each star, i.e. 20 s for the $0.6 M_{\odot}$ CO WD and 37 s for the $0.4 M_{\odot}$ He WD. During the first half of the relaxation, we damp the spurious velocities introduced by discretization errors. During the second half of the relaxation, the stars are left to evolve freely without the damping force, and we check that the density profiles remain unchanged.

After the relaxation, we place both stars in a box with a size of 7.1×10^{11} cm and uniform background density of $\rho = 10^{-5} \text{ g cm}^{-3}$. To avoid large tidal forces when putting the WDs together in the box, we chose the initial distance between the WDs to be 9.4×10^9 cm, which is equal to three times the separation at the point of RLOF. We then artificially shrink the orbit on a timescale larger than the dynamical timescales of the WDs so that potential tidal effects can still take place. This orbital shrinking follows the scheme described in Pakmor et al. (2021), and it is stopped at the point of RLOF, when a steady mass transfer sets in. This happens at an orbital separation of 3.14×10^9 cm, with a total angular momentum of $L = 3.2 \times 10^{50} \text{ g cm}^2 \text{ s}^{-1}$. From this point on, we let the system evolve freely. We run the simulation with the nuclear network disabled during the artificial inspiral in order to reduce the computational cost, as no significant fraction

of mass is expected to undergo any nuclear reaction during this stage. We enable the nuclear network once the artificial orbital shrinking is terminated.

2.3. Prediction of observables

For a precise computation of the optical spectrum emitted by the event, we postprocess the simplified nucleosynthesis of our `AREPO` run by following the thermodynamic trajectories of 10^6 tracer particles during the explosion and using them as an input for a 384 isotope nuclear reaction network (Seitenzahl et al. 2010; Pakmor et al. 2012b; Seitenzahl & Townsley 2017) to obtain more accurate nucleosynthetic yields in the ejecta and assuming solar metallicity (Asplund et al. 2009). The explosion is simulated in `AREPO` until the ejecta reach homologous expansion. At this point, the ejecta structure as determined in the nucleosynthetic postprocessing step is mapped to the three-dimensional Monte Carlo radiative transfer code ARTIS (Sim 2007; Kromer & Sim 2009; Bulla et al. 2015; Shingles et al. 2022) following the methods described by Gronow et al. (2020) to derive synthetic observables. The postprocessed yields of the ejecta structure are mapped to a 50^3 Cartesian grid on which the Monte Carlo radiation transfer is computed. We track 10^8 energy packets as they propagate through the ejecta for 100 logarithmically spaced timesteps between 2 and 60 days after the explosion.

3. Results

3.1. Merger and double detonation

The evolution of the system is visualized in Fig. 1 and in the complementary movies². Both stars are initialized with a dipolar magnetic field with a value of 10 G at the equator; nevertheless, magnetic fields play a minor role in this simulation. When reaching the point of RLOF, He is transferred from the larger, less massive He WD onto the surface of the CO WD. Being composed of fully degenerate matter, the He WD expands as it loses mass, increasing the mass-transfer rate. This shrinks the orbit in a runaway process that ends when the He WD is tidally disrupted by the CO WD after 550 s. The disrupted stellar material initially forms a spiral arm, efficiently transferring angular momentum outwards (Fig. 1d-g). This allows a large fraction of the disrupted gas to spiral inwards, closer to the CO WD, where it begins to form a non-homogeneous He “shell” that completely engulfs the CO WD. This process is complex and we refer the reader to the complementary movies for a better visualization. Due to a tidal interaction, part of the infalling material intersects itself and gets “trapped”, forming an overdense and cold fluid parcel. While the rest of the accreting material circularizes and heats up due to shear and turbulent motions, this overdense structure remains colder with respect to the surrounding gas that forms the He “shell”. As the fluid parcel draws closer to the surface of the CO WD, it gets compressed and increases its density up to $3 \times 10^5 \text{ g cm}^{-3}$.

When this overdense material reaches the surface of the CO WD, it shears against it (the overdense material is best identified in Fig. 2a as the colder region), heating up and compressing the contact region. The shear dredges up a small fraction of C and O from the primary that is mixed with He in the “shell”. In this shearing layer, the density reaches values of up to $3 \times 10^5 \text{ g cm}^{-3}$ and temperatures of 7×10^8 K.

² available on Zenodo (<https://doi.org/10.5281/zenodo.8268166>, showing the temperature, magnetic fields, temperature and kinetic pressure)

¹ Defined as the radius in which 99.9% of the stellar mass is contained

Table 1. Final abundances and energy released by the He and CO detonations, and in the entire event.

	He detonation	CO detonation	Total
Energy released [10^{50} erg]	3.0	3.8	6.8
Yield [$10^{-3} M_{\odot}$]			
^4He	320	0.0	320
^{12}C	4.6	61.6	66.2
^{16}O	1.1	208	209
^{20}Ne	0.4	18.0	18.4
^{24}Mg	0.7	27.2	27.9
^{28}Si	6.7	168	175
^{32}S	16.7	71.8	88.5
^{36}Ar	9.3	9.4	18.6
^{40}Ca	18.8	5.6	24.4
^{44}Ti	6.3	0.0	6.3
^{48}Cr	6.0	0.0	6.0
^{56}Ni	3.3	4.7	8.0

A He detonation takes place 381.5s after the disruption of the He WD. The detonation is shown in Fig.2. The explosion originates from the region between the cold and overdense He structure and the CO WD (Fig.2b & Fig.2f). The shock propagates through the CO WD heating and compressing the material while the detonation wave propagates around the CO WD (Fig. 2c and Fig. 2g) releasing 3×10^{50} erg of nuclear energy (Table 1). The shocked CO does not reach temperatures or densities high enough to trigger burning inside the CO WD as the shock passes through it. The shock wave converges at a distance of 2.7×10^8 cm from the center of the CO WD (Fig. 2d & Fig.2h) 2.7s after the first detonation, compressing the material to densities of $\rho = 1.2 \times 10^7$ g cm³ and temperatures up to $T = 4.5 \times 10^9$ K, igniting a carbon detonation that propagates outward incinerating the CO material and releasing 6.8×10^{50} erg (Table 1). The CO WD is completely disrupted, with the ejecta having a partial axial symmetry due to the interaction with the disrupted stellar material located mainly on the orbital plane.

3.2. Ejecta and radiative transfer

The final yields and explosion energies of the merger are listed in Table 1. Out of the total ejecta mass of about $1 M_{\odot}$, a substantial amount (about 33%) is composed of He that remain unburnt. O contributes around 20% to the total ejecta mass, whereas the iron group elements (IGEs) only constitute less than 5%. The remainder consists of intermediate mass elements (IMEs), with Ca making up around 2.5% of the final composition. The $\sim 0.08 M_{\odot}$ of He that is ignited burns mainly into ^{40}Ca and ^{32}S , and this burning is the origin of all the ^{44}Ti and ^{48}Cr produced in the simulation. A small fraction of the burnt He produces ^{12}C and around 40% of the total ^{56}Ni yield of the event. After the CO detonation a $\sim 30\%$ of the initial ^{12}C remains unburned, while the rest of was burnt to ^{16}O , the majority of the produced IMEs, and 60% of the total ^{56}Ni yield (Table 1).

What stands out in the ejecta composition as listed in Table 1 is the rather low ^{56}Ni abundance compared with a substantial amount of ^{40}Ca . This composition, combined with the low luminosity implied by the low ^{56}Ni yield, suggests that our

model may resemble a Ca-rich transient (see e.g. Taubenberger (2017)). Furthermore, the ^{56}Ni yield also suggests that this is a sub-luminous event compared with a normal SNe Ia.

This is confirmed in our radiative transfer simulations, which predict low-luminosity lightcurves powered by the radioactive decay of ^{56}Ni (Fig. 3) that resemble the Ca-rich transients within the broader class of SN Ia-like objects. The angle-averaged lightcurves show a bolometric peak magnitude of $M_{\text{bol}} \approx -15.7$ mag and a rather slow decline rate of $\Delta m_{15}^{\text{bol}} \approx 1.5$ mag. Furthermore, we observe a substantial viewing angle dispersion in peak magnitudes with values ranging from $M_{\text{bol}} \approx -15.4$ mag to $M_{\text{bol}} \approx -16.0$ mag and decline rates ranging from $\Delta m_{15}^{\text{bol}} \approx 1.4$ mag to $\Delta m_{15}^{\text{bol}} \approx 1.7$ mag. This large scatter can be attributed to the pronounced asymmetry in the ejecta structure as a result of the double detonation explosion mechanism. A detailed analysis of the viewing angle dependence, however, is beyond the scope of this study and will be discussed in future work.

We compare the resulting broad-band and bolometric light curves to several typical Ca-rich transient candidates in Fig. 3, where we find a rather good qualitative agreement, particularly in the *V*- and *R*-band peak magnitudes and decline rates. However, the spectra obtained from our radiative transfer simulation only somewhat resemble the observed spectra of Ca-rich transients, as is illustrated in Fig. 4. While we reasonably reproduce the calcium feature, we consistently lack the feature visible at around 5900 \AA , marked in red in Fig. 4, interpreted as either a He-I or Na-I line.

4. Discussion and conclusions

The cells in the region of He ignition have temperatures of $T \sim 7 \times 10^8$ K and densities of $\rho \sim 3 \times 10^5$ g cm⁻³ with a typical size of ~ 90 km. We also find a small fraction of C (about 15%) mixed into the composition of the detonating material, which is known to facilitate the He ignition. These conditions are consistent with simulations of resolved He detonations (Shen & Moore 2014) where the ignition points have length scales of hundreds of kilometers. We see the ignition of He in several cells and consider it marginally resolved in our simulation. This is not the case for the triggering of the CO detonation, which takes place on centimeter scales (Seitenzahl et al. 2009), i.e. far below the typical resolution of ~ 15 km in the CO detonation ignition region in our simulation. Still, at the point of shock convergence, we measure densities of $\rho = 1.2 \times 10^7$ g cm³ and temperatures of up to $T = 4.5 \times 10^9$ K, which are consistent with those found in simulations of resolved CO detonations (Seitenzahl et al. 2009). Therefore we argue that the detonations we observe in our simulation are physically plausible. One caveat is the simplistic initial composition used for the explosion simulation. More realistic WD models should include ^{22}Ne in the CO material and ^{14}N in the He to represent the metallicity of the original star. It has been shown by that these pollutants facilitate the He ignition Shen & Moore (2014) and they alter the composition of the burning products.

The mass distribution of CO WDs is skewed towards lower masses, and, due to their low central densities, low-mass WDs were previously believed to be very unlikely to produce a thermonuclear explosion. We find that the double detonation mechanism resulting from mergers with massive He WDs can lead to an explosion of such low-mass CO WDs. The He WD companions in the merger result from the cores of RG stars whose envelope is removed in binary interaction. Stars born with masses up to $\sim 2.3 M_{\odot}$ (Kippenhahn et al. 2012) form cores consisting of

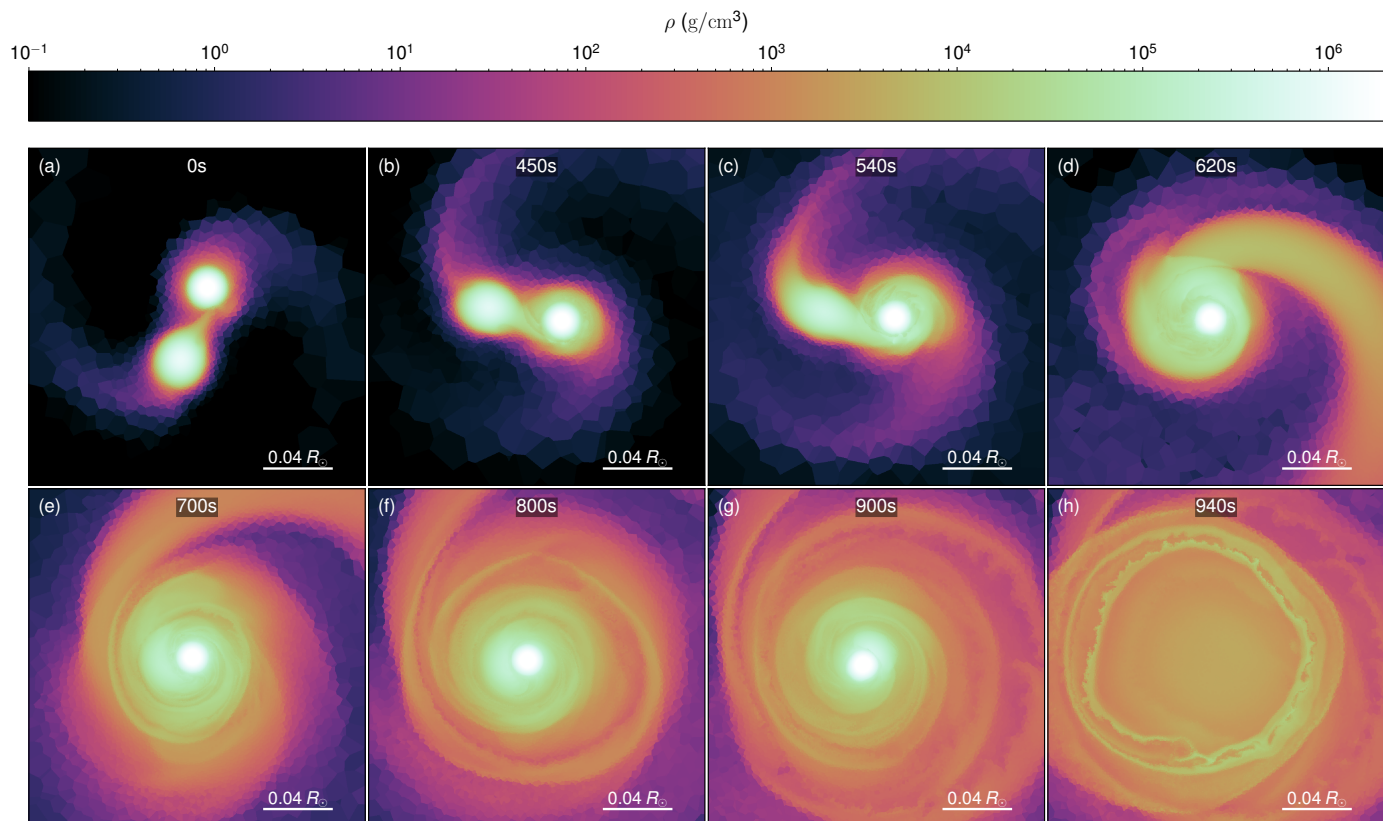


Fig. 1. Hydrodynamic evolution of the WD-WD merger. The panels show slices of the orbital plane color coded with the density from the beginning of the interaction until the moment that the double detonation takes place.

up to $0.48 M_{\odot}$ of degenerate He. However, we expect the mechanism to work only in a very restricted parameter range. The formation and survival of a cold, overdense, structure (part of it originating from the core of the He WD) during the circularization of the accreting material seems to be key in the He ignition mechanism. The survival of this overdense region is expected to depend sensitively on the masses of the components: Increasing the CO WD mass leads to higher central densities which favors the CO ignition, but the increased tidal forces imply that the disruption of the He WD will take place further away from the CO WD and that the disrupted material will be more thoroughly homogenized by the time it is accreted and therefore He ignition may be avoided in the first place. Decreasing the mass of CO will lower the densities even further and, although the survival chances of the overdense He region could increase, the conditions for the CO detonation will be more difficult to meet. Even if the core is able to detonate, less material will be burned and less ^{56}Ni will be produced making the event even fainter. Furthermore, as a lower-mass CO WD is less compact, the accreted He at its surface is more unlikely to trigger a detonation.

In our setup, the He WD had a mass of $0.4 M_{\odot}$. In principle, a more massive He shell will increase chances of triggering both the He and the CO detonations, but as a core of a RG star, its mass cannot exceed $0.48 M_{\odot}$ (Kippenhahn et al. 2012). In contrast, if the mass of the He WD is reduced, its compactness and central density are reduced and therefore tidal disruption will take place at larger distances and the material will have lower densities, diminishing its chances of forming the overdense structure required for He ignition.

The conditions for He ignition seem rather restrictive in the mass ranges of both WDs. Therefore, we do not expect all sim-

ilar systems to undergo thermonuclear explosions, and our scenario leaves room for the formation of R CrB stars from WD mergers.

If the conditions for triggering a detonation are met, the large amount of He mass accumulated on top of the CO WD helps to quickly spread the He detonation around the CO WD. Therefore the convergence of the shockwave is more symmetric than in other scenarios (Fink et al. 2010) and therefore the convergence happens more closely to the center of the CO WD. This is important because the density and temperature of this low-mass object are low, and a more central convergence helps to ignite the second detonation.

The progenitor of our considered system has to evolve through a CE phase. Whether this CE interaction leads to a successful ejection of the RG envelope is a topic of ongoing research. Successful envelope ejection was observed in CE simulations of systems such as that considered here only under the assumption of local thermalization of recombination energy, which is challenged by the possibility of energy transport due to radiation or convection (see Röpke & De Marco 2023, and references therein). If the envelope is successfully ejected, the resulting binary system will consist of a He WD and a CO WD in a tight orbit. The merger and subsequent explosion would then take place after sufficient orbital shrinkage due to the release of gravitational waves. This gives rise to the scenario we have discussed. However, if the envelope is not successfully ejected, the CE event results in the merger between the core of the RG and the companion WD, sometimes called a “failed CE event” or a “CE merger”, see, e.g. Röpke & De Marco (2023). To test whether our proposed explosion mechanism still triggers an explosion when the secondary star is not a He WD but a RG core,

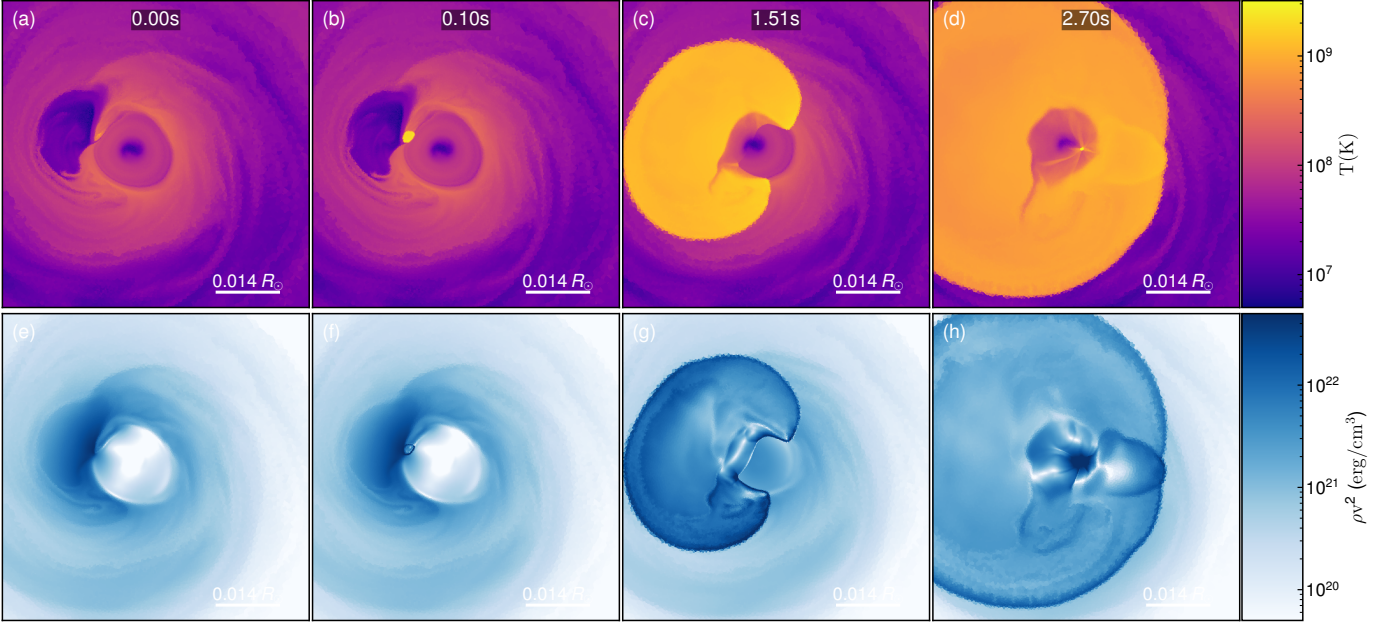


Fig. 2. Columns show snapshots immediately before the first detonation ($t=0$ s), first snapshot after the He ignition ($t=0.1$ s) and the propagation of the shock produced by this detonation through the CO WD ($t=1.51$ s) converging at 2.7×10^8 cm from the center of the CO WD ($t=2.7$ s). *Top:* Temperature in K. *Bottom:* Kinetic pressure in erg/cm^3 .

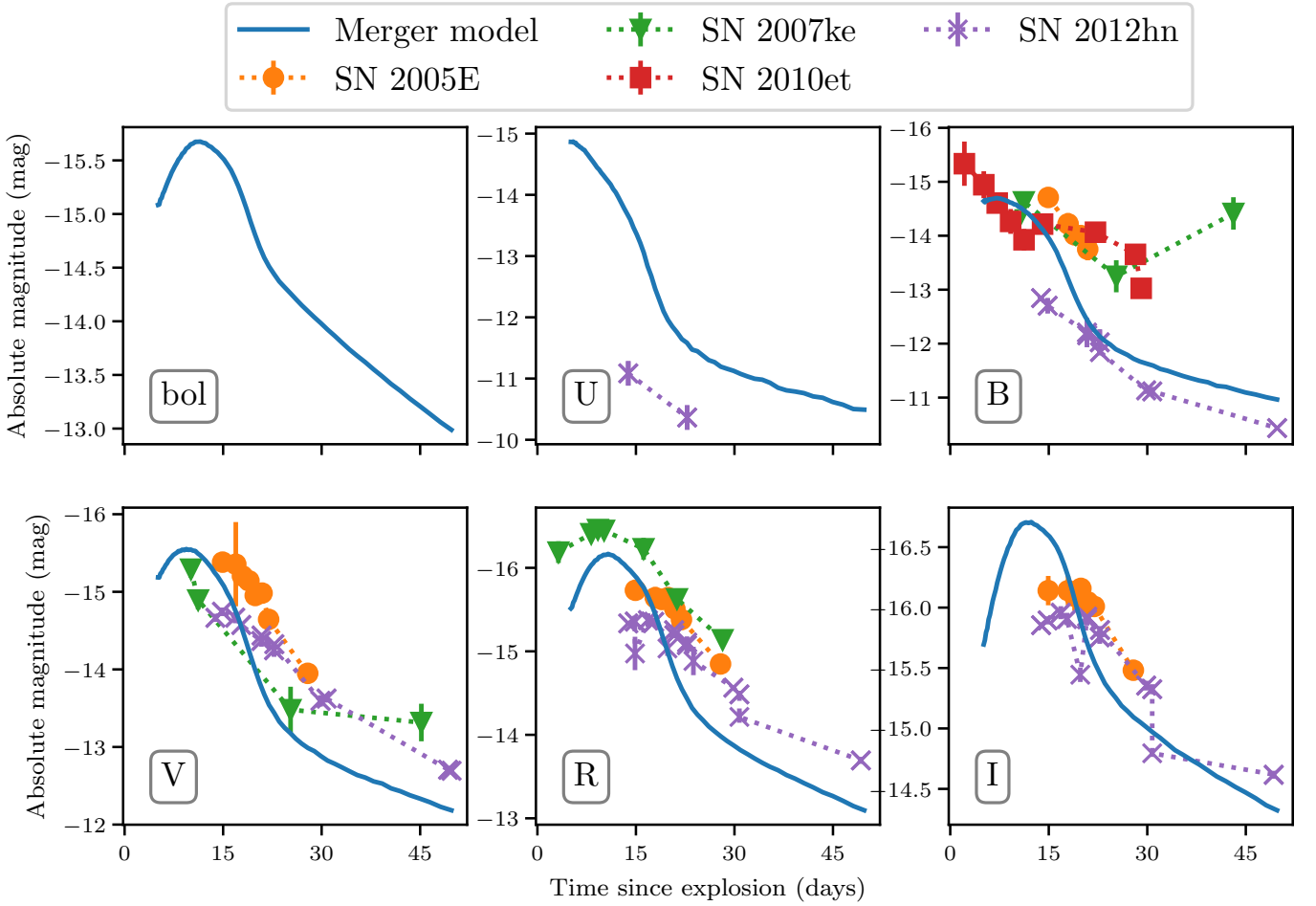


Fig. 3. Bolometric and broadband light curves of the merger model. Here, several Ca-rich transient candidates are plotted as well for comparison: SN 2005E Perets et al. (2010), SN 2007ke, SN 2010et Kasliwal et al. (2012) and SN 2012hn Valenti et al. (2014). All data are taken from the Open Supernova Catalog Guillochon et al. (2017).

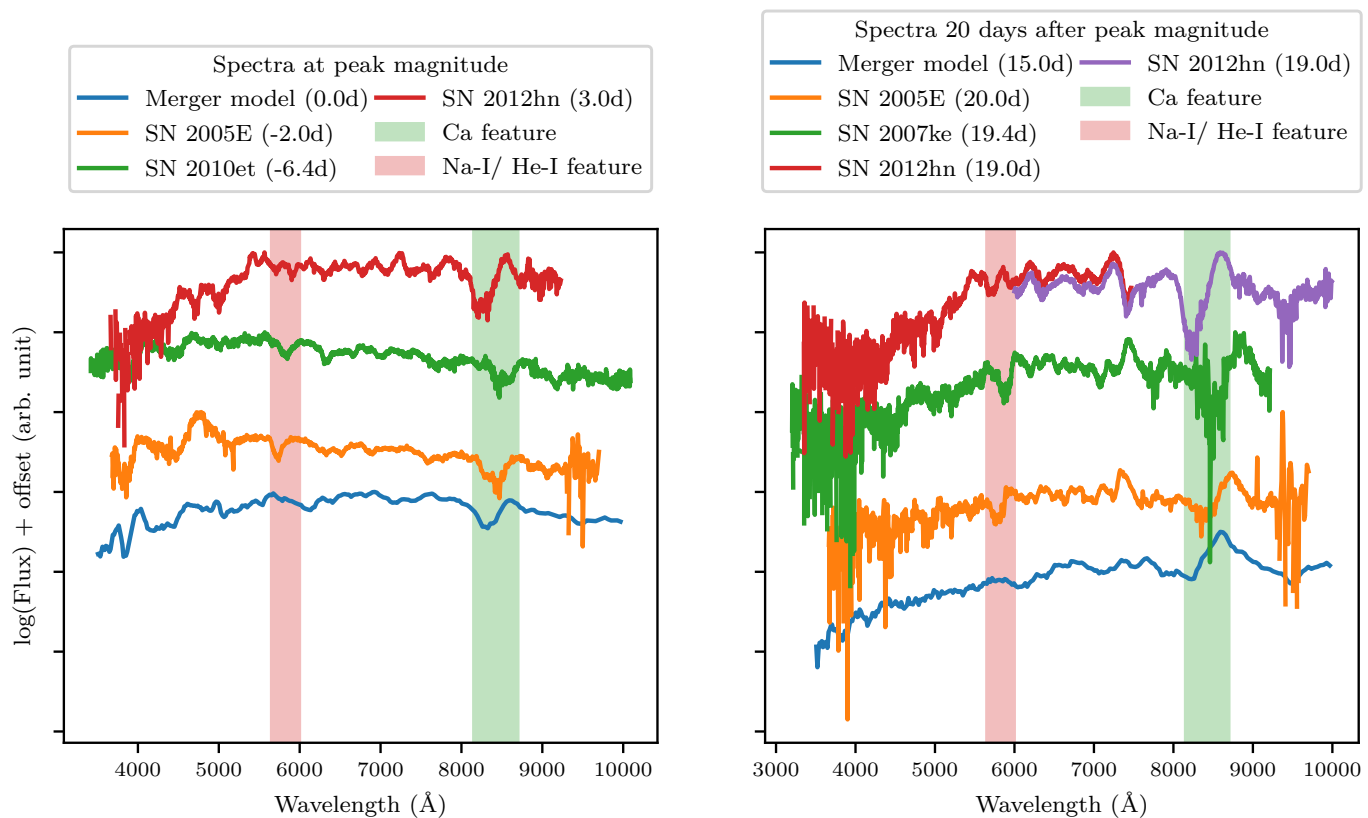


Fig. 4. Spectral comparison between our merger model and various Ca-rich transient candidates (Perets et al. 2010; Kasliwal et al. 2012; Valenti et al. 2014; Shivvers et al. 2019). Here the prominent calcium feature can be seen (green marking) as well as the poorly reproduced Na-I/ He-I feature (red marking). It should be noted that these markings do not indicate the precise location of the respective features, but rather serve as a guide for the eye. All data has been taken from WISeREP (Yaron & Gal-Yam 2012). *Left:* Spectra around peak magnitude. *Right:* Spectra around 20 days after peak magnitude.

we have carried out a second simulation with the same parameters but a He WD with the initially uniform temperature increased to 2×10^7 K. This structure is somewhat less compact than the cold He WD in our original simulation. With this altered setup, we still observe the same explosion mechanism, releasing roughly the same nuclear energy and producing equivalent nucleosynthetic yields. This scenario is reminiscent of the core-degenerate scenario (Kashi & Soker 2011; Ilkov & Soker 2012) for SNe Ia, where the merger between the core of an asymptotic giant branch (AGB) star and a CO WD after a failed CE ejection results in a super-Chandrasekhar mass WD that explodes as a SNe Ia inside the CE. Our setup differs from the original core-degenerate scenario because our explosion results from a double-detonation of a sub-Chandrasekhar mass CO WD due to the merger with a core of a RG star. With the chosen typical mass of a CO WD, this results in an event much fainter than a SN Ia.

This simulation shows that it is possible to produce thermonuclear transients in a realistic scenario that synthesise even less ^{56}Ni and substantially more ^{40}Ca than what is usually obtained in simulations of the double-detonation scenario aiming at modeling SNe Ia (Boos et al. 2021). We reach good agreement with several lightcurves of observed Ca-rich transients, both in shape and peak magnitude. The spectra produced by our model, however, do not reproduce the feature at around 5900 \AA which is a major discrepancy with the observed spectra.

Zenati et al. (2023) reproduce this feature rather well, while it is entirely missing from our spectra. The authors argue that their simulation does not have enough remaining He to pro-

duce strong He features, suggesting that this feature results from sodium. We find, however, that even increasing the sodium content by a factor of 100 the spectral appearance remains virtually unchanged. This suggests that the feature is a He-I line, which ARTIS cannot model in the utilized setup, and the majority of the sodium has been ionized to higher states. It should be pointed out that although Zenati et al. (2023) reproduce this feature, their simulation differs from ours. The key difference is that in their model, the core of the HeCO WD companion is assumed to survive the event. This has significant implications on the ejecta structure and composition, in particular regarding the distribution of He in the ejecta and the subsequent potential imprint of He on the spectra. It remains to be seen if the feature around 5900 \AA is indeed a He-I line or a Na-I line instead. A strong He-I feature, e.g., would suggest that substantial amounts of He are required in the ejecta, making the disruption of the He-carrying companion the more likely scenario, and vice versa. Our results so far indicate that this is a He-I line, which is simply beyond the capabilities of our utilized ARTIS setup.

In the nebular phase of Ca-rich transients typically show a high ratio of Ca/O. Our model predicts a substantial amounts of oxygen in the ejecta resulting from unburnt material and from C-burning at low densities in the outer regions of the WD. Whether this oxygen produces a strong feature in the nebular spectra leading to a conflict with observed nebular spectra of Ca-rich transients has to be tested in detailed radiative transfer simulations that are beyond the scope of this paper. Ca-rich transients are known to also occur far from the centers of their host galax-

ies (Shen et al. 2019). Whether the progenitor system for our mergers are also located far from the center of galaxies must be tested with population synthesis studies. Investigating these questions and the nature of the He-I/ Na-I region remain as open tasks in fully assigning our model as a Ca-rich transient progenitor and will be the focus of future work.

In contrast, if the detonation were to take place inside a CE, the spectra and lightcurve would significantly change due to the interaction of the ejecta with the envelope material, showing hydrogen features in the spectra and likely resembling an interacting SN. This interaction has to be modeled in the framework of radiation hydrodynamics and will be further discussed in Kozyreva et al.³

The transients resulting from these mergers could be faint, but very frequent depending on the sensitivity of the explosion mechanism to the masses of the components. These explosions could be interesting targets for the Zwicky Transient Facility (ZTF Bellm et al. 2019; Graham et al. 2019) or the future Vera Rubin Observatory (Ivezić et al. 2019). Detecting these explosions from both, bare core mergers and inside an envelope, might also give information about the CE mechanism.

ACKNOWLEDGMENTS

J.M-F. and A.H. are fellows of the International Max Planck Research School for Astronomy and Cosmic Physics at the University of Heidelberg (IMPRS-HD) and acknowledge financial support from IMPRS-HD.

This work acknowledges support by the European Research Council (ERC) under the European Unions Horizon 2020 research and innovation programme under grant agreement No. 759253 and 945806, the Klaus Tschira Foundation, and the High Performance and Cloud Computing Group at the Zentrum für Datenverarbeitung of the University of Tübingen, the state of Baden-Württemberg through bwHPC and the German Research Foundation (DFG) through grant no INST 37/935-1 FUGG. The authors gratefully acknowledge the Gauss Centre for Supercomputing e.V. (www.gauss-centre.eu) for funding this project by providing computing time through the John von Neumann Institute for Computing (NIC) on the GCS Supercomputer JUWELS at Jülich Supercomputing Centre (JSC).

References

Asplund, M., Grevesse, N., Sauval, A. J., & Scott, P. 2009, *ARA&A*, 47, 481
 Bellm, E. C., Kulkarni, S. R., Graham, M. J., et al. 2019, *PASP*, 131, 018002
 Boos, S. J., Townsley, D. M., Shen, K. J., Caldwell, S., & Miles, B. J. 2021, *ApJ*, 919, 126
 Bulla, M., Sim, S. A., & Kromer, M. 2015, *MNRAS*, 450, 967
 Cyburt, R. H., Amthor, A. M., Ferguson, R., et al. 2010, *The Astrophysical Journal Supplement Series*, 189, 240
 Fink, M., Röpke, F. K., Hillebrandt, W., et al. 2010, *A&A*, 514, A53
 Graham, M. J., Kulkarni, S. R., Bellm, E. C., et al. 2019, *PASP*, 131, 078001
 Gronow, S., Collins, C., Ohlmann, S. T., et al. 2020, *A&A*, 635, A169
 Gronow, S., Collins, C. E., Sim, S. A., & Röpke, F. K. 2021, *A&A*, 649, A155
 Guillochon, J., Parrent, J., Kelley, L. Z., & Margutti, R. 2017, *The Astrophysical Journal*, 835, 64
 Ilkov, M. & Soker, N. 2012, *MNRAS*, 419, 1695
 Ivezić, Ž., Kahn, S. M., Tyson, J. A., et al. 2019, *ApJ*, 873, 111
 Jacobson-Galán, W. V., Margutti, R., Kilpatrick, C. D., et al. 2020, arXiv e-prints, arXiv:2005.01782
 Kashi, A. & Soker, N. 2011, *MNRAS*, 417, 1466
 Kasliwal, M. M., Kulkarni, S. R., Gal-Yam, A., et al. 2012, *ApJ*, 755, 161
 Kepler, S. O., Kleinman, S. J., Nitta, A., et al. 2007, *MNRAS*, 375, 1315
 Kippenhahn, R., Weigert, A., & Weiss, A. 2012, *Stellar Structure and Evolution* (Berlin Heidelberg: Springer-Verlag)

Kromer, M. & Sim, S. A. 2009, *MNRAS*, 398, 1809
 Liu, Z.-W., Röpke, F. K., & Han, Z. 2023, *Research in Astronomy and Astrophysics*, 23, 082001
 Nelemans, G., Yungelson, L. R., Portegies Zwart, S. F., & Verbunt, F. 2001, *A&A*, 365, 491
 Pakmor, R., Bauer, A., & Springel, V. 2011, *MNRAS*, 418, 1392
 Pakmor, R., Edelmann, P., Röpke, F. K., & Hillebrandt, W. 2012a, *MNRAS*, 424, 2222
 Pakmor, R., Kromer, M., Taubenberger, S., et al. 2012b, *ApJ*, 747, L10
 Pakmor, R., Springel, V., Bauer, A., et al. 2016, *MNRAS*, 455, 1134
 Pakmor, R., Zenati, Y., Perets, H. B., & Toonen, S. 2021, *MNRAS*[arXiv:2103.06277]
 Perets, H. B., Gal-Yam, A., Mazzali, P. A., et al. 2010, *Nature*, 465, 322
 Röpke, F. K. & De Marco, O. 2023, *Living Reviews in Computational Astrophysics*, 9, 2
 Seitenzahl, I. R., Meakin, C. A., Townsley, D. M., Lamb, D. Q., & Truran, J. W. 2009, *ApJ*, 696, 515
 Seitenzahl, I. R., Röpke, F. K., Fink, M., & Pakmor, R. 2010, *MNRAS*, 407, 2297
 Seitenzahl, I. R. & Townsley, D. M. 2017, in *Handbook of Supernovae*, ISBN 978-3-319-21845-8. Springer International Publishing AG, 2017, p. 1955 (Springer), 1955
 Shen, K. J., Boos, S. J., Townsley, D. M., & Kasen, D. 2021, *ApJ*, 922, 68
 Shen, K. J. & Moore, K. 2014, *ApJ*, 797, 46
 Shen, K. J., Quataert, E., & Pakmor, R. 2019, *ApJ*, 887, 180
 Shingles, L. J., Flörs, A., Sim, S. A., et al. 2022, *MNRAS*, 512, 6150
 Shivvers, I., Filippenko, A. V., Silverman, J. M., et al. 2019, *Monthly Notices of the Royal Astronomical Society*, 482, 1545
 Sim, S. A. 2007, *MNRAS*, 375, 154
 Sim, S. A., Röpke, F. K., Hillebrandt, W., et al. 2010, *ApJ*, 714, L52
 Springel, V. 2010, *MNRAS*, 401, 791
 Taubenberger, S. 2017, in *Handbook of Supernovae*, ed. A. Alsabti & P. Murdin (Springer), 317–373
 Timmes, F. X. & Swesty, F. D. 2000, *ApJS*, 126, 501
 Toonen, S., Nelemans, G., & Portegies Zwart, S. 2012, *A&A*, 546, A70
 Valenti, S., Yuan, F., Taubenberger, S., et al. 2014, *Monthly Notices of the Royal Astronomical Society*, 437, 1519
 Waldman, R., Sauer, D., Livne, E., et al. 2011, *ApJ*, 738, 21
 Weinberger, R., Springel, V., & Pakmor, R. 2020, *ApJS*, 248, 32
 Yaron, O. & Gal-Yam, A. 2012, *PASP*, 124, 668
 Zenati, Y., Perets, H. B., Dessart, L., et al. 2023, *The Astrophysical Journal*, 944, 22

³ in prep

3. Conclusions

In this thesis, state-of-the-art 3D MHD simulations of different types of stellar interactions involving WDs were performed, with the aim of shedding light onto poorly understood processes. Specifically, the focus was placed on binary systems that had not previously been studied in this level of detail because of the numerical challenges that they presented.

The first section of this chapter (Sec. 3.1) provides a brief overview of the main results of the individual publications presented in Chapter 2. In the second section (Sec. 3.2), these findings are discussed beyond the scope of the individual publications and presenting possible future research directions.

3.1. Summary of the individual publications

This section summarizes the results and conclusions of each publication. The reader is referred to the original papers for additional information regarding the technical details or the methodology.

Gravitational wave emission from dynamical stellar interactions

GWs emitted by binary stellar systems trace the evolution of their orbital parameters, as their frequencies are intimately related to the frequency and eccentricity of the binary. For the article presented in Sec. 2.1, the computation of GWs in the Newtonian quadrupole approximation was implemented in the 3D MHD code AREPO. Subsequently, three simulations of different stellar interactions taking place on dynamical timescales were performed, in order to study the detectability of GWs released during them with the future LISA space mission (Robson et al., 2019) and what could be learned from such detections.

The first simulation models the merger of two early main-sequence stars with masses of $8 M_{\odot}$ and $9 M_{\odot}$ (same binary system shown by Schneider et al., 2019). The orbit shrinks as the initially more massive star transfers mass to the secondary star, increasing the frequency and amplitude of the GWs until the primary star is disrupted. It was observed that the frequency of the GWs accurately corresponds to two times the orbital frequency of the binary up until the point that the merger takes place. From that point onwards, the amplitude of the released GWs sharply decreases and shifts to higher frequencies, as the signal is now mainly produced by internal oscillations of the merger product. This means that the maximum frequency of the GWs before the merger (and subsequent drop-off in amplitude) can be accurately retrieved by a precise computation of the tidal disruption of the

individual stars, as this point will signal the highest reachable orbital frequency. This can be used to obtain quick estimates for the highest frequency that will be achieved by the GWs released during the inspiral stage of any type of binary system, and check if it is within the sensitivity window of GW observatories. Using the complete GW signal from the 3D MHD simulation (five days of inspiral, three days of post-merger signal), the signal to noise ratio (SNR) that this merger would produce in the detectors of the LISA mission was computed, obtaining values of 6.3×10^{-2} at a distance of 1 kpc. This implies that such an event would be impossible to detect with this space mission, even at relatively short galactic distances. This is mainly due to the mismatch between the maximum frequency of the GWs released by the event and the frequency of peak sensitivity for LISA. Despite the inspiral signal lasting only five days, the GW signal originated during earlier, non-modeled stages will exhibit a lower frequency, being increasingly further from the optimal sensitivity range of LISA.

The second scenario studied is the successful ejection of the envelope during a CE event. During this binary interaction, a small-size, $1 M_{\odot}$ star is engulfed by the envelope of its $2 M_{\odot}$ RG companion. The orbit of the compact star sinks deep into the envelope of the RG, with the star and the core of the giant star orbiting each other, until enough energy is injected into the envelope to eject it and stop the orbital decay at separation of $3.9 R_{\odot}$. The duration of this dynamical stage is on the order of 200 days. From there on, the simulation is continued for a total of two years, during which the orbit remains majorly stable. The frequency of the GWs released by the event covers a range between 7×10^{-7} – 2.5×10^{-2} Hz, accurately matching twice the initial and final orbital frequencies of the system formed by the RG core and the companion. Additionally, there is GW emission at higher frequencies that matches other harmonics of the orbital frequency due to the eccentricity of the orbit (Maggiore, 2007; Creighton and Anderson, 2011). The SNR estimated for this event on the instruments of LISA at a distance of 1kpc is 4.2×10^{-4} , meaning that a CE event that results in such large final orbital separation would also be undetectable at this distance from the observatory. The data of this simulation was used to evaluate the validity of the approximation used by previous semianalytical works (e.g. Ginat et al., 2020; Renzo et al., 2021) of ignoring the effects of the massive envelope in the GW signal. It was found that the envelope leaves almost no imprint in the GW signal, only a small effect at the lowest frequencies. The GW signal can be almost perfectly recovered by computing the signal released exclusively by the core and the companion, proving that the approximation holds true and that the GW signal released by these events indeed fully traces the orbital evolution of the system. Therefore, the GW signal can be recreated with semianalytical models that parametrize the evolution of the orbit, and the detectability of successful CE ejections with LISA will completely depend on the final orbital separation after the event.

The last simulated scenario is the merger of a RG core with a WD companion as a result of a CE event where the envelope is not successfully ejected. The merger plays out as the tidal disruption of the RG core around the more compact WD companion on a timescale of ~ 1000 s. Similarly to the case of the main-sequence star merger, the orbit shrinks as mass transfer takes place, with the frequency of

the GW signal increasing with the orbital frequency, and, again, the amplitude of the waves sharply decreasing the moment the disruption takes place. From this point on, GWs of smaller amplitude are released at higher frequencies, caused by the initial lack of symmetry of the remnant. The simulation is continued for another 1000 s until the remnant is mostly axially symmetric and the GW signal has quieted down except for the internal oscillations that are mostly unresolved. The maximum frequency of the GWs before the disruption and subsequent drop in amplitude is ~ 2.5 Hz, slightly below the estimated value obtained by deriving this value from the tidal disruption radius. This difference is explained by the difficulty in establishing a precise value for the radius of the RG core in the simulation as the core expands when losing mass due to its degenerate nature. The SNR obtained by LISA at 1 kpc for this signal is 6.6, hinting at potential detectability despite the signal lasting only ~ 2000 s. As the only stage of the CE phase that this simulation models is the final disruption of the core, which takes place at GW frequencies above the peak sensitivity of LISA, three toy models were produced in order to model a prior CE event, with three differently parametrized orbital decays. The models produced SNRs for LISA in the range of ~ 10 –200, showing that the detectability of these events will strongly depend on how the orbital decay takes place. Therefore, detections of such events would reveal the precise orbital evolution inside the envelope, and even non-detections could help to put constraints on it, helping to improve the understanding of the CE stage.

Self-consistent magnetohydrodynamic simulation of jet launching in a neutron star – white dwarf merger

Section 2.2 presents the first 3D MHD simulation of a NS–WD merger. This simulation models the event from the onset of mass transfer until the formation of a quasi-toroidal disk around the NS, arising from the debris from the disrupted WD. The simulation featured in the paper was performed using the AREPO code, and although it does not include nuclear reactions, an additional simulation was performed where a nuclear network was coupled to the MHD solver to ensure that the results are not substantially affected by nuclear reactions (this will be discussed in Sec. 3.2).

The simulation shows an unstable mass transfer from the WD onto the NS, shrinking the orbit until the WD is tidally disrupted at a distance of 1.14×10^9 cm from the NS, 90 s after the onset of the mass transfer episode. When the simulation is stopped (~ 150 s after the tidal disruption), the debris from the WD has mostly circularized around the NS, with most of the gas concentrating in the orbital plane. The material forms a puffed up disk, with a thickness comparable to the size of the original WD. Most of the material is located at a distance from the NS similar to the tidal disruption radius of the WD, but with the disk extending up to a radius of $\sim 10^{10}$ cm.

Shear and compression in the accretion stream amplifies the magnetic fields in the gas during the circularization process, and over the course of the simulation, the total magnetic energy of the system increases by more than 7 orders of magnitude due to several physical processes, including magneto-rotational instability

(MRI, [Balbus and Hawley, 1991](#)), Kelvin-Helmholtz instabilities ([Liu et al., 2018](#)), and dynamo processes ([Brandenburg and Subramanian, 2005](#)).

Because the NS is taken as a point mass in this simulation, accretion takes place onto the volume around the NS with a softened gravitational potential. The accretion rate averages $\sim 10^{-4} M_{\odot} \text{ s}^{-1}$ since the disruption of the WD, and peaks at $3 \times 10^{-3} M_{\odot} \text{ s}^{-1}$ the moment that the simulation is stopped due to the numerical issues that arise from that point on.

The accretion, combined with the exceptionally large magnetic fields (ranging between 10^{10} – 10^{13} G inside the disk), powers the launch of bipolar jets perpendicular to the orbital plane. The jets present a strong asymmetry in power, and a high variability during the simulated timescale, shutting on and off, and showing velocities oscillating between 0.05 – $0.1 c$, and luminosities between 10^{47} – 4×10^{47} erg/s. The average thermal neutrino flux measured during the event is 2×10^{48} erg s $^{-1}$.

The binary system releases GWs in the decihertz frequency range until the WD is disrupted. From that point, the GWs sharply decrease in amplitude and increase in frequency, as the inhomogeneities in the disk become the main source of GW radiation. The GW signal from the disruption seems an ideal target for future space-based decihertz GW observatories such as DECIGO ([Seto et al., 2001](#)) or BBO ([Harry et al., 2006](#)), being detectable at distances on the scale of Mpc.

This simulation cannot conclusively predict the final fate of the remnant, as it depends on physics taking place at unresolved scales. If the NS does not collapse into a BH, the event is expected to resemble some fast blue optical transients (FBOTs) with luminosities larger than those of typical kilonovae. In the case of an eventual collapse into a BH, the event could result in a long or ultra-long gamma-ray burst (GRB)-like transient.

Faint calcium-rich transient from a double-detonation of a $0.6 M_{\odot}$ carbon-oxygen white dwarf star

This article presented in Sec. 2.2 shows a 3D MHD simulation coupled to a 55-isotope nuclear reaction network of the merger between a $0.6 M_{\odot}$ COWD and a $0.4 M_{\odot}$ HeWD, performed with the AREPO code. The onset of an unstable mass transfer from the larger HeWD onto the COWD shrinks the orbital separation, until the HeWD is tidally disrupted 550 s after the start of the mass transfer episode, when the distance to the COWD becomes shorter than the tidal disruption radius of the HeWD. The debris from the disrupted HeWD forms an inspiral arm, efficiently transferring angular momentum outwards, and allowing a large fraction of the material to spiral closer to the COWD. This inspiral arm is led by an over-dense parcel of gas. When this parcel of overdense He reaches the surface of the COWD, it shears against it, compressing and heating-up the region until the conditions for He ignition are reached. This ignition takes place under degenerate conditions, and results in an explosive He burning 381.5 s after the disruption of the HeWD. The explosion generates a shock that propagates through the COWD, heating and compressing the material, whereas the detonation wave propagates around it, through the He-shell that has built up around the COWD. The shock-wave converges close to the center of the COWD 2.7 s after the He ignition, in-

creasing the density of the material and heating it up, igniting a carbon detonation that propagates outward, burning the CO material and completely disrupting the COWD. This explosion mechanism is known as a *double-detonation* (Woosley and Weaver, 1994). This simulation shows for the first time the self-consistent formation and ignition of a He-shell arising from the disruption of a HeWD and, additionally, provides strong indication that the double-detonation scenario works for COWDs with masses as low as $0.6 M_{\odot}$ provided that the He-shell is massive enough.

The results of the AREPO simulation were post-processed with a 384-isotope nuclear reaction network to obtain accurate nucleosynthetic yields and with the 3D radiative transfer code ARTIS (Sim, 2007; Kromer and Sim, 2009; Bulla et al., 2015; Shingles et al., 2022) to obtain a synthetic lightcurve and spectra. From the nucleosynthesis, what stands out is the low ^{56}Ni production (less than $10^{-2} M_{\odot}$), coupled to a relatively high abundance of intermediate-mass elements such as ^{40}Ca , ^{32}S and ^{28}Si . Additionally, only a small fraction of the He is burnt, with $0.32 M_{\odot}$ remaining in the ejecta. The lightcurves and spectra produced by the simulation somewhat resemble that of Ca-rich transients, with a measured angle-averaged bolometric peak magnitude of -15.7 mag. The ejecta presents a geometry close to axial symmetry, and therefore a substantial viewing angle dispersion, with the bolometric peak magnitudes ranging between -15.4 mag and -16.0 mag. The spectrum also resembles that of Ca-rich transients, although one of the features at 5900 \AA could not be matched.

The model used for the HeWD is very similar to the degenerate core of a RG star. In fact, the model used for this paper is a colder version of the model used in Sec. 2.1 as the RG core. This means that this explosion mechanism could take place inside a H envelope as a result of a failed CE ejection (this will be further discussed in Sec. 3.2), and such an event could be a target for multi-messenger astronomy, as these events generate GW signals that could be detected by future space-based observatories (as shown in Sec. 2.1).

This simulation shows that even low-mass COWD (which are significantly more abundant than massive COWDs), also have the potential of originating bright transients under the right conditions. The range of masses for the WDs which will result in this interaction leading to a successful double detonation is still unknown, but it is expected to be relatively narrow. This will be discussed in detail in Sec. 3.2.

3.2. Discussion and future work

This section comprises a brief general discussion on the implications of the results of this thesis, followed by a more detailed analysis of each individual publication. The publications included in this thesis have contributed to the scientific knowledge by providing a state-of-the-art representation of a subset of stellar interactions, and also by highlighting some of the remaining gaps in the understanding of their outcomes. These studies emphasize the potential that WDs have to produce energetic transients as a result of dynamical interactions with other stars. Recent advances in numerical techniques and computational capabilities have finally made it possible to accurately explore many of these interactions, but there are still several challenges to overcome and a large parameter space that remains partially unexplored.

In the first place, the CE phase is a key stage in binary evolution, being one of the few possible pathways to shrink the orbital separation of binary systems on scales that can explain the formation of observed systems such as compact binaries (Paczynski, 1976; Lewin et al., 1997; Schreiber and Gänsicke, 2003; Geier et al., 2011; Ritter, 2012; Kruckow et al., 2021), the compact object mergers detected by GW observatories (Kruckow et al., 2016; Kruckow, 2018; Belczynski et al., 2020), or the progenitors of Type Ia SNe (Belczynski et al., 2005) among others. Despite its relevance, this stage presents numerous uncertainties, largely due to the enormous range of scales and physics involved, making it extremely challenging to model (Röpke and De Marco, 2023). As a result of the shortcomings in its modeling, there is still a disparity between observations of post CE systems and the results of simulations. Mainly that the observed values for the final orbital separations are substantially smaller than the ones obtained by simulations (Iaconi and de Marco, 2019), with this parameter having huge implications for the formation of compact binaries, including the ones discussed in Sec. 2.2 and Sec. 2.3.

Another example of how multi-physics, multi-dimensional numerical modeling is required to be able to consistently predict the outcome of dynamical interactions is shown in Sec. 2.3. The type of merger shown in this section was not traditionally expected to result in any significant thermonuclear event. The total mass of the system is substantially below the Chandrasekhar limit, and the initial mass of the COWD is much lower than that of the stars that are currently believed to be the progenitors of Type Ia SNe. However, the complex dynamical evolution of the merger makes it possible for the conditions to ignite carbon inside the COWD to arise, resulting in a new type of thermonuclear transient. The convoluted interplay of physical processes and the wide range of temporal and spatial scales involved in these events taking place on dynamical timescales make predicting their outcome without the use of advanced computations highly complicated. This suggests the potential existence of other important scenarios yet to be discovered as a result of models that do not include all the necessary physics or that resolve all the required scales. Performing ever more accurate simulations will allow for better studies of these events and will help to fill the gaps in the understanding of the processes that originate observed transients, and potentially predict new ones.

GWs from dynamical interactions

The results from Sec. 2.1 show that GWs released during the inspiral phase of binary mergers will only reach frequencies as high as two times the shortest orbital frequency achievable by the system before the merger takes place. For noncompact objects, the large tidal disruption radius of the stars will make the frequency of the GW released by these events too low, far below the optimal frequency of the LISA mission, making them impossible to detect with this instrument. As of today, there is no planned GW detector to cover the GW frequency between nHz and mHz, so the hope of detecting these events with GWs has to be placed in a distant future.

Regarding the GW signals arising from CE events, it is clear that since they dramatically decrease the orbital separation of the system, the GWs released will also cover a wide range of frequencies. Their minimum and maximum values being determined by the initial and final orbital frequencies. For the simulated successful CE ejection scenario, the measured final orbital frequency is 1.7×10^{-5} Hz, which results in GWs of a frequency too low for LISA to detect. It is important to keep in mind the aforementioned mismatch between the orbital separations measured by observations of post-CE systems and the values obtained by numerical simulations (Iaconi and de Marco, 2019). Several proposed explanations for these differences already exist in the literature, including the lack of modeling for the evolution of the core in 3D simulations. Typically, the core is treated as a point mass in these simulations, therefore, disregarding any potential expansion as the envelope is removed. Previous studies using parametrized models of CE have shown that these events could result in GW signals detectable by LISA if the final orbital separations fall below $\sim 1 R_{\odot}$ (Renzo et al., 2021). Observations suggest that many systems may end up with orbital separations below this threshold, challenging the results of 3D simulations. If the GW signals from such events were to be detected, they could give insights on what physics are missing in the current modeling framework of CE evolution and lead to a better understanding of this process, which is key in binary evolution.

This uncertainty in the final orbital separations also blurs the limit on when CE events lead to mergers. It was shown in Sec. 2.1 that the final merger of the core of the giant star and a compact companion inside a CE can lead to a detectable signal. In fact, the maximum frequency reached during the inspiral stage is higher than the frequency corresponding to LISA's peak sensitivity, which means that during the CE phase the frequency of the signal will cross through the optimal frequency range of the detector. This implies that, frequency-wise, the GW signal released during the final stages of these events has the potential of being detected, while, at the same time, tracing the orbital evolution of the system. GWs could therefore provide information about the physical processes that dominate the dynamics at very short orbital separations inside the envelope, and provide the missing link to explain the disparity between the observations of post-CE systems and simulations.

Amplitude-wise, the signals analyzed in this paper are relatively weak and would only be detectable at short distances (between 1–100 kpc) strongly depend-

ing on the exact orbital evolution, mainly on the time that the binary spends at orbital frequencies close to the optimal sensitivity of LISA. The amplitude of the GW signal is proportional to $M_{\text{chirp}}^{5/4}$ with

$$M_{\text{chirp}} = \frac{(m_1 m_2)^{3/5}}{(m_1 + m_2)^{1/5}} \quad , \quad (3.1)$$

and therefore higher masses will lead to larger amplitudes. The two CE events explored in this paper involved binary systems of relatively low mass, with the masses of core and companion totaling $1.36 M_{\odot}$ and $1 M_{\odot}$ for the successful and failed CE ejections respectively. Events involving larger masses would release louder GW signals, potentially leading to improved chances of detection, but this would also result in different outcomes for the CE event. Overall, the final orbital separation will be the key parameter that determines the detectability of these events, and in turn it is one of the aspects of CE evolution that is less constrained.

In Sec. 2.3, it is shown that, when nuclear reactions are taken into account, the CE merger studied in this paper results in a thermonuclear explosion. As the explosion takes place after the disruption of the RG core, when the GW emission has decreased significantly, the conclusions regarding the detectability of the GWs from such events are not affected. Furthermore, such an explosion would make this event a candidate for multi-messenger astronomy, as the explosion occurring inside the envelope would result in a transient resembling a Type II SN (Kozyreva et al., 2024). The detections of GWs arising before the explosion would be one of the methods to distinguish these transients from core-collapse SNe.

NS-WD mergers

Despite AREPO enabling the computation of the first 3D MHD simulation of this type of astrophysical event, there are still substantial limitations in the approach followed in Sect. 2.2. In the first place, in order to make accurate predictions regarding the jet characteristics, which would be relevant for the extraction of observables, the modeling of the jets launched after the disruption of the WD should be improved in several aspects:

- The grid refinement criteria used for the jets falls back to targeting a certain mass per cell. Due to the inherently low density in the jet funnel, the width of the jet is merely resolved by a couple of cells. This is easily addressable by enforcing a larger resolution in this region. Preliminary tests of this fix are already being performed and the result is shown in Fig. 3.1. This figure shows how an increase in the resolution of the jets results in an increase in the jet collimation, also leading to higher maximum velocities.
- The velocities found inside the jet are mildly relativistic (and it seems like the velocities may grow larger with an increased resolution), but the simulation was performed without the use of a relativistic hydrodynamical solver, and therefore the jet is not being accurately treated. There is an existing relativistic solver included in AREPO (Lioutas et al., 2024), but unfortunately it cannot treat magnetic fields, which are what power the jets. The

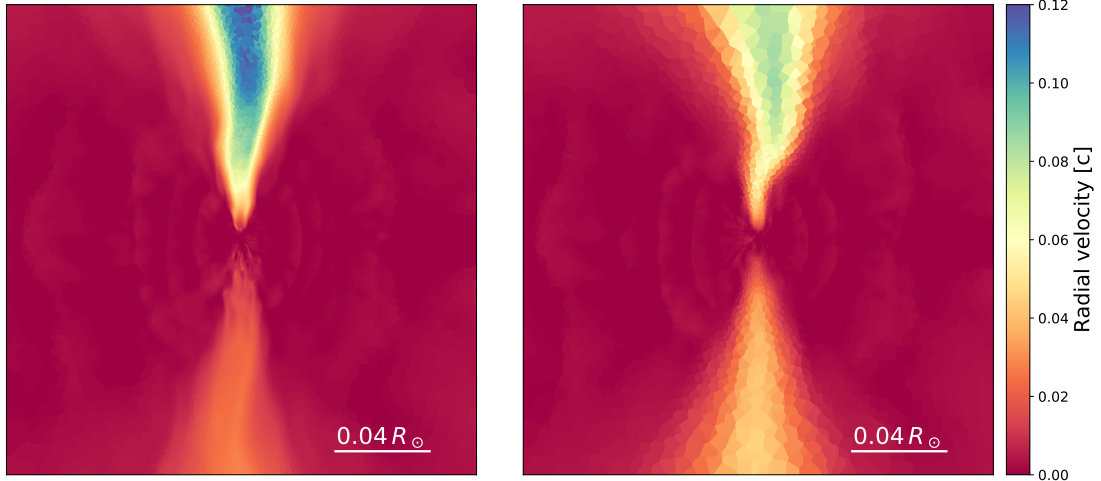


Figure 3.1: Comparison of the morphology and velocities of the jets arising as a result of a NS-WD merger for two different mesh-refinement criteria. The plots show slices perpendicular to the orbital plane of two simulations 150s after the disruption of the WD. The plot on the right shows the standard AREPO refinement. The plot on the left shows an improved refinement, targeting a cell-size 100 times smaller in the jet than the one on the right.

next steps in this direction require either the implementation of a relativistic MHD solver in AREPO, or porting the state of the simulation at the time of the jet launching to another code with a relativistic MHD solver such as ATHENA++ (White et al., 2016; Stone et al., 2020), GRHYDRO (Mösta et al., 2014) or PLUTO (Mignone et al., 2007, 2012). Eulerian codes like these cannot simulate the disruption of the WD, but by the time the jets are launched, the system is in a more axis-symmetric configuration, and its treatment with Eulerian codes could result more feasible.

- As the simulation evolves, the acceleration region from which the jets are launched, moves closer to the NS. The lack of a precise modeling of the NS itself limits the accuracy of the treatment of the acceleration region as it draws closer to the NS.

This last point highlights the main limitation of the simulation: the treatment of the NS as a point mass. Despite AREPO’s capability of covering an extensive range of timescales, the ratio between the minimum resolved timescale and the maximum simulated timescale still constrains this simulation. In the simulation shown in Sec. 2.2, the WD is disrupted ~ 100 s after the onset of the mass transfer episode and, therefore, to properly characterize the event, it is required to simulate time frames on the order of hundreds of seconds. Having a hydrodynamically resolved NS would require¹ time steps on the order of 10^{-7} s, and therefore simulating the entire event would require a number of time steps on the order of 10^9 , which is a factor of 1000 larger than the total number of time steps in the simulation

¹Number based on simulations of resolved NSs (Soultanis et al., 2022; Lioutas et al., 2024)

shown in Sec. 2.2. This makes having a resolved NS currently unachievable in 3D simulations that aim to model this type of event from the onset of mass transfer.

To overcome this challenge, the NS is taken as a point mass particle and its gravitational potential is softened so that the gravitational force does not become infinitely large as the gas gets arbitrarily close to it. Therefore, the hydrodynamical conditions around the NS will depend on the exact shape of this potential, and for this reason anything occurring inside the region with the softened potential or its neighborhood is considered to be unresolved. The size of this region also limits the minimum time step required by the simulation. A softening radius similar to the radius of a NS would result in gravitational forces comparable to those at the surface of an NS, again making the required time steps too small to possibly simulate the entire interaction. For this simulation, a softening radius of 840 km was used in an attempt to balance computational cost and resolution. The lack of a resolved NS means that physical processes such as accretion onto the NS are not modeled, making it difficult to predict the final fate of the remnant, or whether the strong magnetic fields observed in the simulation can advect into the NS originating a magnetar. Such unresolved processes can have effects on larger scales outside the softened region (especially as the jets carry away material from this region), but they would also determine the densities and temperatures reached by the gas in the surroundings of the NS, where most of the nucleosynthesis will take place.

This is the reason why no nuclear reactions were included in the simulation shown in Sec. 2.2. The effects of nuclear reactions were briefly studied in another simulation where the MHD solver was coupled to a 13-isotope nuclear network. It was found that most of the significant nuclear burning takes place inside the unresolved region, and material from there is dredged up by the jets. The hydrodynamical conditions in the proximity of the NS will determine the dominant nuclear reactions, potentially altering the energy injection and the dynamics of the region, and if this takes place under unresolved conditions, it is difficult to assess the validity of the results.

A potential course of action to address this issue is the study of the formation of an accretion disk around a NS and the conditions found inside of it using simulations spanning smaller timeframes. The hydrodynamic state at different stages of the simulation could be used as initial conditions for simulations with resolved NSs to study how the region evolves during short timescales. This could potentially be used to obtain nucleosynthetic yields and compare them with the results of global simulations. Having accurate yields would also be helpful for the extraction of observables and help identify the transients corresponding to these events.

Thermonuclear explosions of low-mass COWDs

The results obtained in Sec. 2.3 are, perhaps, the most unexpected of this thesis. Most of the studies on thermonuclear explosions of COWD have historically focused on high mass stars, as they have commonly been portrayed as the most likely progenitor for Type Ia SNe. The closer the mass of the star to the Chan-

drasekhar limit, the closer the conditions in its interior to those required for the ignition of a runaway C burning. Originally, the ignition scenario involved the transfer of mass from another star onto a COWD close to M_{Ch} until the density and temperature in its interior reached the conditions to trigger an explosion. This scenario was subdivided into two classes, depending on whether the donor star is another WD (double-degenerate scenario, e.g. [Webbink, 1984](#); [Yoon et al., 2007](#)) or a non-degenerate star (single-degenerate scenario, e.g. [Whelan and Iben, 1973](#); [Nomoto et al., 1984](#)).

This scenario has been challenged by the finding of alternative methods to ignite a COWD such as the *double-detonation* scenario ([Woosley and Weaver, 1994](#)). If a COWD presents a He-layer on its surface, either due to being a hybrid HeCO WD or forming the layer during mass transfer, accretion of He-rich material from a companion can lead to an initial He detonation on the surface. This sends a shock inside the COWD, triggering a subsequent C detonation. As the shock can greatly increase the density and temperature inside the COWD, this mechanism enables the explosion of COWD with masses substantially below M_{Ch} (e.g. [Fink et al., 2007](#); [Gronow et al., 2020, 2021](#)). Nevertheless, the explosions must be able to produce a large abundance of ^{56}Ni to power the observed lightcurves of SNeIa, and this production has been shown to decrease as the mass of the COWD decreases ([Sim et al., 2010](#)). For this reason, this scenario has not been explored for COWD masses below $\sim 0.9 M_{\odot}$. A complete and updated review on the topic of Type Ia SNe and their progenitors can be found in [Liu et al. \(2023\)](#).

Lower-mass COWD have lower central densities than their higher-mass counterparts, making the conditions for C ignition more difficult to reach, and producing almost no ^{56}Ni in the case that they are reached. Additionally, as the compactness of WDs increases with the mass, low-mass COWD are larger, and their surface density is substantially lower than that of their higher-mass counterparts, making the initial He ignition more difficult to achieve. These factors made the outcome of the simulation presented in Sec. 2.3 rather surprising. The simulation presents a double-detonation as a result of the merger of a $0.6 M_{\odot}$ COWD with a $0.4 M_{\odot}$ HeWD. There are a couple of factors that make this system overcome the mentioned challenges and result in a successful thermonuclear explosion.

First, the merger product presents an unusually large amount of He. In the standard double-detonation scenario, the COWD is surrounded by a He-layer with masses normally below $0.1 M_{\odot}$. In the scenario shown in Sec. 2.3, the COWD is enveloped in a substantially larger mass of He (Fig. 3.2), with the overdense pocket where He is first ignited having itself a mass of $\sim 0.05 M_{\odot}$. This makes the initial explosion more energetic than in the case of a standard double-detonation scenario, launching a stronger shockwave inside the COWD. This stronger shock is able to create the conditions for explosive C burning inside the COWD despite the central density found in the $0.6 M_{\odot}$ star being much lower than that of massive WDs.

In second place, the ignition of the He-layer in the merger product of the system shown in Sec. 2.3 takes place differently than what is normally seen in standard double-detonation scenarios. In the standard scenario, the substantially larger surface gravity of high-mass COWD, produces an increased density and temperature in the He-shell. This means that the material in this region is close

to the point of ignition, and as a result, a small amount of shear and compression from an accretion stream can trigger the first detonation. In the scenario presented in Sec. 2.3, the density at the surface of the COWD is substantially lower, and the conditions for He ignition are met locally as a result of heating and compression caused by the large, overdense, pocket of He that shears against the surface of the COWD. This interaction increases the temperature and density in the interface region between the COWD and the He pocket until the conditions for an explosive He burning are met. The conditions for this scenario to arise are therefore difficult to predict due to the dynamic nature of the process that results in the formation of these pockets of overdense material. The main factor for the formation of He pockets and their successful ignition seems to be tidal forces. Since the publication of the article shown in Sec. 2.3, several additional simulations have been performed, with different masses for the WDs, in an attempt to narrow down the mass range in which this interaction can take place. Lowering the mass of the HeWD results in a more extended star, and its tidal disruption taking place further away from the COWD. This results in a thinner accretion stream that, for low enough masses of the HeWD, does not form He pockets massive enough to trigger the He ignition. Larger masses for the HeWD were not tested, as those stars would be increasingly difficult to form according to standard stellar evolution. On the other hand, increasing the mass of the COWD has the effect of amplifying the tidal forces, and therefore it also increases the distance at which the HeWD is disrupted. The He pockets may still be formed, but the increased tidal forces mean that the pockets are more likely to be disrupted, forming a more homogeneous accretion stream, and resulting in a less “violent” accretion onto the COWD. The smoother accretion combined with the increased surface gravity leads to a stable burning of the He rather than an explosion. Although more research should be done to elucidate the precise mass range, it seems like this scenario will be restricted to a rather narrow combination of mass ratios and total masses.

Regarding the numerical resolution of the ignition spots, both the He ignition and the C ignition are not resolved in the simulation shown in Sec. 2.3, with typical cell sizes of ~ 90 km and ~ 15 km, in the respective ignition spots. Despite that, the temperatures and densities found in these regions are consistent with those found in 1D simulations of resolved He and C detonations. Resolving the C ignition on these systems is completely out of reach of 3D simulations, as the scales needed to be resolved are on the order of a few centimeters. But in the case of the He ignition, for the conditions found in the presented simulations, the scale of the ignition spot can reach several kilometers (Shen and Moore, 2014). Since the publication of the article shown in Sec. 2.3, another simulation has been performed, where the resolution has been increased locally close to the ignition spot, reaching cell sizes as small as 500 m. This new simulation results in a resolved He ignition, confirming that the ignition observed in Sec. 2.3 is physically plausible.

The double-detonation scenario proposed in Sec. 2.3 is presented as a merger between two isolated WDs, but the formation of such a system and its merger is not trivial. The pathways for the formation of this system should be accurately studied with population synthesis methods. In general, the formation of HeWDs with such high masses is unlikely and will, in most cases, involve stripping a RG

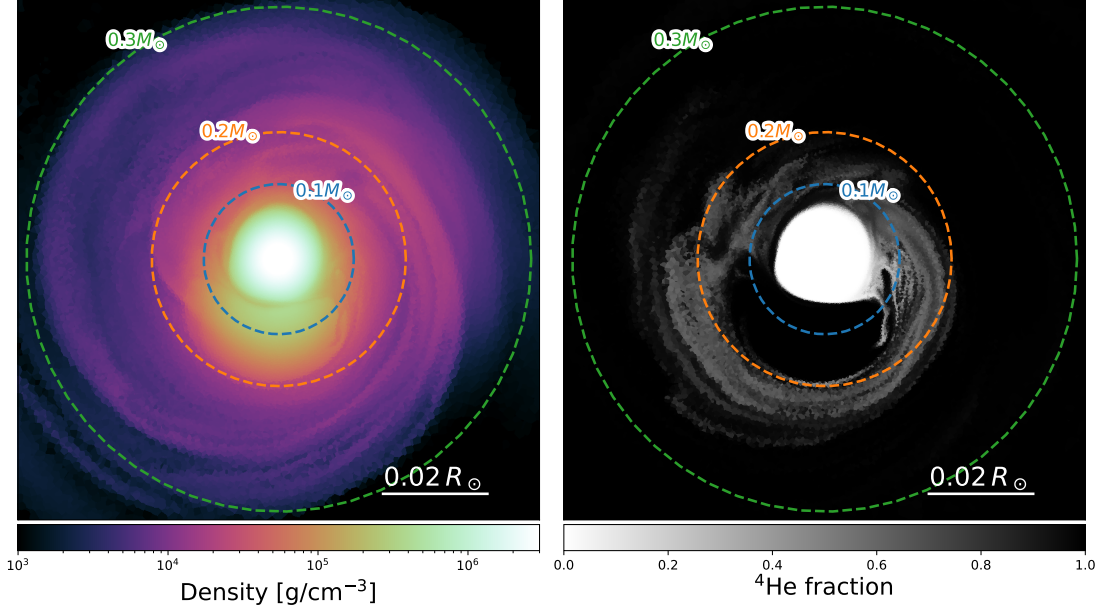


Figure 3.2: Structure of the merger product of Sec. 2.3 moments before the onset of the thermonuclear explosion. The plots show slices perpendicular to the orbital plane. The plot on the left is color coded with the density, while the one in the right shows the ${}^4\text{He}$ fraction. Dashed lines show the cumulative ${}^4\text{He}$ mass contained in that volume.

star of its envelope in a CE event. The HeWD presented shown in that simulation has a mass of $0.4 M_{\odot}$, which is a value close to the maximum core mass that a RG can reach ($\sim 0.48 M_{\odot}$, [Kippenhahn et al., 2012](#)). If a RG star with a degenerate core of this mass is stripped of its envelope by a COWD, the merger will take place after the orbit shrinks due to GW emission. Depending on the final separation after the CE event, this orbital shrinking can take place on a very long timescale, potentially larger than the age of the Universe. On the other hand, if instead of a successful envelope stripping, the outcome of the CE event is a direct merger, this would take place on much shorter timescales. As discussed in Sec. 2.3, this scenario has also been tested, and the merger of the COWD with a degenerate He core of this mass also results in a thermonuclear explosion. The transient arising from this scenario differs substantially to the one described in Sec. 2.3 due to the interaction of the ejecta with the H envelope. This has been studied in another publication ([Kozyreva et al., 2024](#)), where the 1D radiation-hydrodynamics code STELLA ([Blinnikov et al., 2006](#)) was used to predict the observational properties of such interaction. A selection of the synthetic lightcurves produced in this work are shown in Fig. 3.3. In [Kozyreva et al. \(2024\)](#) it is found that if the merger takes place inside a H-rich envelope, the early lightcurve and spectrum of the event resembles that of Type Iip SNe, with the late time evolution showing a mixture of features from Type Ia and Type II SN.

The next steps towards a better understanding of these events involve putting constraints on the mass ranges where the explosions can occur, and using this information to obtain rates for these events using population synthesis methods.

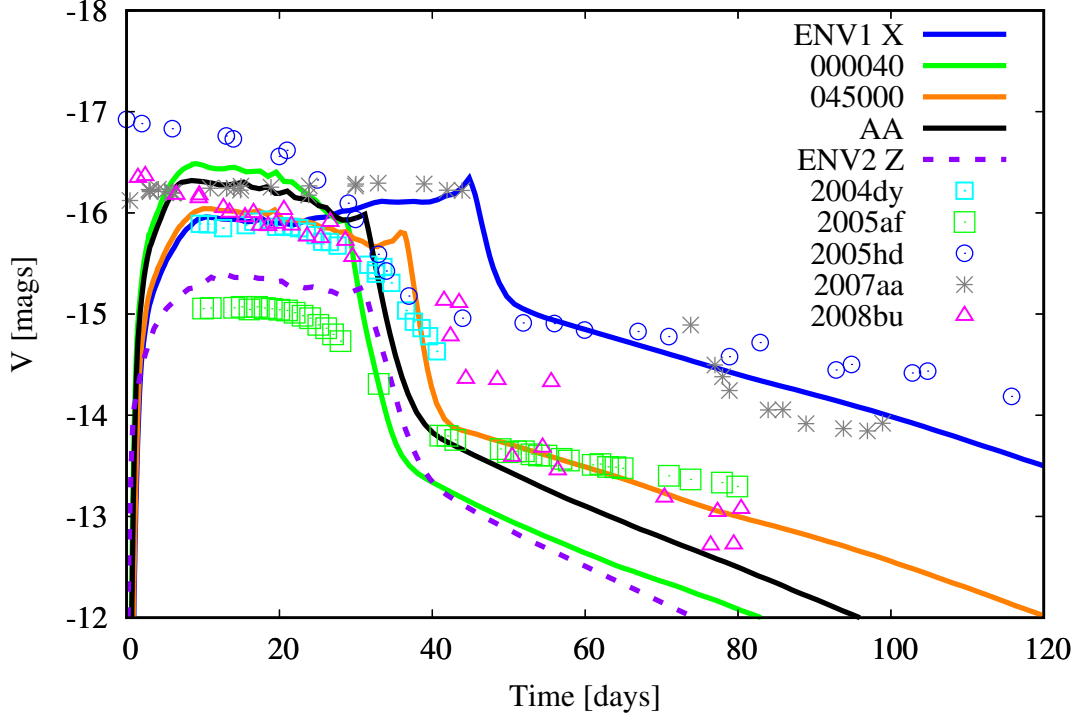


Figure 3.3: Figure shows selected synthetic lightcurves in the V-band produced by the thermonuclear explosion described in Sec. 2.3 if the explosion were to take place embedded in a H-rich envelope. The blue, green, and orange plain lines show the lightcurves produced by the interaction of the ejecta with an “extended” $330 R_{\odot}$ envelope, for different lines of sight. The black line shows the same scenario as the other plain lines, for an angle-averaged model of the ejecta. The purple dashed line shows the lightcurve produced if the ejecta is embedded in a more “compact” $75 R_{\odot}$ envelope, for a line of sight perpendicular to the orbital plane. The colored points represent observational data of selected SN. Figure taken from [Kozyreva et al. \(2024\)](#) and reproduced with permission of the authors.

This will help to understand the likelihood of the described explosion scenario taking place with or without a H envelope surrounding it. Additionally, accurate late time lightcurves and spectra should be produced to attempt to match both cases with observed transients.

3.3. Closing remarks

Numerical modeling is the most precise method for describing dynamical interactions between stars. The simulations presented in this thesis were possible thanks to the nearly-Lagrangian scheme of the code AREPO. These powerful numerical schemes pave the way for a new generation of high-quality simulations of events that were previously impossible to model in such level of detail.

Acknowledgments

I would like to thank the unreasonably large number of people that made it possible for me getting here. First I want to thank my advisor Fritz Röpke for giving me the opportunity, means, supervision, and encouragement needed to carry out my PhD. I would also like to thank Fabian Schneider whom I have always considered my second supervisor and that during these years has always given me the most helpful comments and ideas, and even technical support in my first weeks. I need to thank and apologize to the entirety of the PSO group over these last 4 years, whose work has been continuously disrupted by my loud voice. In the first place, Theo, not only the person that I bothered the most, but probably also my greatest collaborator in improving the general loudness of the office. But also the rest of the current and former group members: Alex, Marco, Giovanni, Robert, Kiril, Hans, Leo, Sabrina, Christian, Manuel, Thomas, David, Melvin, Patrick, and Mike.

I am also extremely grateful to my collaborators, specially to the “common-envelope meeting gang” including Rüdiger Pakmor and Sebastian Ohlmann, who not only provided fantastic ideas, suggestions and feedback, but that without their help I would have never understood AREPO to the level that made these simulations possible.

Of course, I need to acknowledge all the great friends that I have made at HITS over these years. I am specially thankful for the emotional support from Jan, Lynn, and Anna that have been dealing with my daily complaints in every coffee break for the last year. But also to the entirety of the SET group (specially Eva for its unstoppable optimism and encouragement), TOS, MBM and CCC for making live at HITS much more fun.

I also have to thank the people that instilled in me the need to go out for a beer every Wednesday evening: Fede, Cristian, Nick, Michelle, you must know that I have done my best to uphold these values and pass them on to the new generations of PhD students.

Additionally, I express my sincere gratitude to the volleyball community in Heidelberg, and specially to people at the HTV that made me feel so at home. Without them, and the stress relief of volleyball, I would have probably cracked a long time ago. The same goes for all the nice people that joined our weekly football games: Mathias, Saber, Andrei, Max, and many more that have somehow made me reach my peak football level at 28.

I want to also express my gratitude to the people in the University of Amsterdam that made the atmosphere there so ridiculously fun that managed to convince me that doing a PhD was a good idea, specially the great friends that I made during my masters, Jay, Eline, Zack, Andre, Jelle and Annelotte that are always there

for me every time I return to the Netherlands.

I also want to take this moment to appreciate everyone in Spain that has made me who I am. First and foremost the volleyball guys, as those golden years shaped who I am as a person in many ways, and every time I come back to Spain it is as if I had never left. I cannot begin naming people because this is already long enough, but you know who you are. Weirdly, I feel compelled to additionally thank our back-in-the-days head coach Jordi, as I believe he instilled in me a pragmatism and mentality that actually shaped who I am and how I deal with pressure and face adversity. To my friends from Valladolid, Jorge, Juan, Pablo, Marina, Daniel, Edu, Bondan for all the great moments throughout the last two decades. To all the great friends I made at university, that formed what Vilorio described as “those low-maintenance friendships that are always there for you”. I also want to thank Prof. Mariano Santander for giving me the kick that I didn’t know I needed in the direction of Astrophysics with his unparalleled and contagious enthusiasm during his lectures. To the friends that helped me keep (or lose, depending on the day) my sanity during these years with our almost daily “geopolitics” discussions, Alfredo, Marco, Sergio, Lionel, Eli, Vinicius, Aiur and Adrian.

And finally but more importantly to my entire family not only my parents Tomas and Alicia, or my sister Ana, but also to everyone in Cigales and Vallelado because during these years I barely had the time to express how lucky I feel to have such a great, loving family that will always be there for me and support me no matter where I am.

List of publications

Papers used in this thesis:

- [1] **Morán-Fraile, J.**; F. R. N. Schneider; F. K. Röpke; S. T. Ohlmann; R. Pakmor; T. Saultanis; A. Bauswein; **A&A, 672 A9**; *Gravitational Wave emission from dynamical stellar interactions*
- [2] **Morán-Fraile, J.**; F. K. Röpke; R. Pakmor; M. A. Aloy; S. T. Ohlmann; F. R. N. Schneider; G. Leidi; **A&A, 681 A41**; *Self-consistent MHD simulation of jet launching in a neutron star - white dwarf merger*
- [3] **Morán-Fraile, J.**; Holas, A.; F. K. Röpke; R. Pakmor; F. R. N. Schneider; **Accepted for publication in A&A letters**; *Faint calcium-rich transient from a double-detonation of a $0.6 M_{\odot}$ carbon-oxygen white dwarf*

Papers not used in this thesis:

- [1] A. Kozyreva; **Morán-Fraile, J.**; A. Holas; V. A. Bronner; F. K. Röpke; N. Pavlyuk; D. Tsvetkov; **Accepted for publication in A&A**; *Thermonuclear explosions as Type II supernovae*
- [2] Van Son, L. A. C.; De Mink, S. E.; Broekgaarden, F. S.; Renzo, M.; Justham, S.; Laplace, E.; **Morán-Fraile, J.**; Hendriks, D. D.; Farmer, R.; **ApJ 897, 100V**; *Polluting the pair-instability mass gap for binary black holes through super-Eddington accretion in isolated binaries*

Bibliography

- Aasi, J., Abbott, B. P., Abbott, R., Abbott, T., Abernathy, M. R., Ackley, K., Adams, C., Adams, T., Addesso, P., Adhikari, R. X., et al., “Advanced LIGO,” *Classical and Quantum Gravity*, vol. 32, no. 7, p. 074001, 2015, doi:[10.1088/0264-9381/32/7/074001](https://doi.org/10.1088/0264-9381/32/7/074001).
- Abbott, B. P., Abbott, R., Abbott, T. D., Abernathy, M. R., Acernese, F., Ackley, K., Adams, C., Adams, T., Addesso, P., Adhikari, R. X., et al., “GW150914: First results from the search for binary black hole coalescence with Advanced LIGO,” *Physical Review D*, vol. 93, no. 12, p. 122003, 2016a, doi:[10.1103/PhysRevD.93.122003](https://doi.org/10.1103/PhysRevD.93.122003).
- Abbott, B. P., Abbott, R., Abbott, T. D., Abernathy, M. R., Acernese, F., Ackley, K., Adams, C., Adams, T., Addesso, P., Adhikari, R. X., et al., “Observation of Gravitational Waves from a Binary Black Hole Merger,” *Physical Review Letters*, vol. 116, no. 6, p. 061102, 2016b, doi:[10.1103/PhysRevLett.116.061102](https://doi.org/10.1103/PhysRevLett.116.061102).
- Abbott, B. P., Abbott, R., Abbott, T. D., Acernese, F., Ackley, K., Adams, C., Adams, T., Addesso, P., Adhikari, R. X., Adya, V. B., et al., “GW170817: Observation of Gravitational Waves from a Binary Neutron Star Inspiral,” *Physical Review Letters*, vol. 119, no. 16, p. 161101, 2017, doi:[10.1103/PhysRevLett.119.161101](https://doi.org/10.1103/PhysRevLett.119.161101).
- Abbott, B. P., Abbott, R., Abbott, T. D., Acernese, F., Ackley, K., Adams, C., Adams, T., Addesso, P., Adhikari, R. X., Adya, V. B., et al., “Multi-messenger Observations of a Binary Neutron Star Merger,” *The Astrophysical Journal Letters*, vol. 848, no. 2, p. L12, 2017, doi:[10.3847/2041-8213/aa91c9](https://doi.org/10.3847/2041-8213/aa91c9).
- Abbott, B. P., Abbott, R., Abbott, T. D., Acernese, F., Ackley, K., Adams, C., Adams, T., Addesso, P., Adhikari, R. X., Adya, V. B., et al., “GW170817: Measurements of Neutron Star Radii and Equation of State,” *Physical Review Letters*, vol. 121, no. 16, p. 161101, 2018, doi:[10.1103/PhysRevLett.121.161101](https://doi.org/10.1103/PhysRevLett.121.161101).
- Acernese, F., Agathos, M., Agatsuma, K., Aisa, D., Allemandou, N., Allocca, A., Amarni, J., Astone, P., Balestri, G., Ballardin, G., et al., “Advanced Virgo: a second-generation interferometric gravitational wave detector,” *Classical and Quantum Gravity*, vol. 32, no. 2, p. 024001, 2014, doi:[10.1088/0264-9381/32/2/024001](https://doi.org/10.1088/0264-9381/32/2/024001).
- Agazie, G., Anumalapudi, A., Archibald, A. M., Arzoumanian, Z., Baker, P. T., Bécsy, B., Blecha, L., Brazier, A., Brook, P. R., Burke-Spolaor, S., et al., “The

- NANOGrav 15 yr Data Set: Evidence for a Gravitational-wave Background,” *The Astrophysical Journal Letters*, vol. 951, no. 1, p. L8, 2023, doi:[10.3847/2041-8213/acdac6](https://doi.org/10.3847/2041-8213/acdac6).
- Akutsu, T., Ando, M., Arai, K., Arai, Y., Araki, S., Araya, A., Aritomi, N., Aso, Y., Bae, S., Bae, Y., et al., “Overview of KAGRA: Detector design and construction history,” *Progress of Theoretical and Experimental Physics*, vol. 2021, no. 5, p. 49, 2021, doi:[10.1093/PTEP/PTAA125](https://doi.org/10.1093/PTEP/PTAA125).
- Alexander, K. D., Berger, E., Fong, W., Williams, P. K. G., Guidorzi, C., Margutti, R., Metzger, B. D., Annis, J., Blanchard, P. K., Brout, D., et al., “The Electromagnetic Counterpart of the Binary Neutron Star Merger LIGO/Virgo GW170817. VI. Radio Constraints on a Relativistic Jet and Predictions for Late-time Emission from the Kilonova Ejecta,” *The Astrophysical Journal Letters*, vol. 848, no. 2, p. L21, 2017, doi:[10.3847/2041-8213/aa905d](https://doi.org/10.3847/2041-8213/aa905d).
- Almeida, L. A., Sana, H., Taylor, W., Barbá, R., Bonanos, A. Z., Crowther, P., Daminieli, A., de Koter, A., de Mink, S. E., Evans, C. J., et al., “The Tarantula Massive Binary Monitoring. I. Observational campaign and OB-type spectroscopic binaries,” *Astronomy & Astrophysics*, vol. 598, A84, 2017, doi:[10.1051/0004-6361/201629844](https://doi.org/10.1051/0004-6361/201629844).
- Althaus, L. G., Córscico, A. H., Isern, J., and García-Berro, E., “Evolutionary and pulsational properties of white dwarf stars,” *The Astronomy and Astrophysics Review*, vol. 18, no. 4, pp. 471–566, 2010, doi:[10.1007/s00159-010-0033-1](https://doi.org/10.1007/s00159-010-0033-1).
- Arnett, W. D., “A Possible Model of Supernovae: Detonation of ^{12}C ,” *Astrophysics and Space Science*, vol. 5, no. 2, pp. 180–212, 1969, doi:[10.1007/BF00650291](https://doi.org/10.1007/BF00650291).
- Balbus, S. A. and Hawley, J. F., “A Powerful Local Shear Instability in Weakly Magnetized Disks. I. Linear Analysis,” *Astrophysical Journal*, vol. 376, p. 214, 1991, doi:[10.1086/170270](https://doi.org/10.1086/170270).
- Belczynski, K., Bulik, T., and Ruiter, A. J., “New Constraints on Type Ia Supernova Progenitor Models,” *Astrophysical Journal*, vol. 629, no. 2, pp. 915–921, 2005, doi:[10.1086/431578](https://doi.org/10.1086/431578).
- Belczynski, K., Holz, D. E., Bulik, T., and O’Shaughnessy, R., “The first gravitational-wave source from the isolated evolution of two 40-100 Msun stars,” *Nature*, 2016, doi:[10.1038/nature18322](https://doi.org/10.1038/nature18322).
- Belczynski, K., Klencki, J., Fields, C. E., Olejak, A., Berti, E., Meynet, G., Fryer, C. L., Holz, D. E., O’Shaughnessy, R., Brown, D. A., et al., “Evolutionary roads leading to low effective spins, high black hole masses, and O1/O2 rates for LIGO/Virgo binary black holes,” *Astronomy & Astrophysics*, vol. 636, A104, 2020, doi:[10.1051/0004-6361/201936528](https://doi.org/10.1051/0004-6361/201936528).
- Benacquista, M., *An Introduction to the Evolution of Single and Binary Stars*, Springer New York, NY, 2013, doi:[10.1007/978-1-4419-9991-7](https://doi.org/10.1007/978-1-4419-9991-7).

- Berger, M. J. and Olinger, J., “Adaptive Mesh Refinement for Hyperbolic Partial Differential Equations,” *Journal of Computational Physics*, vol. 53, no. 3, pp. 484–512, 1984, doi:[10.1016/0021-9991\(84\)90073-1](https://doi.org/10.1016/0021-9991(84)90073-1).
- Blinnikov, S. I., Röpke, F. K., Sorokina, E. I., Gieseler, M., Reinecke, M., Travaglio, C., Hillebrandt, W., and Stritzinger, M., “Theoretical light curves for deflagration models of type Ia supernova,” *Astronomy & Astrophysics*, vol. 453, no. 1, pp. 229–240, 2006, doi:[10.1051/0004-6361:20054594](https://doi.org/10.1051/0004-6361:20054594).
- Bobrick, A., Davies, M. B., and Church, R. P., “Mass transfer in white dwarf–neutron star binaries,” *Monthly Notices of the Royal Astronomical Society*, vol. 467, no. 3, pp. 3556–3575, 2017, doi:[10.1093/MNRAS/STX312](https://doi.org/10.1093/MNRAS/STX312).
- Bobrick, A., Zenati, Y., Perets, H. B., Davies, M. B., and Church, R., “Transients from ONe white dwarf – neutron star/black hole mergers,” *Monthly Notices of the Royal Astronomical Society*, vol. 510, no. 3, pp. 3758–3777, 2022, doi:[10.1093/mnras/stab3574](https://doi.org/10.1093/mnras/stab3574).
- Brandenburg, A. and Subramanian, K., “Astrophysical magnetic fields and nonlinear dynamo theory,” *Physics Reports*, vol. 417, no. 1-4, pp. 1–209, 2005, doi:[10.1016/j.physrep.2005.06.005](https://doi.org/10.1016/j.physrep.2005.06.005).
- Buldgen, G., “Current problems in stellar evolution,” *arXiv e-prints*, arXiv:1902.10399, 2019, doi:[10.48550/arXiv.1902.10399](https://doi.org/10.48550/arXiv.1902.10399).
- Bulla, M., Sim, S. A., and Kromer, M., “Polarization spectral synthesis for Type Ia supernova explosion models,” *Monthly Notices of the Royal Astronomical Society*, vol. 450, no. 1, pp. 967–981, 2015, doi:[10.1093/mnras/stv657](https://doi.org/10.1093/mnras/stv657).
- Burmester, U. P., Ferrario, L., Pakmor, R., Seitenzahl, I. R., Ruiter, A. J., and Hole, M., “AREPO White Dwarf merger simulations resulting in edge-lit detonation and run-away hypervelocity companion,” *Monthly Notices of the Royal Astronomical Society*, vol. 000, pp. 1–20, 2023, doi:[10.1093/mnras/stad1394](https://doi.org/10.1093/mnras/stad1394).
- Carvalho, A., Marinhojr, R. M., and Malheiro, M., “Mass-Radius Relation for White Dwarfs Models at Zero Temperature,” *Journal of Physics: Conference Series*, vol. 706, no. 5, p. 052016, 2016, doi:[10.1088/1742-6596/706/5/052016](https://doi.org/10.1088/1742-6596/706/5/052016).
- Chandrasekhar, S., “The Maximum Mass of Ideal White Dwarfs,” *Astrophysical Journal*, vol. 74, p. 81, 1931, doi:[10.1086/143324](https://doi.org/10.1086/143324).
- Chini, R., Hoffmeister, V. H., Nasseri, A., Stahl, O., and Zinnecker, H., “A spectroscopic survey on the multiplicity of high-mass stars,” *Monthly Notices of the Royal Astronomical Society*, vol. 424, no. 3, pp. 1925–1929, 2012, doi:[10.1111/j.1365-2966.2012.21317.x](https://doi.org/10.1111/j.1365-2966.2012.21317.x).
- Courant, R., Friedrichs, K., and Lewy, H., “Über die partiellen Differenzgleichungen der mathematischen Physik,” *Mathematische Annalen*, vol. 100, pp. 32–74, 1928, doi:[10.1007/BF01448839](https://doi.org/10.1007/BF01448839).

- Creighton, J. D. and Anderson, W. G., *Gravitational-Wave Physics and Astronomy. An Introduction to Theory, Experiment and Data Analysis*, Wiley-VCH, 2011, ISBN 9783527408863, doi:[10.1002/9783527636037](https://doi.org/10.1002/9783527636037).
- Damiani, C. and Lanza, A. F., “Evolution of angular-momentum-losing exoplanetary systems - Revisiting Darwin stability,” *Astronomy & Astrophysics*, vol. 574, p. A39, 2015, doi:[10.1051/0004-6361/201424318](https://doi.org/10.1051/0004-6361/201424318).
- Darwin, G. H., “VIII. The determination of the secular effects of tidal friction by a graphical method,” *Proceedings of the Royal Society of London*, vol. 29, no. 196-199, pp. 168–181, 1879.
- de Kool, M., van den Heuvel, E. P. J., and Pylyser, E., “An evolutionary scenario for the black hole binary A0620-00.” *Astronomy & Astrophysics*, vol. 183, pp. 47–52, 1987.
- de Mink, S. E., Cantiello, M., Langer, N., Yoon, S. C., Brott, I., Glebbeek, E., Verkoulen, M., and Pols, O. R., “Rotational mixing in close binaries,” in Deng, L. and Chan, K. L. (editors), “The Art of Modeling Stars in the 21st Century,” vol. 252, pp. 365–370, 2008, doi:[10.1017/S1743921308023223](https://doi.org/10.1017/S1743921308023223).
- Eggenberger, P., Meynet, G., Maeder, A., Hirschi, R., Charbonnel, C., Talon, S., and Ekström, S., “The Geneva stellar evolution code,” *Astrophysics and Space Science*, vol. 316, no. 1-4, pp. 43–54, 2008, doi:[10.1007/s10509-007-9511-y](https://doi.org/10.1007/s10509-007-9511-y).
- Eggleton, P., *Evolutionary Processes in Binary and Multiple Stars*, Cambridge Astrophysics, Cambridge University Press, 2006, doi:[10.1017/CBO9780511536205](https://doi.org/10.1017/CBO9780511536205).
- Eggleton, P. P. P., “Approximations to the radii of Roche lobes,” *The Astrophysical Journal*, vol. 268, p. 368, 1983, doi:[10.1086/160960](https://doi.org/10.1086/160960).
- Einstein, A., “Die Feldgleichungen der Gravitation,” *Sitzungsberichte der Königlich Preußischen Akademie der Wissenschaften*, pp. 844–847, 1915.
- EPTA Collaboration, Antoniadis, J., Babak, S., Bak Nielsen, A. S., Bassa, C. G., Berthereau, A., Bonetti, M., Bortolas, E., Brook, P. R., Burgay, M., et al., “The second data release from the European Pulsar Timing Array. I. The dataset and timing analysis,” *Astronomy & Astrophysics*, vol. 678, A48, 2023a, doi:[10.1051/0004-6361/202346841](https://doi.org/10.1051/0004-6361/202346841).
- EPTA Collaboration, InPTA Collaboration, Antoniadis, J., Arumugam, P., Arumugam, S., Babak, S., Bagchi, M., Bak Nielsen, A. S., Bassa, C. G., Bathula, A., et al., “The second data release from the European Pulsar Timing Array. III. Search for gravitational wave signals,” *Astronomy & Astrophysics*, vol. 678, A50, 2023b, doi:[10.1051/0004-6361/202346844](https://doi.org/10.1051/0004-6361/202346844).
- EPTA Collaboration, InPTA Collaboration, Antoniadis, J., Arumugam, P., Arumugam, S., Babak, S., Bagchi, M., Nielsen, A. S. B., Bassa, C. G., Bathula, A., et al., “The second data release from the European Pulsar Timing Array. II. Customised pulsar noise models for spatially correlated gravitational

- waves,” *Astronomy & Astrophysics*, vol. 678, A49, 2023c, doi:[10.1051/0004-6361/202346842](https://doi.org/10.1051/0004-6361/202346842).
- Ferlito, F., Springel, V., Davies, C. T., Hernández-Aguayo, C., Pakmor, R., Barrera, M., White, S. D. M., Delgado, A. M., Hadzhiyska, B., Hernquist, L., et al., “The MillenniumTNG Project: the impact of baryons and massive neutrinos on high-resolution weak gravitational lensing convergence maps,” *Monthly Notices of the Royal Astronomical Society*, vol. 524, no. 4, pp. 5591–5606, 2023, doi:[10.1093/mnras/stad2205](https://doi.org/10.1093/mnras/stad2205).
- Fernández, R., Margalit, B., and Metzger, B. D., “Nuclear-dominated accretion flows in two dimensions – II. Ejecta dynamics and nucleosynthesis for CO and ONe white dwarfs,” *Monthly Notices of the Royal Astronomical Society*, vol. 488, no. 1, pp. 259–279, 2019, doi:[10.1093/mnras/stz1701](https://doi.org/10.1093/mnras/stz1701).
- Fernández, R. and Metzger, B. D., “Nuclear Dominated Accretion Flows in Two Dimensions. I. Torus Evolution with Parametric Microphysics,” *Astrophysical Journal*, vol. 763, no. 2, 108, 2013, doi:[10.1088/0004-637X/763/2/108](https://doi.org/10.1088/0004-637X/763/2/108).
- Fink, M., Hillebrandt, W., and Röpke, F. K., “Double-detonation supernovae of sub-Chandrasekhar mass white dwarfs,” *Astronomy & Astrophysics*, vol. 476, no. 3, pp. 1133–1143, 2007, doi:[10.1051/0004-6361:20078438](https://doi.org/10.1051/0004-6361:20078438).
- Geier, S., Classen, L., and Heber, U., “The Fast-rotating, Low-gravity Subdwarf B Star EC 22081-1916: Remnant of a Common Envelope Merger Event,” *The Astrophysical Journal Letters*, vol. 733, no. 1, L13, 2011, doi:[10.1088/2041-8205/733/1/L13](https://doi.org/10.1088/2041-8205/733/1/L13).
- Ginat, Y. B., Glanz, H., Perets, H. B., Grishin, E., and Desjacques, V., “Gravitational waves from in-spirals of compact objects in binary common-envelope evolution,” *Monthly Notices of the Royal Astronomical Society*, vol. 493, no. 4, pp. 4861–4867, 2020, doi:[10.1093/mnras/staa465](https://doi.org/10.1093/mnras/staa465).
- Glanz, H., Perets, H. B., and Pakmor, R., “Thermonuclear explosion criteria for direct and indirect collisions of CO white dwarfs: a study of the impact-parameter threshold for detonation,” *arXiv e-prints*, arXiv:2309.03300, 2023, doi:[10.48550/arXiv.2309.03300](https://doi.org/10.48550/arXiv.2309.03300).
- Goicovic, F. G., Springel, V., Ohlmann, S. T., and Pakmor, R., “Hydrodynamical moving-mesh simulations of the tidal disruption of stars by supermassive black holes,” *Monthly Notices of the Royal Astronomical Society*, vol. 487, no. 1, pp. 981–992, 2019, doi:[10.1093/mnras/stz1368](https://doi.org/10.1093/mnras/stz1368).
- Goldstein, A., Veres, P., Burns, E., Briggs, M. S., Hamburg, R., Kocevski, D., Wilson-Hodge, C. A., Preece, R. D., Poolakkil, S., Roberts, O. J., et al., “An Ordinary Short Gamma-Ray Burst with Extraordinary Implications: Fermi-GBM Detection of GRB 170817A,” *The Astrophysical Journal Letters*, vol. 848, no. 2, p. L14, 2017, doi:[10.3847/2041-8213/aa8f41](https://doi.org/10.3847/2041-8213/aa8f41).

- Grand, R. J. J., Gómez, F. A., Marinacci, F., Pakmor, R., Springel, V., Campbell, D. J. R., Frenk, C. S., Jenkins, A., and White, S. D. M., “The Auriga Project: the properties and formation mechanisms of disc galaxies across cosmic time,” *Monthly Notices of the Royal Astronomical Society*, vol. 467, no. 1, pp. 179–207, 2017, doi:[10.1093/mnras/stx071](https://doi.org/10.1093/mnras/stx071).
- Gronow, S., Collins, C., Ohlmann, S. T., Pakmor, R., Kromer, M., Seitenzahl, I. R., Sim, S. A., and Röpke, F. K., “SNe Ia from double detonations: Impact of core-shell mixing on the carbon ignition mechanism,” *Astronomy and Astrophysics*, vol. 635, p. A169, 2020, doi:[10.1051/0004-6361/201936494](https://doi.org/10.1051/0004-6361/201936494).
- Gronow, S., Collins, C. E., Sim, S. A., and Röpke, F. K., “Double detonations of sub-MChCO white dwarfs: Variations in Type Ia supernovae due to different core and He shell masses,” *Astronomy and Astrophysics*, vol. 649, p. A155, 2021, doi:[10.1051/0004-6361/202039954](https://doi.org/10.1051/0004-6361/202039954).
- Harms, J., Ambrosino, F., Angelini, L., Braitto, V., Branchesi, M., Brocato, E., Cappellaro, E., Coccia, E., Coughlin, M., Ceca, R. D., et al., “Lunar Gravitational-wave Antenna,” *The Astrophysical Journal*, vol. 910, no. 1, p. 1, 2021, doi:[10.3847/1538-4357/abe5a7](https://doi.org/10.3847/1538-4357/abe5a7).
- Harry, G. M., Fritschel, P., Shaddock, D. A., Folkner, W., and Phinney, E. S., “Laser interferometry for the Big Bang Observer,” *Classical and Quantum Gravity*, vol. 23, no. 15, pp. 4887–4894, 2006, doi:[10.1088/0264-9381/23/15/008](https://doi.org/10.1088/0264-9381/23/15/008).
- Heger, A., Langer, N., and Woosley, S. E., “Presupernova Evolution of Rotating Massive Stars. I. Numerical Method and Evolution of the Internal Stellar Structure,” *The Astrophysical Journal*, vol. 528, no. 1, pp. 368–396, 2000, doi:[10.1086/308158](https://doi.org/10.1086/308158).
- Hirai, R. and Mandel, I., “A Two-stage Formalism for Common-envelope Phases of Massive Stars,” *The Astrophysical Journal Letters*, vol. 937, no. 2, L42, 2022, doi:[10.3847/2041-8213/ac9519](https://doi.org/10.3847/2041-8213/ac9519).
- Horst, L., Hirschi, R., Edelmann, P. V. F., Andrásy, R., and Röpke, F. K., “Multidimensional low-Mach number time-implicit hydrodynamic simulations of convective helium shell burning in a massive star,” *Astronomy & Astrophysics*, vol. 653, A55, 2021, doi:[10.1051/0004-6361/202140825](https://doi.org/10.1051/0004-6361/202140825).
- Hulse, R. A. and Taylor, J. H., “Discovery of a pulsar in a binary system.” *The Astrophysical Journal Letters*, vol. 195, pp. L51–L53, 1975, doi:[10.1086/181708](https://doi.org/10.1086/181708).
- Hut, P., “Stability of tidal equilibrium,” *Astronomy & Astrophysics*, vol. 92, no. 1-2, pp. 167–170, 1980.
- Hut, P., “Tidal evolution in close binary systems.” *Astronomy & Astrophysics*, vol. 99, pp. 126–140, 1981.

- Iaconi, R. and de Marco, O., “Speaking with one voice: simulations and observations discuss the common envelope α parameter,” *Monthly Notices of the Royal Astronomical Society*, vol. 490, no. 2, pp. 2550–2566, 2019, doi:[10.1093/MNRAS/STZ2756](https://doi.org/10.1093/MNRAS/STZ2756).
- Ivanova, N., Justham, S., Chen, X., De Marco, O., Fryer, C. L., Gaburov, E., Ge, H., Glebbeek, E., Han, Z., Li, X.-D., et al., “Common envelope evolution: where we stand and how we can move forward,” *The Astronomy and Astrophysics Review 2013 21:1*, vol. 21, no. 1, pp. 1–73, 2013, doi:[10.1007/S00159-013-0059-2](https://doi.org/10.1007/S00159-013-0059-2).
- Kalogera, V., Belczynski, K., Kim, C., Oshaughnessy, R., and Willems, B., “Formation of double compact objects,” *Physics Reports*, vol. 442, no. 1-6, pp. 75–108, 2007, doi:[10.1016/j.physrep.2007.02.008](https://doi.org/10.1016/j.physrep.2007.02.008).
- Kippenhahn, R., Weigert, A., and Weiss, A., *Stellar Structure and Evolution*, Astronomy and Astrophysics Library, Springer Berlin Heidelberg, Berlin, Heidelberg, 2012, ISBN 978-3-642-30255-8, doi:[10.1007/978-3-642-30304-3](https://doi.org/10.1007/978-3-642-30304-3).
- Koester, D. and Chanmugam, G., “REVIEW: Physics of white dwarf stars,” *Reports on Progress in Physics*, vol. 53, no. 7, pp. 837–915, 1990, doi:[10.1088/0034-4885/53/7/001](https://doi.org/10.1088/0034-4885/53/7/001).
- Kotake, K. and Kuroda, T., “Gravitational Waves from Core-Collapse Supernovae,” in Alsabti, A. W. and Murdin, P. (editors), “Handbook of Supernovae,” p. 1671, Springer, 2017, doi:[10.1007/978-3-319-21846-5_9](https://doi.org/10.1007/978-3-319-21846-5_9).
- Kozyreva, A., Moran-Fraile, J., Holas, A., Bronner, V. A., Roepke, F. K., Pavlyuk, N., Mironov, A., and Tsvetkov, D., “Thermonuclear explosions as Type II supernovae,” *arXiv e-prints*, arXiv:2401.10401, 2024, doi:[10.48550/arXiv.2401.10401](https://doi.org/10.48550/arXiv.2401.10401).
- Kromer, M. and Sim, S. A., “Time-dependent 3D spectrum synthesis for type Ia supernovae,” *Monthly Notices of the Royal Astronomical Society*, vol. 398, no. 4, pp. 1809–1826, 2009, doi:[10.1111/j.1365-2966.2009.15256.x](https://doi.org/10.1111/j.1365-2966.2009.15256.x).
- Kruckow, M. U., *Binary star population synthesis - Progenitors of gravitational wave driven mergers*, Ph.D. thesis, Rheinische Friedrich Wilhelms University of Bonn, Germany, 2018.
- Kruckow, M. U., Neunteufel, P. G., Di Stefano, R., Gao, Y., and Kobayashi, C., “A Catalog of Potential Post-Common Envelope Binaries,” *Astrophysical Journal*, vol. 920, no. 2, 86, 2021, doi:[10.3847/1538-4357/ac13ac](https://doi.org/10.3847/1538-4357/ac13ac).
- Kruckow, M. U., Tauris, T. M., Langer, N., Kramer, M., and Izzard, R. G., “Progenitors of gravitational wave mergers: binary evolution with the stellar grid-based code COMBINE,” *Monthly Notices of the Royal Astronomical Society*, vol. 481, no. 2, pp. 1908–1949, 2018, doi:[10.1093/mnras/sty2190](https://doi.org/10.1093/mnras/sty2190).

- Kruckow, M. U., Tauris, T. M., Langer, N., Szécsi, D., Marchant, P., and Podsiadlowski, P., “Common-envelope ejection in massive binary stars. Implications for the progenitors of GW150914 and GW151226,” *Astronomy & Astrophysics*, vol. 596, A58, 2016, doi:[10.1051/0004-6361/201629420](https://doi.org/10.1051/0004-6361/201629420).
- Lattimer, J., “Neutron Stars and the Nuclear Matter Equation of State,” *Annual Review of Nuclear and Particle Science*, vol. 71, no. 1, pp. 433–464, 2021, doi:[10.1146/annurev-nucl-102419-124827](https://doi.org/10.1146/annurev-nucl-102419-124827).
- Lau, M. Y., Hirai, R., González-Bolívar, M., Price, D. J., De Marco, O., and Mandel, I., “Common envelopes in massive stars: towards the role of radiation pressure and recombination energy in ejecting red supergiant envelopes,” *Monthly Notices of the Royal Astronomical Society*, vol. 512, no. 4, pp. 5462–5480, 2022, doi:[10.1093/mnras/stac049](https://doi.org/10.1093/mnras/stac049).
- Leidi, G., Andrassy, R., Higl, J., Edelmann, P. V. F., and Röpke, F. K., “Turbulent dynamo action and its effects on the mixing at the convective boundary of an idealized oxygen-burning shell,” *Astronomy & Astrophysics*, vol. 679, A132, 2023, doi:[10.1051/0004-6361/202347621](https://doi.org/10.1051/0004-6361/202347621).
- Lewin, W. H. G., van Paradijs, J., and van den Heuvel, E. P. J., *X-ray Binaries*, Cambridge Astrophysics, Cambridge University Press, 1997, ISBN 9780521599344.
- Lidov, M. L., “The evolution of orbits of artificial satellites of planets under the action of gravitational perturbations of external bodies,” *Planetary and Space Science*, vol. 9, no. 10, pp. 719–759, 1962, doi:[10.1016/0032-0633\(62\)90129-0](https://doi.org/10.1016/0032-0633(62)90129-0).
- Lioutas, G., Bauswein, A., Soutanis, T., Pakmor, R., Springel, V., and Röpke, F. K., “General relativistic moving-mesh hydrodynamic simulations with AREPO and applications to neutron star mergers,” *Monthly Notices of the Royal Astronomical Society*, vol. 528, no. 2, pp. 1906–1929, 2024, doi:[10.1093/mnras/stae057](https://doi.org/10.1093/mnras/stae057).
- Liu, Y., Chen, Z. H., Zhang, H. H., and Lin, Z. Y., “Physical effects of magnetic fields on the Kelvin-Helmholtz instability in a free shear layer,” *Physics of Fluids*, vol. 30, no. 4, p. 044102, 2018, doi:[10.1063/1.5004473](https://doi.org/10.1063/1.5004473).
- Liu, Z., Roepke, F. K., and Han, Z., “Type Ia Supernova Explosions in Binary Systems: A Review,” *Research in Astronomy and Astrophysics*, vol. 23, no. 8, p. 082001, 2023, doi:[10.1088/1674-4527/acd89e](https://doi.org/10.1088/1674-4527/acd89e).
- Maeder, A., “Evidences for a bifurcation in massive star evolution. The ON-blue stragglers,” *Astronomy and astrophysics (Berlin. Print)*, vol. 178, no. 1, pp. 159–169, 1987.
- Maggiore, M., *Gravitational Waves: Volume 1: Theory and Experiments*, Oxford University Press, 2007, ISBN 9780198570745, doi:[10.1093/acprof:oso/9780198570745.001.0001](https://doi.org/10.1093/acprof:oso/9780198570745.001.0001).

- Manchester, R. N., “The International Pulsar Timing Array,” *Classical and Quantum Gravity*, vol. 30, no. 22, p. 224010, 2013, doi:[10.1088/0264-9381/30/22/224010](https://doi.org/10.1088/0264-9381/30/22/224010).
- Marchant, P. and Bodensteiner, J., “The Evolution of Massive Binary Stars,” *arXiv e-prints*, arXiv:2311.01865, 2023, doi:[10.48550/arXiv.2311.01865](https://doi.org/10.48550/arXiv.2311.01865).
- Marinacci, F., Vogelsberger, M., Pakmor, R., Torrey, P., Springel, V., Hernquist, L., Nelson, D., Weinberger, R., Pillepich, A., Naiman, J., et al., “First results from the IllustrisTNG simulations: radio haloes and magnetic fields,” *Monthly Notices of the Royal Astronomical Society*, vol. 480, no. 4, pp. 5113–5139, 2018, doi:[10.1093/mnras/sty2206](https://doi.org/10.1093/mnras/sty2206).
- Mason, B. D., Hartkopf, W. I., Gies, D. R., Henry, T. J., and Helsel, J. W., “The High Angular Resolution Multiplicity of Massive Stars,” *The Astronomical Journal*, vol. 137, no. 2, pp. 3358–3377, 2009, doi:[10.1088/0004-6256/137/2/3358](https://doi.org/10.1088/0004-6256/137/2/3358).
- Metzger, B. D., “Kilonovae,” *Living Reviews in Relativity*, vol. 20, no. 1, p. 3, 2017, doi:[10.1007/s41114-017-0006-z](https://doi.org/10.1007/s41114-017-0006-z).
- Metzger, B. D., Martínez-Pinedo, G., Darbha, S., Quataert, E., Arcones, A., Kasen, D., Thomas, R., Nugent, P., Panov, I. V., and Zinner, N. T., “Electromagnetic counterparts of compact object mergers powered by the radioactive decay of r-process nuclei,” *Monthly Notices of the Royal Astronomical Society*, vol. 406, no. 4, pp. 2650–2662, 2010, doi:[10.1111/J.1365-2966.2010.16864.X](https://doi.org/10.1111/J.1365-2966.2010.16864.X).
- Mezzacappa, A. and Zanolin, M., “Gravitational Waves from Neutrino-Driven Core Collapse Supernovae: Predictions, Detection, and Parameter Estimation,” *arXiv e-prints*, arXiv:2401.11635, 2024, doi:[10.48550/arXiv.2401.11635](https://doi.org/10.48550/arXiv.2401.11635).
- Mignone, A., Bodo, G., Massaglia, S., Matsakos, T., Tesileanu, O., Zanni, C., and Ferrari, A., “PLUTO: A Numerical Code for Computational Astrophysics,” *The Astrophysical Journal Supplement Series*, vol. 170, no. 1, pp. 228–242, 2007, doi:[10.1086/513316](https://doi.org/10.1086/513316).
- Mignone, A., Zanni, C., Tzeferacos, P., van Straalen, B., Colella, P., and Bodo, G., “The PLUTO Code for Adaptive Mesh Computations in Astrophysical Fluid Dynamics,” *The Astrophysical Journal Supplement Series*, vol. 198, no. 1, 7, 2012, doi:[10.1088/0067-0049/198/1/7](https://doi.org/10.1088/0067-0049/198/1/7).
- Moe, M. and Di Stefano, R., “Mind Your Ps and Qs: The Interrelation between Period (P) and Mass-ratio (Q) Distributions of Binary Stars,” *The Astrophysical Journal Supplement Series*, vol. 230, no. 2, 15, 2017, doi:[10.3847/1538-4365/aa6fb6](https://doi.org/10.3847/1538-4365/aa6fb6).
- Moreno, M. M., Schneider, F. R. N., Röpkke, F. K., Ohlmann, S. T., Pakmor, R., Podsiadlowski, P., and Sand, C., “From 3D hydrodynamic simulations of common-envelope interaction to gravitational-wave mergers,” *Astronomy & Astrophysics*, vol. 667, A72, 2022, doi:[10.1051/0004-6361/202142731](https://doi.org/10.1051/0004-6361/202142731).

- Mösta, P., Mundim, B. C., Faber, J. A., Haas, R., Noble, S. C., Bode, T., Löffler, F., Ott, C. D., Reisswig, C., and Schnetter, E., “GRHydro: a new open-source general-relativistic magnetohydrodynamics code for the Einstein toolkit,” *Classical and Quantum Gravity*, vol. 31, no. 1, p. 015005, 2014, doi:[10.1088/0264-9381/31/1/015005](https://doi.org/10.1088/0264-9381/31/1/015005).
- Naiman, J. P., Pillepich, A., Springel, V., Ramirez-Ruiz, E., Torrey, P., Vogelsberger, M., Pakmor, R., Nelson, D., Marinacci, F., Hernquist, L., et al., “First results from the IllustrisTNG simulations: a tale of two elements - chemical evolution of magnesium and europium,” *Monthly Notices of the Royal Astronomical Society*, vol. 477, no. 1, pp. 1206–1224, 2018, doi:[10.1093/mnras/sty618](https://doi.org/10.1093/mnras/sty618).
- Nakar, E., “Short-hard gamma-ray bursts,” *Physics Reports*, vol. 442, no. 1-6, pp. 166–236, 2007, doi:[10.1016/j.physrep.2007.02.005](https://doi.org/10.1016/j.physrep.2007.02.005).
- Nakar, E., “The electromagnetic counterparts of compact binary mergers,” *Physics Reports*, vol. 886, pp. 1–84, 2020, doi:[10.1016/j.physrep.2020.08.008](https://doi.org/10.1016/j.physrep.2020.08.008).
- Narayan, R., Paczynski, B., and Piran, T., “Gamma-ray bursts as the death throes of massive binary stars,” *The Astrophysical Journal*, vol. 395, p. L83, 1992, doi:[10.1086/186493](https://doi.org/10.1086/186493).
- Nelemans, G., Verbunt, F., Yungelson, L. R., and Portegies Zwart, S. F., “Reconstructing the evolution of double helium white dwarfs: envelope loss without spiral-in,” *Astronomy & Astrophysics*, vol. 360, pp. 1011–1018, 2000, doi:[10.48550/arXiv.astro-ph/0006216](https://doi.org/10.48550/arXiv.astro-ph/0006216).
- Nelemans, G., Yungelson, L. R., and Portegies Zwart, S. F., “The gravitational wave signal from the Galactic disk population of binaries containing two compact objects,” *Astronomy & Astrophysics*, vol. 375, no. 3, pp. 890–898, 2001, doi:[10.1051/0004-6361:20010683](https://doi.org/10.1051/0004-6361:20010683).
- Nelson, D., Springel, V., Pillepich, A., Rodriguez-Gomez, V., Torrey, P., Genel, S., Vogelsberger, M., Pakmor, R., Marinacci, F., Weinberger, R., et al., “The IllustrisTNG simulations: public data release,” *Computational Astrophysics and Cosmology*, vol. 6, no. 1, 2, 2019, doi:[10.1186/s40668-019-0028-x](https://doi.org/10.1186/s40668-019-0028-x).
- Nomoto, K., Nomoto, and K., “Evolution of 8-10 solar mass stars toward electron capture supernovae. I - Formation of electron-degenerate O + NE + MG cores.” *Astrophysical Journal*, vol. 277, pp. 791–805, 1984, doi:[10.1086/161749](https://doi.org/10.1086/161749).
- Ohlmann, S. T., *Hydrodynamics of the Common Envelope Phase in Binary Stellar Evolution.*, Ph.D. thesis, Ruprecht-Karls University of Heidelberg, Germany, 2016.
- Ohlmann, S. T., Röpke, F. K., Pakmor, R., and Springel, V., “Constructing stable 3D hydrodynamical models of giant stars,” *Astronomy & Astrophysics*, vol. 599, p. 5, 2017, doi:[10.1051/0004-6361/201629692](https://doi.org/10.1051/0004-6361/201629692).

- Ondratschek, P. A., Röpke, F. K., Schneider, F. R., Fendt, C., Sand, C., Ohlmann, S. T., Pakmor, R., and Springel, V., “Bipolar planetary nebulae from common-envelope evolution of binary stars,” *Astronomy & Astrophysics*, vol. 660, p. L8, 2022, doi:[10.1051/0004-6361/202142478](https://doi.org/10.1051/0004-6361/202142478).
- Paczynski, B., “Common Envelope Binaries,” *IAUS*, vol. 73, p. 75, 1976.
- Pakmor, R., Bauer, A., and Springel, V., “Magnetohydrodynamics on an unstructured moving grid,” *Monthly Notices of the Royal Astronomical Society*, vol. 418, no. 2, pp. 1392–1401, 2011, doi:[10.1111/j.1365-2966.2011.19591.x](https://doi.org/10.1111/j.1365-2966.2011.19591.x).
- Pakmor, R., Kromer, M., Taubenberger, S., and Springel, V., “Helium-ignited Violent Mergers as a Unified Model for Normal and Rapidly Declining Type Ia Supernovae,” *The Astrophysical Journal Letters*, vol. 770, no. 1, L8, 2013, doi:[10.1088/2041-8205/770/1/L8](https://doi.org/10.1088/2041-8205/770/1/L8).
- Pakmor, R., Springel, V., Bauer, A., Mocz, P., Munoz, D. J., Ohlmann, S. T., Schaal, K., and Zhu, C., “Improving the convergence properties of the moving-mesh code AREPO,” *Monthly Notices of the Royal Astronomical Society*, vol. 455, no. 1, pp. 1134–1143, 2016, doi:[10.1093/mnras/stv2380](https://doi.org/10.1093/mnras/stv2380).
- Pakmor, R., Springel, V., Coles, J. P., Guillet, T., Pfrommer, C., Bose, S., Barrera, M., Delgado, A. M., Ferlito, F., Frenk, C., et al., “The MillenniumTNG Project: the hydrodynamical full physics simulation and a first look at its galaxy clusters,” *Monthly Notices of the Royal Astronomical Society*, vol. 524, no. 2, pp. 2539–2555, 2023, doi:[10.1093/mnras/stac3620](https://doi.org/10.1093/mnras/stac3620).
- Pakmor, R., Zenati, Y., Perets, H. B., and Toonen, S., “Thermonuclear explosion of a massive hybrid HeCO white dwarf triggered by a He detonation on a companion,” *Monthly Notices of the Royal Astronomical Society*, vol. 503, no. 4, pp. 4734–4747, 2021, doi:[10.1093/mnras/stab686](https://doi.org/10.1093/mnras/stab686).
- Paschalidis, V., Liu, Y. T., Etienne, Z., and Shapiro, S. L., “Merger of binary white dwarf–neutron stars: Simulations in full general relativity,” *Physical Review D*, vol. 84, no. 10, p. 104032, 2011, doi:[10.1103/PhysRevD.84.104032](https://doi.org/10.1103/PhysRevD.84.104032).
- Paschalidis, V., MacLeod, M., Baumgarte, T. W., and Shapiro, S. L., “Merger of white dwarf–neutron star binaries: Prelude to hydrodynamic simulations in general relativity,” *Physical Review D*, vol. 80, no. 2, p. 024006, 2009, doi:[10.1103/PhysRevD.80.024006](https://doi.org/10.1103/PhysRevD.80.024006).
- Paxton, B., Bildsten, L., Dotter, A., Herwig, F., Lesaffre, P., and Timmes, F., “Modules for Experiments in Stellar Astrophysics (MESA),” *The Astrophysical Journal Supplement Series*, vol. 192, no. 1, pp. 3–35, 2011, doi:[10.1088/0067-0049/192/1/3](https://doi.org/10.1088/0067-0049/192/1/3).
- Paxton, B., Cantiello, M., Arras, P., Bildsten, L., Brown, E. F., Dotter, A., Mankovich, C., Montgomery, M. H., Stello, D., Timmes, F. X., et al., “Modules for Experiments in Stellar Astrophysics (MESA): Planets, Oscillations, Rotation,

- and Massive Stars,” *The Astrophysical Journal Supplement Series*, vol. 208, no. 43pp, p. 4, 2013, doi:[10.1088/0067-0049/208/1/4](https://doi.org/10.1088/0067-0049/208/1/4).
- Paxton, B., Marchant, P., Schwab, J., Bauer, E. B., Bildsten, L., Cantiello, M., Dessart, L., Farmer, R., Hu, H., Langer, N., et al., “Modules for Experiments in Stellar Astrophysics (MESA): Binaries, Pulsations, and Explosions,” *The Astrophysical Journal Supplement Series*, vol. 220, no. 1, p. 15, 2015, doi:[10.1088/0067-0049/220/1/15](https://doi.org/10.1088/0067-0049/220/1/15).
- Paxton, B., Smolec, R., Schwab, J., Gaudy, A., Bildsten, L., Cantiello, M., Dotter, A., Farmer, R., Goldberg, J. A., Jermyn, A. S., et al., “Modules for Experiments in Stellar Astrophysics (MESA): Pulsating Variable Stars, Rotation, Convective Boundaries, and Energy Conservation,” *The Astrophysical Journal Supplement Series*, vol. 243, no. 1, 10, 2019, doi:[10.3847/1538-4365/ab2241](https://doi.org/10.3847/1538-4365/ab2241).
- Peters, P. C., “Gravitational Radiation and the Motion of Two Point Masses,” *Physical Review*, vol. 136, no. 4B, pp. B1224–B1232, 1964, doi:[10.1103/PhysRev.136.B1224](https://doi.org/10.1103/PhysRev.136.B1224).
- Peters, P. C. and Mathews, J., “Gravitational Radiation from Point Masses in a Keplerian Orbit,” *Physical Review*, vol. 131, no. 1, pp. 435–440, 1963, doi:[10.1103/PhysRev.131.435](https://doi.org/10.1103/PhysRev.131.435).
- Pillepich, A., Nelson, D., Hernquist, L., Springel, V., Pakmor, R., Torrey, P., Weinberger, R., Genel, S., Naiman, J. P., Marinacci, F., et al., “First results from the IllustrisTNG simulations: the stellar mass content of groups and clusters of galaxies,” *Monthly Notices of the Royal Astronomical Society*, vol. 475, no. 1, pp. 648–675, 2018, doi:[10.1093/mnras/stx3112](https://doi.org/10.1093/mnras/stx3112).
- Powell, J., Müller, B., Aguilera-Dena, D. R., and Langer, N., “Three dimensional magnetorotational core-collapse supernova explosions of a 39 solar mass progenitor star,” *Monthly Notices of the Royal Astronomical Society*, vol. 522, no. 4, pp. 6070–6086, 2023, doi:[10.1093/mnras/stad1292](https://doi.org/10.1093/mnras/stad1292).
- Renzo, M., Callister, T., Chatziioannou, K., van Son, L. A. C., Mingarelli, C. M. F., Cantiello, M., Ford, K. E. S., McKernan, B., and Ashton, G., “Prospects of Gravitational Wave Detections from Common Envelope Evolution with LISA,” *The Astrophysical Journal*, vol. 919, no. 2, p. 128, 2021, doi:[10.3847/1538-4357/ac1110](https://doi.org/10.3847/1538-4357/ac1110).
- Ritter, H., “Formation and evolution of cataclysmic variables .” *Memorie della Societa Astronomica Italiana*, vol. 83, p. 505, 2012.
- Robson, T., Cornish, N. J., and Liu, C., “The construction and use of LISA sensitivity curves,” *Classical and Quantum Gravity*, vol. 36, no. 10, p. 105011, 2019, doi:[10.1088/1361-6382/ab1101](https://doi.org/10.1088/1361-6382/ab1101).
- Röpke, F. K. and De Marco, O., “Simulations of common-envelope evolution in binary stellar systems: physical models and numerical techniques,” *Living Reviews*

- in Computational Astrophysics*, vol. 9, no. 1, 2, 2023, doi:[10.1007/s41115-023-00017-x](https://doi.org/10.1007/s41115-023-00017-x).
- Röpke, F. K. and Sim, S. A., “Models for Type Ia Supernovae and Related Astrophysical Transients,” *Space Science Reviews*, vol. 214, no. 4, pp. 72, 2018, doi:[10.1007/s11214-018-0503-8](https://doi.org/10.1007/s11214-018-0503-8).
- Ruiter, A. J., “Type Ia supernova sub-classes and progenitor origin,” *Proceedings of the International Astronomical Union*, vol. 15, no. S357, pp. 1–15, 2019, doi:[10.1017/S1743921320000587](https://doi.org/10.1017/S1743921320000587).
- Ryu, T., de Mink, S. E., Farmer, R., Pakmor, R., Perna, R., and Springel, V., “Close encounters of star-black hole binaries with single stars,” *Monthly Notices of the Royal Astronomical Society*, vol. 527, no. 2, pp. 2734–2749, 2024, doi:[10.1093/mnras/stad3082](https://doi.org/10.1093/mnras/stad3082).
- Sana, H. and Evans, C. J., “The multiplicity of massive stars,” in Neiner, C., Wade, G., Meynet, G., and Peters, G. (editors), “Active OB Stars: Structure, Evolution, Mass Loss, and Critical Limits,” vol. 272, pp. 474–485, 2011, doi:[10.1017/S1743921311011124](https://doi.org/10.1017/S1743921311011124).
- Sana, H., de Mink, S. E., de Koter, A., Langer, N., Evans, C. J., Gieles, M., Gosset, E., Izzard, R. G., Le Bouquin, J.-B., and Schneider, F. R. N., “Binary Interaction Dominates the Evolution of Massive Stars,” *Science*, vol. 337, no. 6093, pp. 444–446, 2012, doi:[10.1126/science.1223344](https://doi.org/10.1126/science.1223344).
- Sand, C., Ohlmann, S. T., Schneider, F. R., Pakmor, R., and Röpke, F. K., “Common-envelope evolution with an asymptotic giant branch star,” *Astronomy and Astrophysics*, vol. 644, p. A60, 2020, doi:[10.1051/0004-6361/202038992](https://doi.org/10.1051/0004-6361/202038992).
- Savchenko, V., Ferrigno, C., Kuulkers, E., Bazzano, A., Bozzo, E., Brandt, S., Chenevez, J., Courvoisier, T. J.-L., Diehl, R., Domingo, A., et al., “INTEGRAL Detection of the First Prompt Gamma-Ray Signal Coincident with the Gravitational-wave Event GW170817,” *The Astrophysical Journal*, vol. 848, no. 2, p. L15, 2017, doi:[10.3847/2041-8213/aa8f94](https://doi.org/10.3847/2041-8213/aa8f94).
- Schneider, F. R., Ohlmann, S. T., Podsiadlowski, P., Röpke, F. K., Balbus, S. A., Pakmor, R., and Springel, V., “Stellar mergers as the origin of magnetic massive stars,” *Nature*, vol. 574, no. 7777, pp. 211–214, 2019, doi:[10.1038/s41586-019-1621-5](https://doi.org/10.1038/s41586-019-1621-5).
- Schreiber, M. R. and Gänsicke, B. T., “The age, life expectancy, and space density of Post Common Envelope Binaries,” *Astronomy & Astrophysics*, vol. 406, pp. 305–321, 2003, doi:[10.1051/0004-6361:20030801](https://doi.org/10.1051/0004-6361:20030801).
- Seitenzahl, I. R., Herzog, M., Ruiter, A. J., Marquardt, K., Ohlmann, S. T., and Röpke, F. K., “Neutrino and gravitational wave signal of a delayed-detonation model of type Ia supernovae,” *Physical Review D - Particles, Fields, Gravitation and Cosmology*, vol. 92, no. 12, p. 124013, 2015, doi:[10.1103/PhysRevD.92.124013](https://doi.org/10.1103/PhysRevD.92.124013).

- Seto, N., Kawamura, S., and Nakamura, T., “Possibility of Direct Measurement of the Acceleration of the Universe Using 0.1 Hz Band Laser Interferometer Gravitational Wave Antenna in Space,” *Physical Review Letters*, vol. 87, no. 22, p. 221103, 2001, doi:[10.1103/PhysRevLett.87.221103](https://doi.org/10.1103/PhysRevLett.87.221103).
- Shen, K. J. and Moore, K., “The Initiation and Propagation of Helium Detonations in White Dwarf Envelopes,” *The Astrophysical Journal*, vol. 797, no. 1, p. 46, 2014, doi:[10.1088/0004-637X/797/1/46](https://doi.org/10.1088/0004-637X/797/1/46).
- Shingles, L. J., Flörs, A., Sim, S. A., Collins, C. E., Röpke, F. K., Seitenzahl, I. R., and Shen, K. J., “Modelling the ionization state of Type Ia supernovae in the nebular phase,” *Monthly Notices of the Royal Astronomical Society*, vol. 512, no. 4, pp. 6150–6163, 2022, doi:[10.1093/mnras/stac902](https://doi.org/10.1093/mnras/stac902).
- Shipman and L., H., “Masses and radii of white-dwarf stars. III. Results for 110 hydrogen-rich and 28 helium-rich stars.” *Astrophysical Journal*, vol. 228, pp. 240–256, 1979, doi:[10.1086/156841](https://doi.org/10.1086/156841).
- Siess, L., “Evolution of massive AGB stars. II. model properties at non-solar metallicity and the fate of Super-AGB stars,” *Astronomy & Astrophysics*, vol. 476, no. 2, pp. 893–909, 2007, doi:[10.1051/0004-6361:20078132](https://doi.org/10.1051/0004-6361:20078132).
- Sijacki, D., Vogelsberger, M., Genel, S., Springel, V., Torrey, P., Snyder, G. F., Nelson, D., and Hernquist, L., “The Illustris simulation: the evolving population of black holes across cosmic time,” *Monthly Notices of the Royal Astronomical Society*, vol. 452, no. 1, pp. 575–596, 2015, doi:[10.1093/mnras/stv1340](https://doi.org/10.1093/mnras/stv1340).
- Sim, S. A., “Multidimensional simulations of radiative transfer in Type Ia supernovae,” *Monthly Notices of the Royal Astronomical Society*, vol. 375, no. 1, pp. 154–162, 2007, doi:[10.1111/j.1365-2966.2006.11271.x](https://doi.org/10.1111/j.1365-2966.2006.11271.x).
- Sim, S. A., Röpke, F. K., Hillebrandt, W., Kromer, M., Pakmor, R., Fink, M., Ruiter, A. J., and Seitenzahl, I. R., “Detonations in Sub-Chandrasekhar-mass C+O White Dwarfs,” *The Astrophysical Journal Letters*, vol. 714, no. 1, pp. L52–L57, 2010, doi:[10.1088/2041-8205/714/1/L52](https://doi.org/10.1088/2041-8205/714/1/L52).
- Soberman, G. E., Phinney, E. S., and Heuvel, E. P. J. v. d., “Stability Criteria for Mass Transfer in Binary Stellar Evolution,” *Astronomy and Astrophysics*, vol. 327, no. 2, pp. 620–635, 1997.
- Soker, N., “Supernovae Ia in 2017: a long time delay from merger/accretion to explosion,” *Science China Physics, Mechanics & Astronomy 2018 61:4*, vol. 61, no. 4, pp. 1–10, 2018, doi:[10.1007/S11433-017-9144-4](https://doi.org/10.1007/S11433-017-9144-4).
- van Son, L. A. C., De Mink, S. E., Broekgaarden, F. S., Renzo, M., Justham, S., Laplace, E., Morán-Fraile, J., Hendriks, D. D., and Farmer, R., “Polluting the Pair-instability Mass Gap for Binary Black Holes through Super-Eddington Accretion in Isolated Binaries,” *The Astrophysical Journal*, vol. 897, no. 1, p. 100, 2020, doi:[10.3847/1538-4357/ab9809](https://doi.org/10.3847/1538-4357/ab9809).

- Soultanis, T., Bauswein, A., and Stergioulas, N., “Analytic models of the spectral properties of gravitational waves from neutron star merger remnants,” *Physical Review D*, vol. 105, no. 4, 043020, 2022, doi:[10.1103/PhysRevD.105.043020](https://doi.org/10.1103/PhysRevD.105.043020).
- Springel, V., “E pur si muove: Galilean-invariant cosmological hydrodynamical simulations on a moving mesh,” *Monthly Notices of the Royal Astronomical Society*, vol. 401, no. 2, pp. 791–851, 2010, doi:[10.1111/j.1365-2966.2009.15715.x](https://doi.org/10.1111/j.1365-2966.2009.15715.x).
- Springel, V., Pakmor, R., Pillepich, A., Weinberger, R., Nelson, D., Hernquist, L., Vogelsberger, M., Genel, S., Torrey, P., Marinacci, F., et al., “First results from the IllustrisTNG simulations: matter and galaxy clustering,” *Monthly Notices of the Royal Astronomical Society*, vol. 475, no. 1, pp. 676–698, 2018, doi:[10.1093/mnras/stx3304](https://doi.org/10.1093/mnras/stx3304).
- Stone, J. M., Tomida, K., White, C. J., and Felker, K. G., “The Athena++ Adaptive Mesh Refinement Framework: Design and Magnetohydrodynamic Solvers,” *The Astrophysical Journal Supplement Series*, vol. 249, no. 1, 4, 2020, doi:[10.3847/1538-4365/ab929b](https://doi.org/10.3847/1538-4365/ab929b).
- Taubenberger, S., “The Extremes of Thermonuclear Supernovae,” in Alsabti, A. W. and Murdin, P. (editors), “Handbook of Supernovae,” p. 317, Springer International Publishing, 2017, doi:[10.1007/978-3-319-21846-5_37](https://doi.org/10.1007/978-3-319-21846-5_37).
- Tauris, T. M. and van den Heuvel, E. P. J., *Physics of Binary Star Evolution. From Stars to X-ray Binaries and Gravitational Wave Sources*, Princeton Series in Astrophysics, Princeton University Press, Princeton, 2023, ISBN 9780691239262, doi:[doi:10.1515/9780691239262](https://doi.org/10.1515/9780691239262).
- The International Pulsar Timing Array Collaboration, Agazie, G., Antoniadis, J., Anumalapudi, A., Archibald, A. M., Arumugam, P., Arumugam, S., Arzoumanian, Z., Askew, J., Babak, S., et al., “Comparing recent PTA results on the nanohertz stochastic gravitational wave background,” *arXiv e-prints*, arXiv:2309.00693, 2023, doi:[10.48550/arXiv.2309.00693](https://doi.org/10.48550/arXiv.2309.00693).
- Toonen, S., Perets, H. B., Igoshev, A. P., Michaely, E., and Zenati, Y., “The demographics of neutron star – white dwarf mergers,” *Astronomy & Astrophysics*, vol. 619, p. A53, 2018, doi:[10.1051/0004-6361/201833164](https://doi.org/10.1051/0004-6361/201833164).
- Troja, E., Piro, L., van Eerten, H., Wollaeger, R. T., Im, M., Fox, O. D., Butler, N. R., Cenko, S. B., Sakamoto, T., Fryer, C. L., et al., “The X-ray counterpart to the gravitational-wave event GW170817,” *Nature*, vol. 551, no. 7678, pp. 71–74, 2017, doi:[10.1038/nature24290](https://doi.org/10.1038/nature24290).
- Vigna-Gómez, A., Neijssel, C. J., Stevenson, S., Barrett, J. W., Belczynski, K., Justham, S., de Mink, S. E., Müller, B.-H. B., Podsiadlowski, P., Renzo, M., et al., “On the formation history of Galactic double neutron stars,” *Monthly Notices of the Royal Astronomical Society*, vol. 000, no. 3, pp. 1–22, 2018, doi:[10.1093/mnras/sty2463](https://doi.org/10.1093/mnras/sty2463).

- Vogelsberger, M., Genel, S., Springel, V., Torrey, P., Sijacki, D., Xu, D., Snyder, G., Bird, S., Nelson, D., and Hernquist, L., “Properties of galaxies reproduced by a hydrodynamic simulation,” *Nature*, vol. 509, no. 7499, pp. 177–182, 2014, doi:[10.1038/nature13316](https://doi.org/10.1038/nature13316).
- Vynatheya, P., Ryu, T., Pakmor, R., de Mink, S. E., and Perets, H. B., “Simulating the tidal disruption of stars by stellar-mass black holes using moving-mesh hydrodynamics,” *arXiv e-prints*, arXiv:2310.14852, 2023, doi:[10.48550/arXiv.2310.14852](https://doi.org/10.48550/arXiv.2310.14852).
- Webbink, R. F., “Double white dwarfs as progenitors of R Coronae Borealis stars and type I supernovae.” *Astrophysical Journal*, vol. 277, pp. 355–360, 1984, doi:[10.1086/161701](https://doi.org/10.1086/161701).
- Weinberger, R., Springel, V., and Pakmor, R., “The AREPO Public Code Release,” *The Astrophysical Journal Supplement Series*, vol. 248, no. 2, p. 32, 2020, doi:[10.3847/1538-4365/ab908c](https://doi.org/10.3847/1538-4365/ab908c).
- Weisberg, J. M., Taylor, J. H., and Fowler, L. A., “Gravitational waves from an orbiting pulsar,” *Scientific American*, vol. 245, pp. 74–82, 1981, doi:[10.1038/scientificamerican1081-74](https://doi.org/10.1038/scientificamerican1081-74).
- Whelan, J. and Iben, J., Icko, “Binaries and Supernovae of Type I,” *Astrophysical Journal*, vol. 186, pp. 1007–1014, 1973, doi:[10.1086/152565](https://doi.org/10.1086/152565).
- White, C. J., Stone, J. M., and Gammie, C. F., “An Extension of the Athena++ Code Framework for GRMHD Based on Advanced Riemann Solvers and Staggered-mesh Constrained Transport,” *The Astrophysical Journal Supplement Series*, vol. 225, no. 2, 22, 2016, doi:[10.3847/0067-0049/225/2/22](https://doi.org/10.3847/0067-0049/225/2/22).
- Woosley, S. E. and Weaver, T. A., “Sub-Chandrasekhar Mass Models for Type IA Supernovae,” *Astrophysical Journal*, vol. 423, p. 371, 1994, doi:[10.1086/173813](https://doi.org/10.1086/173813).
- Yoon, S. C., Podsiadlowski, P., and Rosswog, S., “Remnant evolution after a carbon-oxygen white dwarf merger,” *Monthly Notices of the Royal Astronomical Society*, vol. 380, no. 3, pp. 933–948, 2007, doi:[10.1111/j.1365-2966.2007.12161.x](https://doi.org/10.1111/j.1365-2966.2007.12161.x).
- Zenati, Y., Bobrick, A., and Perets, H. B., “Faint rapid red transients from Neutron star – CO white-dwarf mergers,” *Monthly Notices of the Royal Astronomical Society*, vol. 493, no. 3, pp. 3956–3965, 2020, doi:[10.1093/mnras/staa507](https://doi.org/10.1093/mnras/staa507).
- Zenati, Y., Perets, H. B., and Toonen, S., “Neutron star–white dwarf mergers: early evolution, physical properties, and outcomes,” *Monthly Notices of the Royal Astronomical Society*, vol. 486, no. 2, pp. 1805–1813, 2019, doi:[10.1093/mnras/stz316](https://doi.org/10.1093/mnras/stz316).
- Zhu, C., Pakmor, R., Kerkwijk, M. H., and Chang, P., “Magnetized moving mesh merger of a carbon-oxygen white dwarf binary,” *Astrophysical Journal Letters*, vol. 806, no. 1, p. L1, 2015, doi:[10.1088/2041-8205/806/1/L1](https://doi.org/10.1088/2041-8205/806/1/L1).

Zwick, L., Capelo, P. R., Bortolas, E., Mayer, L., and Amaro-Seoane, P., “Improved gravitational radiation time-scales: significance for LISA and LIGO-Virgo sources,” *Monthly Notices of the Royal Astronomical Society*, vol. 495, no. 2, pp. 2321–2331, 2020, doi:[10.1093/mnras/staa1314](https://doi.org/10.1093/mnras/staa1314).